THERMAL MECHANICAL ANALYSIS OF SPRAG CLUTCHES

FINAL TECHNICAL REPORT

NATIONAL AERONAUTICS AND SPACE ADMINISTRATION
GRANT

NAG3-653

ROBERT L. MULLEN
RONALD JOSEPH ZAB
ANTONIUS S. KURNIAWAN

CASE WESTERN RESERVE UNIVERSITY

July 7, 1992

ABSTRACT

This report describes work done at Case Western Reserve University on the Thermal Mechanical analysis of sprag helicopter clutches. The report is presented in two parts. The first part is a description of a test rig for the measurement of the heat generated by high speed sprag clutch assemblies during cyclic torsional loading. The second part describes a finite element modeling procedure for sliding contact.

The test rig provides a cyclic torsional load of 756 inch-pounds at 5000 rpm using a four-square arrangement. The sprag clutch test unit was placed between the high speed pinions of the circulating power loop. The test unit was designed to have replaceable inner and outer races, which contain the instrumentation to monitor the sprag clutch. The torque loading device was chosen to be a water cooled magnetic clutch, which is controlled either manually or through a computer.

In the second part of the report, a Generalized Eulerian-lagrangian formulation for Non-linear Dynamic problems is developed for solid materials. This formulation is derived from the basic laws and axioms of continuum mechanics. The novel aspect of this method is that we are able to investigate the physics in the spatial region of interest as material flows though it without having to follow material points.

A finite element approximation to the governing equations is developed. Iterative Methods for the solution of the discrete finite element equations are explored. A FORTRAN program to implement this formulation is developed and a number of solutions to problems of sliding contact are presented.

TABLE OF CONTENTS

PART ONE

Chapter I

INTRODUCTION

This investigation involves the development of a test rig that will simulate a cyclic type of loading on a helicopter sprag clutch and obtain data on the heat generated by the sprag clutch. In a helicopter power train, there are three main components, the engines, the main transmissions, and the rotor. The location of the sprag clutch in the drive train is in one of two places. The first place is between the engine and the main transmission and the other location would be after the first reduction in the main transmission. In both cases, the clutch performs the same function. The major difference is the speed of the clutch. If the clutch location is next to the engine, the clutch needs to operate at speeds of up to 20,000 rpm. The second location in the transmission allows the clutch to operate at lower speeds, approximately 5000 rpm. Although the lower speed is a plus, the torque that it must transmit is proportionally higher. A typical cross section of a helicopter transmission is shown in figure 2 and an enlarged view of the sprag clutch area is shown in figure 3.

The sprag clutch is a commonly used type of overrunning clutch in helicopter transmissions. The principal by which the sprag clutch operates is that of a wedge. The inner and

outer races are concentric circular cylinders. The sprags wedge themselves between the races to transmit torque. A section of a sprag is illustrated in figure 1. The clutch package consists of an inner and outer race, one or two rows of sprags, one or two retainers, and an energizing spring. In the transmissions, the outer race is the driving member and the inner race is the driven member.

If the outer race attempts to rotate faster than the inner race, the energizing spring will cause the sprags to come in contact with both races. The frictional forces at the interface between the races and the sprag will rotate the sprags in a counterclockwise direction about their centers. Because the "y" dimension of the sprags exceeds the radial distance between the races, "x", the sprags become wedged between the races. Once this occurs the two races become locked together and the clutch will transmit torque.

If the inner race attempts to rotate faster than the outer race, the frictional forces will cause the sprags to rotate in the clockwise direction. Since the "z" dimension of the sprags is less than the radial distance between the races, the sprags do not wedge. This will allow the two races to rotate independently of one another. The energizing spring forces the sprags to remain in contact with both races, during this mode.

The sprag clutch can operate in three different modes. The first is when the engine is driving the transmission, the clutch would be in the locked mode. The second is the full speed overrunning mode. The clutch will be in this mode when one engine is not operating in flight and but mainly during start-up. The last mode is the differential speed mode. This mode occurs when the two engines are operating at approximately the same speed but not exactly. In this mode the sprags switch between the locked mode and overrunning mode.

The sprag clutch differential speed mode is the primary interest in this project. The history of the sprag clutch, in the helicopter transmissions, has seen a repetitive pattern of mechanical problems.

A typical failure cycle starts with the sprag clutch overheating. The overheating of the sprag clutch would be caused by friction between the sprags and the two races. This heating would occur during the differential speed or full overrunning modes. Once the overheating is noted, the method used to correct the problem is to increase the cooling of the clutch, which is to modify the oil supply system. The oil supply system pressure is increased, which will increase the oil flow to the clutch and thereby

increase the cooling of the clutch. The next step is the repetition of the same problem. The sprag clutch would still continue to overheat, so the pressure is increased again. This would continue until the oil seals fail. The required action to correct this problem, is to decrease the oil pressure. At this point, the cycle would repeat since the clutch would overheat again.

Before this investigation, a computer analysis was developed for the sprag clutch and the area of heat generation was modeled. The computer analysis was being developed to aid in the design of the sprag clutch. The next phase of the project requires the verification of the computer analysis and this will be accomplished by the development of a test rig.

Chapter II

TORSIONAL LOADING METHODS

The first portion of this project was to determine the method to load the sprag clutch to simulate the torsional loading. Several methods can be used to apply the torsional load. Each method was analyzed to determine the suitability, since each method have certain benefits and drawbacks.

One of the basic methods of load testing power transmission components is using a motor generator test system. The concept that could be used in this project, is to use a motor to drive the outer race of the sprag clutch. The sprag clutch would then transmit the torque to the inner race and finally drive the generator.

The power is dissipated electrically, normally through a resistor bank. While this system is straight forward, the main draw back is the size of the motor. The motor needs to be as large as the power required for the test. Also the speeds involved for the test would require utilizing a speed increaser for the drive side and a speed decreaser for the generator side. Another variation on this method is to change the generator to a mechanical brake. The same drawbacks occur with the brake.

The other basic method to apply a the torsion load to the sprag clutch are all based on the "four-square" test setup. The typical four square system comprises of two identically geared gear transmissions. The two gear transmissions are set up with their low speed and high speed shafts in line with each other. Normally the low speed shafts are rigidly connect and the high speed shafts are connect utilizing some type of device that can twist one shaft relative to the other shaft. As the system is set up, the entire gear system can be torsionally loaded using the twisting device independently of the drive motor. The main advantage with this type of test system is that only the lost power needs to be supplied to the test setup. The external drive system needs to be only as large as the losses in the four square setup.

The requirements of the project are such that the torsion load needs to be applied and controlled remotely, while the gears are running. The major advantages of this type of system is the loads can be varied through suitable programmable controls and the loads can be changed without shutting down the four square setup. Also, there is less wear on the four square since the loads are applied after the test rig is up to operating speed. There are several type of devices that can be used to apply the torsional load in this method. Each method was analyzed to determine

the suitability and each will be described briefly.

The first method examined uses a planetary gear set to apply the torque to the four square test setup. Figure 4 is a sketch of the this gear arrangement. Shaft 1 and shaft 2 are the shafts coming from each gear set of the four square setup. These two shafts are not directly connected and will allow one shaft to be rotated relative to the other shaft. Shaft 1 has the sun gear mounted on it and the planet carrier holding the planet gears is connected to shaft 2. The ring gear is located around the planets as in a normal planetary system. As long as the ring gear is stationary, there is a constant ratio between the two shafts. Rotating the ring gear introduces a relative twist between the two shafts. The ring gear can be accurately adjusted to give the torque required for the test.

This method was promising with only a few draw backs. The planetary is rotating at one of the connecting shaft speeds, which in this case, would be from 3000 to 5000 rpm. Also, the rotation of the ring gear that would introduce the torque into the system, had to be done while the planetary is rotating. This method was not chosen.

Another method to apply torque into the four square was to use a hydraulic rotatory actuator. The actuator uses the

water wheel principal to create the relative twist between the two shafts. A high pressure pump pushes oil through one on the rotating shafts and out between the vanes of the rotor and stator. The oil forces the vanes apart, which cause the shafts to twist. The oil pressure and size of the vanes can be adjusted to vary the amount of twist. A drawing of a typical system can be found in figure 5.

This method is an excellent method to apply torque. Using a high oil pressure the size of the actuator is relatively small and easily built into the test setup, but was also not chosen. The major problem with this type of system is the oil must be introduced through a rotating union. With shaft speeds in the 3000 to 5000 rpm range, the union becomes costly and only one manufacture was able to meet the requirements for the test setup. The torque actuator was also found to be a costly item for the torque needed for the test and the rotational speeds involved.

The next method considered involves changing one set of gears in the four square setup to an elliptical gear set. The elliptical gears are made to rotate about their geometric centers. Also, the gears would be identical, which will allow the system to be balanced. The other gear set in the four square setup would be a one to one gear set. By varying the major and minor axis of the ellipse,

the ratio between the rotation of one shaft to the other can be plotted. Figure 6 is a typical representation of one rotation of the elliptical gear set. This motion, when connected to a standard gear set, would induce a cyclical twist on the system.

The elliptical gears can be manufactured using modern CNC equipment. At first this seemed to be an acceptable method. If more than one torque level is required, a new gear set is required for each level. This would be an expensive test method. The other problem is powering the four square setup. The power required to drive these gears through the speed variations would have to be supplied by an external source, the drive motor. The other four square setups only requires a motor large enough to over come the losses in the system. This method was not chosen due to the high costs involved.

The next method that was investigated uses a magnetic clutch and two gear sets which have different ratios, which is required for the magnetic clutch to function. In this arrangement the sprag clutch is used to connect one set of shafts and the magnetic clutch is used to connect the other set of shafts. The reason for the different ratios is to have the rotor, of the magnetic clutch, connected to one shaft and the drum, of the magnetic clutch, connected to

the other shaft, to rotate at slightly different speeds. Also, the rotor is rotating inside the drum of the magnetic clutch. The controls for the magnetic clutch vary a field coil which is wrapped around the drum. As the coil is energized, magnetic lines of force from the coil flow into the drum through the rotor and back through the drum to the coil. These lines of force and the relative motion between the drum and rotor produce eddy currents in the drum. These currents create an electromagnetic force which transmits torque between the drum and rotor.

This system has several benefits and some draw backs. This system is easily controlled through the clutch controller, which controls the field coil. The device can be interfaced with a programmable controller and the cyclic type loading required is easily accomplished. The one problem with this system is the same problem as was just discussed with the elliptical gears. The power for the torque wound into the system must be supplied by an external source. The power source is the drive motor in this case.

The magnetic clutch arrangement was the method that was finally chosen. The basic equipment for this four square setup was located in storage from an old test rig designed to test roller planetary drives. The test rig was an excellent fit to the requirements of the sprag clutch test.

Chapter III

PRELIMINARY HARDWARE INSPECTION

The test rig was in relatively good shape and required some repair before modifying it for the sprag clutch test. The test rig consisted of several components that were mounted to a reinforced I-beam frame. The four square system used to Philadelphia gear increasers, which are located at each end of the I-beam frame. Between the slow speed shaft, a Louis Allis magnetic clutch was connected to one gear box and the other end was connect through a jack shaft and Lebow torque transducer to the other gear box. The high speed shafts of each gear box was connected by two jack shafts and another Lebow torque transducer.

The gear increasers have different ratios, which is required to have the magnetic clutch function as a torque applying device. One gear case has a ratio of 1.286 and 1.500 ratio on the other gear box. Both gear increasers had name plates on them and the rating of each gear box was found. The 1.500 ratio increaser was rated at 758 horsepower at a speed of 3550 rpm input and a 3.0 service factor. The other increaser was rated at 731 horsepower at an input speed of 3300 rpm and a 3.0 service factor. Both increasers have an oil circulating system, which services two functions. The first is that the system supplies oil to the gears and bearings and the second is that it filters

the oil and pumps it through a heat exchanger to cool the oil. Each gear case contains the oil sump required for the increaser.

The magnetic clutch was rated at 170 horsepower and has a maximum speed of 3490 rpm. The name plate data also listed the cooling water requirements of 3 gallons per minute and water pressure from 30 to 100 psi. The controller for the clutch was a type MC2 MOD 7.

The last item to identify are the two Lebow torque transducers. The model numbers were the same, model 1605-5K and listed the capacity at 5000 inch pounds at a maximum speed of 15000 rpm.

Before the project continued any further the test rig components had to be checked out and any storage damage repaired and tested. After the test rig was delivered, a visual check of the components indicated that water was left in the cooling systems. On the increasers, the heat exchangers were found with cracked end caps, which probably occurred when the water in them froze. Also the piping to the magnetic clutch was cracked, again frozen water was probably the cause. The magnetic clutch piping was replaced and new end caps were obtained for the heat exchangers. The heat exchangers were pressure tested in insure that the

internal tubing was not damaged. Both heat exchangers were pressurized to 100 psi and no leaks were found.

The gear increaser's inspection covers were removed to inspect the gears and bearings. The gear cases were found with oil in their sumps and the gears and bearings showed no signs of rust or damage. The increaser shafts were rotated by hand and no problems were found.
At this point, the mechanical equipment was determined to be in good shape.

The next step in the test rig check out was to couple a motor to the increaser and run the system at operating speed. Since the test design speed was set at 5000 rpm, the motor input shaft will be coupled to the slow speed shaft of the increaser. The spin test motor was an AC drive of 75 horsepower at 3600 rpm. Coupled to the 1.500 ratio gear increaser, the high speed shaft will have a speed of 5400 rpm, which is higher than design speed but for a temporary spin test the higher speed will not be a problem.

A motor base was fabricated to raise the motor to the proper height to be coupled to the slow speed shaft and a gear coupling was purchased to couple the shafts together. Electrical power was temporally hooked up to an electrical cabinet. The electrical cabinet contained the contactors

for the large drive motor, contactors for the lubrication motors on the increasers, and the control for the magnetic clutch. The drive motor was aligned to the increaser shaft and the gear coupling was bolted together. The final hook up involved the water cooling system. For a temporary test, cooling would not be a necessity, but the hook up was made to check out the entire system. The water system was connected in a series type circuit. The water enters one heat exchanger, then through the other heat exchanger, and finally through the magnetic clutch to the drain. The magnetic clutch has a solenoid controlled valve controlling the water flow and the clutch must be powered up to allow the water to flow through the system.

Once all connections were made, the initial test was to insure that the lubrication systems on the two increasers were supplying oil to the gear mesh and bearings. Removing the inspection covers allowed a visual inspection of the lubrication system, which was found in excellent condition. Next the water supply was turned on and the clutch was powered on, which opened the solenoid valve. The water flow was established at a slow rate, since a long term test was not going to be done. After these checks were made, the main drive motor was powered up. The test rig was brought up to speed and monitored for a short time before energizing the clutch. With the test rig running with no

problems, the clutch was energized to apply a torque on the four square rig. The torque, which is controlled by a potentiometer, was varied from zero to the maximum of 170 horsepower. The two Lebow transducers were not checked out since the instrumentation to operate them was unavailable.

The conclusion of the no load spin test and the loaded spin test was the entire mechanical system is fully operational. The four square rig can be modified to accept the sprag clutch test modification.

Chapter IV

EVOLUTION OF DESIGN

The preliminary design concept for the sprag clutch test unit was based on the concept of keeping the modifications on the four square rig to a minimum, and thereby holding down the cost of the hardware. Since the sprag test unit needs to run at a speed of 5000 rpm, the unit is to be placed on the high speed shaft line of the four square test rig. This shaft line initially consists of a jack shaft, connected to the Lebow transducer, and another jack shaft connecting the Lebow transducer to the other gear increaser. The only logical location for the sprag test unit was to replace one jack shaft with the test unit. The magnetic clutch is directly opposite of the longer jack shaft. The outside diameter of the magnetic clutch is large, only allowing a shaft approximately four inches in diameter to be next to the magnetic clutch. This would not allow the sprag test unit any room, since the sprag clutch outer race is expected to be six inches in diameter and that does not include any type of enclosure. The other jack shaft, on the other side of the Lebow transducer does allow more room. The only obstacle to clear is the Lebow transducer on the low speed shaft line.

The preliminary design had two main physical constraints. The first constraint is the maximum width of the sprag test

unit had to a maximum of twelve inches wide or six inches from the centerline of the sprag clutch. The other constraint is the over all length on the test unit. The length which is determined by the space between the torque transducer and the increaser shaft, is only twenty-five inches. The design concept for the sprag test unit was developed and an arrangement of the unit was drawn up. Figure 7 is the drawing of the unit. This design consisted of two separate shafts, one to be the inner race of the sprag clutch and the other to be outer race. The outer race was made as a movable sleeve that is attached to the shaft by a Ringfeder, which is a mechanical wedge type clamping collar. Each shaft is supported by a set of ball bearings that are captured in the housing by two retaining lips. A small axial clearance will allow for some thermal growth in the shaft but will support any thrust that may develope. The shafts were sealed using a commercially available labyrinth seal. The cost for this feature is higher than using a rubber lip seal, but due to the speed of the shafting the cost difference would pay off in the long term. Also the unit would need to be disassembled in order to change sprag clutches. The housing that will enclose the sprag clutch shafting is fabricated using standard steel plate and the housing is split in the horizontal plane for ease of assembly and disassembly.

This design was reviewed and was found to be acceptable, although several changes were discussed. The main disadvantage of this design was compactness of the design. Since the maximum length could only be twenty-five inches long, the bearing spans were short and the area which held the sprag clutch was very tight and would be difficult to work in. Several additional requirements were also determined to be needed after the original meetings. The sprag clutch would need to be lubricated in a similar manner as it is done in the actual transmission. The lubrication oil is supplied to the clutch through the inner race of the clutch. Therefore the test unit needs to be redesigned to allow this feature. The next problem was the test data that was planned, required electrical access to the sprag clutch area.

These changes were discussed and a revised design would need to be done. The major problem was to supply lubrication oil to the clutch as well as getting the transducer signals from the shaft. The way in which the system is designed the only access to the clutch area is through the increaser shaft and then through the inner sprag clutch shaft. The other side was not accessible due to the Lebow transducer. This unit could not be hollow bored to get access from that side. This was determined to be unacceptable since transducer readings need to be

obtained from the outer race also.

The decision to redesign was made. The new parameters added to the design requirements were as follows. The new design had to incorporate some means to lubricate the sprag clutch and electrical access to the sprag clutch area, for both the inner and outer races. A major change in the initial design considerations was also made. The Lebow torque transducer on this high speed shaft line is removed, thus allowing the sprag test unit to grow in length. Also the other long jack shaft will be replaced depending on the final length of the sprag test unit. The torque transducer which is being removed will be replaced by a strain gage torque transducer built into the new jack shaft. The new design was then developed.

The second design was completed and figure 8 is the arrangement of this design. The design was similar to the previous design but several new features were added. The bearing arrangement was still the same as before except the bearing span was larger than before. On this design the bearings were all the same, which will minimize the number of spares to be on hand. The area where the sprag clutch is located was increased in length to allow easier access to the clutch. The clutch area, inner and outer races, were redesigned to simulate the actual configuration of the

shafting in the transmission. The space between the two shafts was increased, which will enable the sprag clutch to be changed without total disassembly of the test unit housing.

The oil lubricating system was also revised. The oil supply for the sprag clutch will be done through the use of two lubricating collars. These collars, which consist of an outer ring of steel and two inner rings of bronze, will ride on the shafts and oil will be pumped into the center cavity of the bronze. The collars will act as a free floating non-rotating sleeve bearing. The two shafts are to have several cross drilled and rifle drilled holes that will pipe the oil to the clutch area. Two dams on the inner chamber walls were added to impede any oil flow that may come from the inner shaft bearings.

The two shafts were rifle drilled to allow access for the various instrumentation connections as required by the test. On the shaft that holds the outer race tube, a groove was added to this shaft for alignment of the sprag clutch to the inner race. The long jack shaft was also replaced with a rifle drilled shaft and a small area necked down for the strain gage torque transducer. Figure 25 is a plan view of the new layout of the four square rig.

The design review committee was assembled to review the new design. The design was accepted, since it covered the revised design criteria. The design was being scrutinized for the cost of replacing parts damaged due to a catastrophic failure of a sprag clutch. The outer race, which is the tube shaped part, was acceptable since the remaining part of the shaft would be undamaged. The inner race shaft was the item that needed to be redesigned. A failure of the sprag clutch would destroy the inner race portion and since it is integral with the remaining part of the shaft, the whole shaft must be replaced. Another change was requested for the outer race tube. The wall thickness was duplicated from the actual part geometry, but for the initial tests, the wall will be doubled in thickness. This part can be turned down during later tests if required. Four radial tapped holes were added to the outer race tube. This will add the ability to meter the oil flow out of the inner cavity. The oil lubrication holes that run through the shafts will be changed to end in a tapped hole. This will allow for special orifice set screws to be used to adjust the flow into the sprag clutch. The design was then revised with the new parameters.

The third and final design was again brought before the design review committee. The new design required some major changes to the sprag clutch shafts. Figure 22 is the

arrangement of the final design. Two significant changes can be seen when comparing this design to the previous design.

The first change was a redesign of the inner race shaft. The end of the shaft was changed to include a flange area. This flange inner race portion is now the replaceable unit that was requested by the review committee. The flange area is specially design with two body fitted bolts. These bolts perform two functions, the first is to carry the torsional load and the second is to align the oil lubrication holes between the two parts. The joint is designed with two o-rings on the flange face to seal the oil from penetrating the pilot area and entering the rifle drilled hole in the center of the shaft. The flange area also has six other bolts clamping the joint together. This will add to the torsional holding ability of the body fitted bolts by the frictional forces developed between the two parts.

The other major revision involves the bearing and housing locking arrangement. The housing up to this point was design to be entirely symmetrical, which would enable the shaft assemblies to be swapped. This feature allows for other type of sprag clutches to installed into this test rig. Therefore the changes on one shaft are copied to the other shaft for the sake of symmetry. The inner race shaft

required a new bearing arrangement, since the large flange was added to the end. The bearing assembly on the previous shaft could be done from either end, because the bearing bores were larger than the shaft ends. With the large flange, a large bore bearing is required to clear this diameter. This in turn would cause clearance problems for fitting the sprag clutch test unit onto the existing four square rig and the larger bearing would reach the operating limits of the bearing. Due to these problems, the bearing design was changed to have a one ended assembly. The inner bearing would now require a lock nut to secure it to the shaft and the outer bearing was changed since the backing shoulder for the bearing had to be less than the bearing bore of the inner bearing.

With these changes and the other minor changes requested from the last review, the design of the sprag clutch test unit was accepted. The entire engineered package was released to manufacture the test unit.

Several other items were also designed along with the test unit. The test unit had to be attached to the I-beam frame of the four square rig. The method that was chosen, required a support plate that is bolted and pinned to the I-beam frame. On this plate, pads are welded and tapped to accept the bolting pattern from the sprag clutch test unit.

After the shafts are properly aligned, this unit can also be pinned in place.

The other item that was designed is a motor stand. This is required to raise the motor to the correct height so it can be coupled to the gear increasers slow speed shaft. This stand was not built. A change in the motor specifications required a v-belt pulley system to be added. The motor was no longer required to be at the same height as the increaser shafts. A commercially adjustable motor base plate was used to secure the motor to the floor plate and tension the v-belts.

As the project was reviewed by the fabrication shop, several requested were made to change the housing design. The original housing was designed using current industry practice. The design took into consideration the cost of materials, fabrication, and machining. The order listed is from least to most expensive process. The test unit was issued to NASA machine shop for building and the cost of fabrication and machining is the same. Therefore the housing design was changed to minimize the cost of producing it. The changes reduced the number of plate sizes as well as the number of pieces to be welded together. Another change was made per their request to line bore the bearing bores in the housing to the largest diameter and

eliminate the counter bore on the inner walls. These changes were all done. The elimination of the inner counter bore required a redesign of the inner oil dam to make it an inner retainer plate and oil dam. Also the outer bearing required a bearing sleeve to be designed to reduce the bore back down to the smaller size required. After these changes no other changes were requested and the design was manufactured.

Chapter V

DESIGN CALCULATIONS

The four square test rig had to be designed or the existing hardware had to be analyzed to insure that the rig is safe to run. Therefore the mechanical components were checked out and the base load for the analysis was based on a service factor 1.0 rating on the motor, which is 200 horsepower at the input speed of 3333 rpm or 5000 rpm at the sprag clutch. From figure 25, the input is into the low speed shaft of the gear box on the left. The ratio in this increaser is 1.500, which will run the high speed shaft at a speed of 5000 rpm, the design speed of the test rig.

The primary area that was analyzed was the gear sets in the two gear boxes. The gears were rated using the American Gear Manufactures Associations rating practice for high speed gear boxes, which is AGMA 421.06 standard. The results of the calculations are listed in figures 32A and 32B for the 1.500 ratio gear box and figures 32C and 32D for the 1.2857 ratio gear box. The safety factor for the gear boxes are 16.21 and 18.4 respectively. The bearings for the geared shafts were also analyzed using the procedure from the Timken Company design manual. The AGMA standard for gear increasers requires the bearings to have a minimum life of at least 5000 hours of B-10 life. Both gear cases utilize the same bearings on the high and low

speed shafts. The life calculations, figures 33A, 33B, 33C, and 33D, were done and in all cases the bearing lives exceeded the requirement by more than 100 times.

The other bearings that were analyzed are the roller bearings used in the test rig. The shafts are subjected to only torsional loads, therefore the only load on these bearings is due to the weight of the shafts. The life calculations, figure 34, shows that the bearing life is over 100000 hours of life, which is more than 20 times the minimum required in the gear boxes.

The four square components are all connected by commercially available gear tooth couplings. The rig uses three different sizes, sizes 1.5W, 2.0W, and 2.5W. Using the deign guide from the manufacture, the maximum speed for each size was checked to insure that no coupling exceeds the maximum value. The couplings maximum speed are 6500, 5600, and 5000 rpm respectively. The coupling torque ratings was also checked and the following list was complied.

Coupling Torque Capacity

Size	3333 rpm	3888 rpm	5000 rpm
1.5W	899 hp	1049 hp	1350 hp
2.0W	1666 hp	1944 hp	2500 hp
2.5W	2999 hp	3499 hp	4500 hp

The minimum safety factor, 4.49, was calculated from the above list. The other area to check on the couplings is the torsional holding capacity of the shaft to coupling fit. The couplings were designed to have a slip fit to a metal to metal type fit to allow ease of assembly and the results of the analysis is listed in figure 35. From the analysis the minimum safety factor was found to be 2.57 and figure 36 is a typical printout of the analysis of the press fit and key on the couplings.

The two other areas that require a torsional holding ability is the flange connection that attaches the inner sprag race to the test rig shaft and the Ringfeder connection between the outer sprag race to the test rig shaft. The Ringfeder, which is a mechanical crimping device, is used to hold the outer race to the test rig shaft. The analysis was done by the application department of the Ringfeder Corporation, since the rotational speed required them to analyze the application. The torsional holding capacity from their analysis, which are based on the dimensions of the various parts, was found to be 5180 foot-pounds. The safety factor is 24.6 based on the 200 horsepower load. The flange connection has two body fitted bolts, which are used as the primary torsional transmitting component. The load that these bolts can carry is 2760

foot-pounds. This is based on using grade 8 bolts, 3/8 diameter, with a shear strength of 60000 psi, on a 2.50 radius. The safety factor is 13.1 based on the 200 horsepower load.

The shafting on the test rig was checked and the highest stressed areas were located on each shaft line. The low speed shaft line has the smallest diameter on the jack shaft between the Lebow load cell and the magnetic clutch. The diameter of this section is 1.375 inches and the material is heat treated to 180 brinell. The torsion stress on this shaft is 6351 psi and with a torsion yield stress of 31000 psi. The safety factor is 4.88 On the high speed shaft line the smallest area is located on the jack shaft and is the area where the gages will be located. The shaft diameter is 1.118 inches and the shaft has an inner diameter of 0.50 inches. This shaft is also heat treated to 330 brinell and has a torsion yield stress of 49000 psi. The torsion stress on this shaft is 9570 psi, which computes to a safety factor of 5.12

The shafts were also checked for their critical speed by using Rayleigh's method. Each shaft was analyzed using a deflection program that develops the deflection of the shaft based on shaft weight plus any external loads that may be present. With the deflections and the weight of each

section calculated, the critical speed of each shaft was computed. The following list are the first natural speed of the various shafts in the four square rig.

Low speed increaser shaft	93917 rpm
Low speed jack shaft	4831 rpm
Low speed increaser shaft	139419 rpm
High speed increaser shaft	29459 rpm
High speed jack shaft	11172 rpm
Test rig outer race shaft	103447 rpm
Test rig inner race shaft	93220 rpm
High speed increaser shaft	26632 rpm

From this list, the only shaft of concern is the low speed jack shaft. The maximum speed that this shaft will see is 3888 rpm, which is 24% lower than the first critical speed.

The next requirement was to examine the gears, outer sprag clutch race, and inner clutch race flange connection for centrifugal stresses and the bursting velocity of the parts can be determined. The tensile strength of the pinions is 47100 psi, for the gears it is 50400 psi, and for the flange and outer race of the sprag clutch it is 85000 psi. Using these values the maximum velocity of the various items can be found. They are respectively 686 fps, 709 fps, and 921 fps. The pinions and gears in the two gear boxes have different diameters. The maximum speed for the pinions is found by using the largest diameter of the two. The

largest diameter is 9.6289 inches and the maximum speed is 16327 rpm. The same procedure is done for the gears and the maximum speed is 12577 rpm. The maximum speed for the flange and outer race is 35179 rpm. The minimum safety factor for this calculation is 3.26, based on the design speed of 5000 rpm on the high speed shaft and 3888 rpm on the low speed shaft.

The magnetic clutch is a commercial item that was manufactured by Louis Allis. The catalog rating for the clutch is 3120 inch-pounds at a maximum output speed of 3490 rpm. This is equivalent to 170 horsepower. Since the input speed to the gear increaser is 3333 rpm, this is also the output speed of the clutch because the motor drives directly into the output side of the clutch. The only other requirement is for the input shaft to be at least 35 rpm faster than the output. The input shaft which is driven through the other increaser runs at a speed of 3888 rpm. The magnetic clutch is the torque limiter for the four square rig, since the maximum torque that can be locked into the rig is 3120 inch-pounds. This results in a safety factor over the motor horsepower of 1.17

The Lebow torque and speed transducer is located in the low speed shaft line, which runs at a speed of 3888 rpm. The load cell is rated at 5000 inch-pounds with a maximum speed

of 15000 rpm. This results in a safety factor of 3.85 on speed and 1.54 on the motor load of 200 horsepower.

The last concern was the containment of fragments should any of the rotating elements fail. The major elements analyzed were the drive belt shield, the two increaser gear boxes, and the test rig that housed the sprag clutch. All of these rotating elements were encased using a low carbon steel. The gear increasers were analyzed assuming two different modes of failure. The first is the failure of a portion of a tooth to a whole tooth. The safety factor to contain this mode of failure is 5.2 The second mode of failure would be if the rim of a gear would break off and the analysis was based on any one piece having 25% of the total energy of the blank. A 2.21 factor of safety for containment was calculated for this mode.

The next major area was the sprag clutch inner and outer races. For this analyses the entire energy of the inner and outer race was used to determine if the housing would contain a failure. A minimum safety factor of 2.35 was determined for a failure in this unit. The final analysis was done on the drive belt systems enclosure. For this analysis the belts energy was used to determine if the enclosure was sufficient to contain a failure. A 9.05 factor of safety was calculated for this area.

In conclusion, the four square test rig does meet the requirement of a 1.50 minimum safety factor. The rig is over designed due to two effects. The first is the four square rig, less the test rig, was available from a previous test, which allowed for project funds to be redirected into other areas of the rig. The other effect is the physical size of the mechanical components and the requirements for the lubrication and instrumentation resulted in safety factors higher than required. The four square rig was approved by the NASA safety committee and was given a safety permit.

Chapter VI

ASSEMBLY INSTRUCTIONS

The sprag clutch test unit and the entire four square rig is to be assembled in a test cell at NASA Lewis Research Center. The assembly will be conducted by the engineers and technicians at NASA. The following text was compiled to provide instructions for the assembly of the test unit and the assembly of test unit to the I-beam frame. The following instructions are divided into two parts. The first part is work that had to be preformed before the test unit could be assembled to the four square rig. The preliminary work also prepares the rig for later assembly work. The second part is the instructions to assemble the test rig, install the instrumentation, and assemble it to the four square rig.

Part 1: Preliminary Assembly

The following work can be done before obtaining the new parts for the test rig. The order in which the work is done, does not have to be followed exactly but hopefully it is a logical approach.

1) Remove the coupling on the gear box shaft, ratio 1.5, which is opposite the Louis Allis Magnetic Clutch. This coupling and key will not be reused.

2) Remove all bolts on all four couplings between the two gear boxes, this is the shaft line opposite the clutch shaft line. This shaft line consists of a floating shaft, the Lebow transducer, and another smaller floating shaft. The bolts for the large coupling size 2.0W will be used and two sets of bolts for the size 1.5W will be used. One set of bolts for the size 1.5W will not be reused.

3) On the first floating shaft (2" diameter), there is a Waldron 2.0W flex coupling and a Waldron 1.5W flex coupling on either end. Press these two couplings off and save the couplings only. The keys and the shaft must be discarded. These couplings will be used and need to be altered per drawing C-88-9-14-5-C.

4) The other floating shaft (1.375" diameter) will not be used and can be discarded.

5) Remove the Lebow Transducer from it's pedestal and remove the couplings. The keys and the transducer are not to be used. The rigid coupling half will be used and must be altered per drawing C-88-9-14-5-D and the flex half needs to be altered per drawing C-88-9-14-5-C.

6) Remove the transducer stand, which the Lebow transducer from step 5 was mounted on. This will not be used and it is

discarded.

7) On both gear boxes disconnect the union that connects the lubrication pump and filter from all the piping on the top half of the gear boxes. This will allow the top half of the gear case to be removed without disassembling the entire lubrication system.

8) On both gear boxes remove all bearing screws and all flange bolts that secure the top of the gear case to the bottom of the gear case.

9) Carefully remove the top half of both gear cases.

10) Carefully remove the input shaft pinion from both gear boxes. These shafts must be altered per drawing C-88-9-14-8-C, which calls for the shafts to be rifled drilled. All bearings, retainer plates and couplings must be removed to avoid damage to these elements when it is machined. PLEASE TAG all parts so they can be replaced to the same shaft and place on these parts.

11) If the shaft seals for these shafts are damaged, they must be ordered to be able to replace them when reassembly is done.

12) Cover the open gear cases so dirt or other foreign material does not get into the gear cases.

Part 2: Assembly Instruction for The Test Rig

Inspect all parts to be assured all tolerances have been obtained. All parts should be properly deburred and all metal chips removed from all drilled holes especially the shaft cross drilled and thur holes. At this point several sub-assemblies can be done. These sub-assemblies must be done in order and must be completed before final assembly of the test rig. The numbers given for each part listed in the instructions is the bill of material number. The bill of material can be used to obtain the drawing number of each part. For the test rig, the assembly drawing, C-88-9-14-12, can be used as a quick reference for bill of material numbers and the any part in question. The drawings and bill of material can be located on figures 11 through 30.

Inner Clutch Shaft Assembly

1) Clean and degrease the 6 inch flange area on the shaft, BOM number 17, and the 6 inch flange area on the clutch inner race part, BOM number 46.

2) Locate the o-rings, BOM numbers 50 and 51, as well as the six flange bolts, BOM number 48, and the two body fitted bolts and nuts, BOM number 47.

3) The heads of these bolts must be drilled so after assembly they can be wired together to prevent them from loosening during the operation of the test rig.

4) The two flange parts can now be assembled. First place the o-rings in their appropriate grooves. This area can be greased to hold the o-rings in place if need be. The flange area should be totally degreased. With the o-rings in place the flanges can be joined. Line up the two body fitted holes and put the body fitted bolts into these holes. The remaining six bolts can be screwed into the holes. The 3/8 inch bolts should be torqued to 37.1 foot-pounds and the 3/8 inch body fitted bolts should be torqued to 29.5 foot-pounds. These bolts must be wired together to prevent loosening.

Shaft Assemblies

Both shafts have identical bearing assemblies so this procedure must be done for each test rig shaft.

1) The bearings for these shafts must be heated before they

are assembled to the shafts. Remove the bearings from their protective wrappings and heat them in an oil bath or a quartz type oven to about 200 degrees fahrenheit.

2) While the bearings are heating, the two shafts are placed so the keyed shaft end is straight up.

3) After the bearings are at the proper temperature, the inner bearings, BOM number 5 can be put on the shafts.

4) The Speith locknut, BOM number 45, can be put on the shaft to lock this bearing in place. After the bearing is cooled to room temperature, the locknut is tightened using a spanner wrench and the face bolts must be tightened to lock the nut in place. These bolts should be torqued to 75 inch-pounds.

5) The next part to put on these shafts is the lubricating collar, BOM number 7. The lubricating collar has a bronze inner sleeve. This sleeve must be oiled before assembly. Also apply a coat of oil to the shaft on the shaft diameter from the locknut to the tapered section near the end of the shaft. This will help prevent damage to the bronze sleeve during assembly. After these parts are oiled, carefully slide the lubricating collars onto the shafts. They are symmetrical so they can be place on the shaft either side

first.

6) The other bearing, BOM number 6, can now be assembled to the shaft. After the bearing is cooled down, locate the outer bearing sleeve, BOM number 56. This part should slide over the bearing's outer race. The flange end should be on the keyed shaft extension end.

7) These shafts can be placed aside for later final assembly.

Housing Sub-Assembly

1) Locate the two inner retainer plates dams, BOM number 16, and saw cut the retainer plates in half per the blueprint, if they have not already been cut.

2) Locate the 3/8 - 16 bolts with drilled heads, BOM number 25, and bolt the inner retainer plate in place. These bolts must be wired together to prevent them from loosening during operation of the test rig.

3) The two locking screws, BOM number 9, can now be threaded into the top of the housing. They should be torqued to a value of 90.5 foot-pounds.

4) The internal lube system can now be put into the box. The schematic for the lube system is shown on drawing C-88-9-14-11. For lubricating the bearings on each side, come out of one 3/8 inch NPT port in the housing wall with a short nipple. Next a tee can be added to the nipple. From this tee, each side will run to the bearing using tubing. At the end of this tubing, place an orifice that will spray into the bearing. The shaft assemblies can be used to adjust the orifice location. These lubrication parts should be securely attached to the inner walls with clamps and screws.

5) Using one shaft as an assembly aid, position the lubricating collar to straddle the cross drilled holes in the shaft. Now measure the length of hose required to go from the other 3/8 inch port to the bottom of the collar. Note that the taped hole in this collar must point toward the bottom of the shaft. The length should be long enough to allow for one coil of hose to sit on the bottom of the housing. The reason for the coil of hose is to eliminate any side loads on the collar. Once the length of hose is known, cut two pieces of hose. On one end of the hose attach a fitting to go to a 3/8 inch NPT and this end will be threaded into the lubricating collar. The other end should have a male end of a quick disconnect coupling. The female end is attached to the 3/8 inch NPT port in the

housing wall.

6) Clean the housing of all metal chips and debris.

Bearing Adjustment

1) Clean the housing splits to remove all dirt and remove any sharp edges that may be on this split. The o-ring for the split will not be required for this procedure.

2) Place the two shaft assemblies into the housing. With the inspection opening, in the bottom of the housing facing you, the flange shaft will be on the right side and the non-flange shaft will be on the left side. The lubricating collars must be centered over the cross drilled holes on each shaft and the blind hole, located 180 degrees from the hose connection, must point straight up.

3) The top half of the housing can now be place on the bottom half. The proper orientation should be to have the face and split side pins all lined up. With the top in it's proper position, carefully lower the housing, but make sure the locking screws are lining up with the lubricating collar's holes. The 1 inch NPT ports, in the top of the housing, can be used to aid in the alignment of these parts.

4) With the top of the housing in place, locate the 26 bearing boss screws, BOM number 26, and hand tighten these in the appropriate holes.

5) Using a lead hammer, carefully tap the ends of the two shafts inward to seat the inner bearing on the shoulder in the housing. Repeat this several times to assure that the bearing are seated properly.

6) The 26 bearing boss screws can now be torqued down. These bolts should be torqued to 90.5 foot-pounds.

7) The bearing retainer plates, BOM number 15, and the bearing retainer plate screws, BOM number 23, must be located. Place the retainer plate on the end of the shaft and slide it into place on the housing. Line up the holes and hand tighten the bolts in place. Using a wrench snug these bolts tight, DO NOT torque these bolts down. Repeat this procedure for the other side of the test rig.

8) The retainer plates were designed so there will be a gap between the housing face and the retainer plate. Using feeler gages, make sure the retainer plates are parallel to the housing face.

9) Measure the gage between the housing face and the retainer plates. Match mark the housing and the retainer plate to make sure the retainer plates are returned to the proper side.

10) Remove the retainer plates from the housing. The retainer plates will need to be machined to obtain the proper clearances in the bearings. The amount of material to remove from the hub of the retainer plate will be the value measured using the feeler gage, add to this value .010 inches, then subtract the thickness of a paper gasket material. Each side must be done using this method, separately, since the feeler gage readings may be different.

Retainer Plate Assembly

1) Locate the retainer plates that have been machined for proper bearing clearances, BOM number 15, and the Inpro Seal, BOM number 4. The only part of the Inpro Seal needed is the stator or outer ring of the seal.

2) Clean and degrease all parts. If the Inpro Seal was shipped with a stator o-ring it must be discarded since it will not be required.

3) The stator half of the Inpro Seal needs to be cooled down to insert it into the retainer plate. This can be done using dry ice or liquid nitrogen. After the stator is cooled down, these parts can be assembled. The stator will drop into the pilot bore in the retainer plate.

4) Place these parts aside and allow them to come up to room temperature.

Clutch Sleeve Assembly

1) Two parts and one sub assembly are required for this section. The parts are the clutch sleeve, BOM number 11, the Ringfader shrink disc, BOM number 9, and the non-flange shaft subassembly.

2) The first step is to check the Ringfader. If it is assembled then jump to the next step but if it is not assembled it must be put together. Take the ring that is threaded and place it on a table. Next put the internal wedged ring on to the threaded ring. The o-ring is put on the face of the threaded ring and the other ring can now be placed on the o-ring. Using three bolts equally spaced, hand tighten the shrink disc together. The remaining bolts can then be hand tightened into the remaining holes. This assembly can now be moved.

3) The Ringfader shrink disc can now be assembled on to the clutch sleeve. The bolts of the shrink disc will be facing out.

4) The shaft sub-assembly can be inserted into the clutch sleeve. Insert about three inches of shaft into the sleeve. With the sleeve at this location, start tightening the shrink disc bolts. Refer to the instruction sheet received with the shrink disc for the proper order. If no instructions are found, the bolts must be tightened in a rotating star pattern. The bolts need not be torqued to the maximum value. They only need to be tightened until the sleeve grips the shaft and will not move.

Clutch Lubrication Orifice Installation

The final lubrication of the clutch is controlled by the installation of twelve set screws, BOM number 49. Depending on the test that may be run these set screws may be altered to vary the flow of lubricant to the clutch. The four set screws are placed in the end of each shaft and four set screws are located in the clutch collar sleeve. The reason for the lube orifices in the flange shaft is to lubricate the clutch through the inner race, which is accomplished by small holes that are place in this part. The lube orifices

in the other shaft will allow lubricant to flow through the clutch in an axial direction. The lube orifices in the clutch collar can be used to control the lubricant that is trapped in the inner cavity.

Thermocouple Installation

With all the mechanical sub-assembly done, the thermocouples that are required to monitor the clutch must be installed. The thermocouple wires should be long enough to go through the shaft and through the gear increaser shafts to the slip rings on the ends of the shafts. The wires are to be feed through the hole in the center of the shafts. At the clutch end of each shaft, the center drilled hole is threaded to allow for some type of fitting to prevent the lubricant from going through the shafts.

Jack Shaft and Torsional Load Transducer

1) Locate the jack shaft, BOM number 31, and thoroughly clean out the through hole and the two cross drilled holes. Using needle files remove any burrs that occurred at the intersection of the through hole and cross drilled holes.

2) The next step is to install the torsional gages to the shaft to make the load cell. Two complete bridges will be

installed. One will be a spare, if the active bridge is damaged the backup can easily be switched over to.

3) The necked down portion is where the gages will be installed. This area has been polished and should not require any sanding. Using the appropriate layout tools, a circumferential line should be lightly scribed on this section half way between the two shoulders. Next four equally spaced axial lines need to be lightly scribed on this section.

4) After the layout of these lines, clean the area with the conditioner solution. Wipe this area dry and use the neutralizer over this same area. Again wipe the area dry.

5) Remove one gage from the strain gage package, BOM number 44, and place the gage on a clean glass plate. Using mylar tape, place a long piece of tape over the gage. Carefully peel the tape back. The gage will be attached to the tape. Using the tape, align the gage with a set of cross lines on the shaft. Repeat this for the remaining three cross lines.

6) Locate two pieces of terminal strips with four terminals on the strip. Using mylar tape, place the terminal strip in front of each hole that was cross drilled through the shaft.

7) With all gages and terminal strips in place, carefully peel back each item and clean the back of them using the neutralizer solution.

8) These gages and terminal strips will be glued to the shaft using M-Bond 610 adhesive. Follow the instructions for mixing the adhesive and prepare a batch. Apply the adhesive to the back of each gage, the terminal strips, and the areas of the shaft where these items will be. Following the instructions, the adhesive must be allowed to air dry before continuing.

9) Carefully put the gages and terminal strips down on to the shaft, using the tape to hold them in place. Wrap this area with a piece of teflon sheet and use the mylar tape to hold it in place. Next cut a piece of silicone gum to cover this area, again use the mylar tape to hold it in place. The final step is to locate some flexible metal strips and place these over the gages and terminal strips. A hose type clamp is put over the metal and tightened to put a slight compressive load on this area, about 40 to 50 psi.

10) The entire shaft must be placed in a temperature controlled oven set at 350 degree fahrenheit. The time to cure the adhesive is one hour after the shaft is up to the 350 degree temperature.

11) After the shaft is removed and allowed to cool down to room temperature, the gage area is stripped down. Remove the clamps, metal strips, silicone gum, teflon tape and the mylar tape that is over the gages. Using an eraser from a pencil, carefully clean all terminal areas on the gages and terminal strips. Do not rub the eraser over the gages, this may damage them.

12) Using figure 31, the gages must be wired. The thin wires are glued to the shaft using M-Coat B. There will be two complete bridges on this shaft. The gages that are 180 degrees apart complete one bridge.

13) After the bridges are fully connected to the terminal strips, the bridge must be checked out. Using an ohm meter the following readings are found if the bridge is operating properly. Across the corners of the bridge, the meter should read 350 ohms and across any gage, the reading should be 262.5 ohms. The last check should be for a ground circuit between any terminal strip and the shaft. This should be an open circuit.

14) If both bridges check out, the lead wires can be connected up. Cut two pieces of four conductor wire with a shield at least 3 feet long, since the wires must be feed

through the increaser pinion shaft to the slip rings. Feed the wires through the cross drilled holes and out the nearest end of the shaft. Once this is completed connect the wires as shown on figure 31, repeat this procedure for the other terminal strip. The cross drilled holes must be filled with a silicone type caulk to secure the wires in place.

15) The bridge can now be connected up to a strain indicator and the bridge is balanced. After setting the gain on the instrument to a high value, twist the shaft by hand. If the bridge is operational the reading on the instrument will move and reversing the twisting will reverse the sign on the reading.

16) If both bridges check out, the entire area can be coated with M-Coat A. This is be done several times to build up a thick coating. Following this the entire area can be coated with a RTV type silicone to aid in protecting the gaged area.

17) A coupling is assembled on both ends of the torque shaft, which will complete this assembly. The larger flex coupling, BOM number 41, will be put on the short end of the shaft, closest to the strained gaged area and the end with the wires. The small rigid coupling, BOM number 40,

will be put on the long end of the shaft. Both couplings require keys, BOM number 17, and set screws, BOM number 30. The couplings should slide onto the shaft and are flush with the ends of the shaft. Tighten the set screws in place.

Final Test Rig Assembly

After all the sub-assemblies are done, the test rig can now be assembled. During this assembly the sprag clutch can be installed if desired or it is installed after the rig is put together.

1) The bottom half of the housing must be prepared for the final assembly. The first step is to make sure the housing is free from all dirt or any other foreign material. With the bottom housing inspection opening face you, obtain the o-ring material, BOM number 21, and cut the required lengths to create the split seal.

2) The shaft, with the clutch sleeve, is put into the housing. The radial pin in the outer bore must be lined up with one of the holes in the bearing sleeve. This shaft goes on the left side of the housing. The quick connect coupling for the lubrication collar is connected on the inside of the housing. The Ringfader shrink disc bolts are

be loosened to allow the sleeve to slide on the shaft. After it is free to slide, move the clutch sleeve to the left, the reason for this is to allow the other shaft enough room to be placed into the housing. Care must be exercised to insure that any thermocouples are not damaged.

3) The shaft, with the flange, is placed into the housing on the right side. The radial pin in the outer bore must be lined up with one of the holes in the bearing sleeve. The lubrication collar on this side should also be connected to the coupling inside the housing.

4) The next step is to install the sprag clutch. The reason is to check out the shaft alignment. After the checkout, the sprag clutch can be removed until the test rig housing is mounted to the I-beam frame. The sprag clutch should slide into the clutch sleeve on the left side of the housing. Next the snap ring, BOM number 13, is installed to hold the clutch in place. The entire clutch sleeve and Ringfader shrink disc slides to the right and the sprag clutch will slide over the shaft on the right. The shaft on the left has a groove in it and the sleeve's proper position is to have the entire groove showing. This will position the sprag clutch over the inner race. The clutch can be removed if all checks are completed.

5) The top half of the housing is lowered into place. The face pins are used to align the housing and the lubricating collars must be aligned with the locking bolts in the top of the housing. The bearing boss screws, BOM number 26, are screwed in place. At this point only hand tight.

6) The retainer plate assembly and retainer plate screws must be located. The retainer plates were match marked and must be put on the correct side of the housing. Remember to put the paper gasket on the shaft before sliding the retainer plate on. The retainer plate screws should be snugged up to align the housing and seat the bearings. After this has been done, loosen the retainer plate bolts, but do not remove them from the housing.

7) The bearing boss screws and the flange screws can now be torqued down. The bearing boss screws should be torqued to 90.5 foot-pounds. Finally the retainer plate screws should be torqued to 37.1 foot-pounds.

8) The rotor half of the Inpro seal can installed on each shaft end. To help in the installation a light coat of oil can be applied to the shaft ends. The rotor half has an inner o-ring that will secure it to the shaft. The rotor half is put on the shaft and pushed up until it is flush with the stator half of the seal. The rotor half of the

seal should back off from the stator half by 0.002 to 0.005 inches.

9) The gear couplings, BOM number 19, and keys, BOM number 17, must be located. These couplings are two couplings that were reworked previously. First put the keys in the keyways on the shafts. Then place the coupling sleeve on the shaft. The inner coupling hub can be placed on the end of the shafts and the set screws, BOM number 18, can be tightened into place. The gear teeth on the coupling hub must be greased with a coupling grease and the coupling sleeve is pulled into place.

10) The inspection plate, BOM number 20, the inspection plate screws, BOM number 24, and the o-ring material, BOM number 21, must be located. The o-ring is cut to size for each plate and can be held in place with some grease. The inspection plates can be installed on the housing. These screws should be torqued to 37.1 foot-pounds.

11) The support plate, BOM number 2, is placed on the I-beam frame to check alignment of the holes in the plate to the tapped holes in the I-beam frame. If the holes need to be opened up due to any misalignment, it must be done before continuing.

12) The support plate, BOM number 2, is bolted to the I-beam frame. Using a plumb line from the center of the increaser shaft, line up the centerline of the tapped holes in the support plate and using five one inch bolts, bolt the support plate to the I-beam frame. These bolts should be torqued to 709.0 foot-pounds.

13) Finally all the NPT ports must be plugged using pipe plugs, BOM numbers 53 and 54. The entire test rig is sealed and is ready to be connected to the I-beam frame.

Final Assembly to I-Beam Frame

For the final assembly of the four square rig, there are two main sub-assemblies needed, the test rig and the jack shaft torque transducer.

1) The first step is to locate 0.06 shim that will be put under the bolts of the test rig. These will be used to get the first adjustment on the height alignment of the test rig.

2) The test rig can be lifted with a crane and the bottom of the unit must be cleaned and stoned to remove any nicks or burrs. The inspection plate on the front of the unit must be facing toward you. Carefully move the test rig over

the support plate and feed the wires through the increaser shaft on the right side. At this point lower the test rig onto the support plate but do not remove all the tension from the crane. The test rig should be able to move by pushing on the rig. Move the test rig to pull the side away from the increaser gear box out.

3) The jack shaft must be located and while holding the shaft the wires from the torque transducer is on your left. The wires coming out of the test rig on the left side are feed through the jack shaft. With all the wires coming out of the left side of the jack shaft carefully feed these wires through the increaser pinion shaft on the other side. These two sub-assemblies should be kinked in between them.

4) Carefully slide the test rig and jack shaft in toward the center of the I-beam structure and at the same time keeping tension on the wires coming out of each increaser. After the jack shaft and test rig are in line with the increaser shafts, put bolts in couplings to hold the jack shaft in place and put the base bolts, BOM number 22, into the holes. All these bolts should only be hand tight. The gasket between the flanges of the couplings should be in place before the bolts are put in place.

5) The test rig must be aligned with the increaser shaft.

The alignment on height can be done using shims under the test rig. The sleeves on the couplings joining the increaser to the test rig must be pulled back. Using a straight edge on the two coupling hubs, move the test rig until the rig is center and adjust the shims to move the test rig up and down. The maximum misalignment is 0.005 inches. The other adjustment is the gap between the coupling, which should be 0.125 inches, and the angular alignment, which should not exceed 0.005 inches. This can be checked by using feeler gages to measure the gap between the top of the coupling and the bottom of the coupling. If there is any difference between the readings, shim is added to the front end of the test rig or the rear of the test rig depending on the movement required.

6) With the test rig aligned, tighten the base bolts to lock the test rig in place. These bolts should be torqued to 90.5 foot-pounds. Recheck the alignment of the test rig to the increaser and if realignment is necessary repeat the procedure to align the couplings. When the box is aligned, the test rig should be dowel pined to the support plate and the support plate should be doweled to the I-beam frame. Each must be pined in at least two places this will eliminate the need for future alignment if the test rig needs to be removed.

7) At this point the coupling bolts should be torqued to their required values. The size 1015 bolts should be torqued to 31 foot-pounds and the size 1020 bolts should be torqued to 75 foot-pounds. These couplings should also be pumped full of coupling grease using the fittings in the sleeves of the couplings.

8) The slip ring adapters, BOM numbers 28 and 32, set screws, BOM number 30, and the slip ring adaptor keys, BOM number 29 and 33, can now be assembled to the ends of the increaser shafts. The wires coming out of the end of the shaft are feed through the adapters and the adapters should slide onto the ends of the shafts. Each shaft has a different diameter and the appropriate adaptor must be found for each side. With the key in place the set screws are tightened in place. Next the slip rings, BOM number 42, are screwed to the adaptor using the socket head screws, BOM number 43. The wires can be divided into two equal numbers and laid into the milled slot under the slip ring counter bore. These wires can then be cut to the appropriate lengths and soldered to the terminals on the slip ring base.

9) The entire I-beam frame must be bolted to the floor plate. There are several holes in the frame that can be used as well as finger clamps can be used.

10) The lubrication system must be connected to the test rig. Refer to drawing C-88-9-14-11 for the schematic of the lubrication system, which shows the various connections to the test rig. The return oil drain line can be connected to any one of the four one inch NPT drain holes in the bottom of the test rig housing. Also the water lines to the increaser heat exchangers and the magnetic clutch must be connected to the inlet ports and the returns should also be piped, if this work has not been done.

11) The drive system can be installed. First the two pulleys are installed. The smaller of the two is placed on the increaser shaft and the larger one will be placed onto the motor shaft. The motor can be placed onto the motor base plate and bolted in place. This motor and base plate assembly should then be lined up with the pulley on the increaser shaft and should be on the side away from the slip ring assembly. The drive belts can be put on the two pulleys and they can be used to align the motor with the increaser shaft. With the motor lined up, the motor base plate can be bolted to the floor plate. The tension adjustment screws on the base plate can be used to properly tension the drive belts.

12) The final hook up is for all the electrical connections

on the test rig. The slip rings on each end of the increaser shafts and the Lebow torque transducer can be connected to the instrumentation in the control room. The lubrication motors on the increaser must be connected to the appropriate power source. Also the instrumentation on the increaser gear boxes must be connect to the control room. The lubrication system for the test rig, the magnetic clutch, and the drive motor must be connected to power and to the control room. Refer to the electrical drawings for the wiring diagrams for this test cell.

13) The final check is to run the lubrication systems and verify that all elements are getting lubricant. Also the water cooling system can be checked. If any leaks occur they must be repaired and rechecked.

14) The clutch test rig is now completely assembled and can now be run under a no load spin test.

Chapter VI

CONTROL SYSTEMS AND OPERATING PROCEDURES

The various control systems on the clutch engagement test rig are used to preform three main functions. The first function is for test set up and operation, the second is for the test rig alarms and emergency shutdown, and the third is for data acquisition. The three control systems of the clutch engagement test rig are for the DC drive system, the magnetic clutch, and the test assembly lubrication system.

The basic components of the drive system are the 200 HP shunt wound motor, the DC drive controller, and the Fenner motor speed controller. The DC motor has been equipped with an external blower assembly for armature ventilation. A safety feature on the motor is a thermal sensor for motor over temperature indication. The DC drive controller provides a variable DC output voltage, which is supplied to the motor armature. Speed regulation is accomplished through the use of a tachometer feedback system. The safety features of the controller are as follows. First the DC armature loop contactor is set up for a positive disconnect when the stop button is pushed or when an under voltage occurs. The next is high speed current limiting SCR semi-conductor fuses on both the AC and DC faults. A fault trip circuit that will shut down the DC drive and the entire

drive system cannot be restarted until the fault is cleared and manually reset. The other protection features are for a DC overload of the armature, a field loss, current limit, and phase loss protection.

The Fenner programmable digital controller has many advanced features. Some of the features are five preset setpoints to allow quick change of operating conditions, multiple formats for implementing speed control commands, and the ability to provide accurate digital control to the DC drive system. The controller also contains a RS-422 communication port allowing communication between the controller and a host computer.

The magnetic clutch controls are relatively simple. The basic safety controls for the magnetic clutch consist of a low water pressure and over temperature limit switches. These devices will provide visual alarms and are connected to the shutdown circuits on the DC drive systems. The other controls on the magnetic clutch are the manual and automatic mode switch and the engage and disengage set pots. When the system is in the manual mode a center off double throw toggle switch will be operated to provide the preset voltages from the set pots to engage and disengage the magnetic clutch. The automatic mode will allow the host computer to control the voltages to engage and disengage

the magnetic clutch.

The lubrication systems for the sprag clutch test rig consists of pump, motor, heat exchanger, and a 40 gallon oil reservoir. The lubrication system supplies oil to the bearings that support the shafts and to the sprag clutch assembly. The oil supply to the sprag clutch can be supplied from either side of the assembly and initially one side will be disconnect and only oil from the inner race will be utilized. The system is monitored with pressure transducers, flow meters, and thermocouples. These devices are connected into the shutdown circuits and visual alarms.

The only other system on the test rig is the lubrication systems on the two speed increasers. These oil systems are self contained to provide oil to the bearings and gear teeth. In the system, a filter and heat exchanger in the circulation loop are used to clean and cool the oil. The controls used on this system are for low water pressure, oil temperature, and low oil pressure. These controls are connected into the alarm and shutdown circuits. The entire test rig is also monitored by several vibration pickups. These are also connected to the shutdown circuits.

The last system is the data acquisition to be used during a test run. The collection of data for the clutch

engagement rig will be done with a Zenith 286 personal computer. The computer will monitor various items, for example speeds, torques, oil flow, oil pressure, oil temperature, vibrations, clutch race temperatures, as well as others. A chart recorder will also be used to develope a history file on the test runs.

The procedure to use before operating the test rig was developed by using check sheets. The start up procedure begins with a pre-run check of the Test Cell Basement, which contains the electrical cabinets, water valves and the lubrication system for the test rig; next the Test Cell, which contains the clutch engagement test rig; and finally the Control Room, which contains all the controls for the clutch test rig. After all checks are complete, an experiment can run. Following the experiment, a shut down procedure was also developed. Both of these procedures are found in Appendix 1.

During the normal operation of the test rig, a procedure was developed to assure that all systems are functioning properly. During the normal operation of the test rig the automatic safety system is in operation. A table was developed to list the limits that are monitored by the safety system. In Appendix 2, the normal operating procedure and operating limits of the test rig are found.

If the safety system does not respond or an unexpected failure occurs, the operator has an emergency shutdown button and the drive system will shut down. The lubrication system is independent from the drive system and will continue to operate when the DC drive system is shut down. The lubrication system does have a separate operator emergency shutdown button. If the lubrication system malfunctions and is shut down by either the operator or the automatic safety system, the DC drive system will automatically stop.

The last procedure to deal with is for emergency procedures. In Appendix 3, a chart is found that lists the various hazards, causes, effects, and recommendations. Also given in Appendix 3 is the procedure to follow for an emergency shut down.

Chapter VIII

EXPERIMENTAL PROCEDURE

The purpose of this test program is to investigate the heat generated due to friction between the sprags and the inner or outer races. The method that will be used to obtain the temperature data will be thermocouples located on the inner and outer race of the sprag clutch.

During the operation of the sprag clutch, the sprags are not attached to any one point on the race. When the sprags engage, there will be a little slippage until the sprags lock in place. Due to this movement, several thermocouples will be placed in the inner and outer race. The spacing between the thermocouples was chosen to be 4.5 degrees, which will increase the chances of at least on sprag locking up over a thermocouple. The inner race, figure 15, and the outer race, figure 8, will be modified to allow 8 thermocouples to be placed on the sprag race surface. The shortest distance between any two thermocouples was 0.125 inches and the distance between the thermocouples on the inner race is 0.112 inches. The solution to this problem was the stagger the locations in a zig-zag pattern, with 4 locations separated by a distance of 0.054 inches from the other four locations.

The location of the thermocouples for the inner race is

shown on figure 38. The outer race was also modified using the same zig-zag pattern and angular spacing, refer to figure 39. The thermocouples were brazed into the surface of the races and the leads were run through the hole down the center of the shaft. The data will be taken out through the use of slip rings on the end of the speed increaser high speed shafts.

The experiments to be preformed will determine the influence of several variables on the generation of heat between the sprags and the sprag races. The specific variables are shaft speed, torque, oil temperature, and oil flow.

The initial work done with the test rig will be to become familiar with conducting the experiments and controlling the various systems that control the test rig. After the initial break in, the first series of tests will be conducted. This first series will be broken down into four separate parts. During these tests three of the four variables will be held constant while the fourth variable is changed to predetermined levels.

In the first test, the shaft speed will be the variable that is adjusted. The shaft speed will be varied starting at 3000 rpm, to 4000 rpm, and finally to the maximum speed

of the test rig which is 5000 rpm. During this test the torque level will be set at the maximum level of 260 foot pounds, the oil flow will be at 0.8 gallons per minute, and the oil temperature will be held at a constant temperature to be set during the test runs.

The second variable to be investigated will be the torque. The torque level will be adjusted starting at 156 foot pounds, to 208 foot pounds, and finally to a level of 260 foot pounds. During this test the shaft speed will be set at 5000 rpm, oil flow at 0.8 gallons per minute, and the oil temperature will be held constant, which is the value determined during the shaft speed tests.

The third test will be to vary the oil flow. The oil flow to the clutch will be increased and decreased in increments of 0.1 gallons per minute. When these tests are conducted the shaft speed will be set at 5000 rpm and the torque level will be at 260 foot pounds. The oil temperature will also be held at a constant level, the same temperature determined during the shaft speed tests. When this test is run the sprag clutch will require close monitoring. As the oil flow is decreased, the ability to cool the clutch will decrease and damage or failure of the clutch may occur.

The last variable is the oil temperature. The temperature

of the oil will be increased and decreased then feed into the sprag clutch. The shaft speed will be at 5000 rpm, the oil flow will be at 0.8 gallons per minute, and the torque will be at 260 foot pounds. During this test, as with the oil flow test, close monitoring of the clutch will be required. As the oil temperature is increased the ability to cool the clutch will be decreased and damage or failure of the clutch can occur.

After the first test, each of the other tests will repeat one test, when the shaft speed is at 5000 rpm, the torque is at 260 foot pounds, the oil flow is at 0.8 gallons per minute, and the oil temperature is at the level determined during the first test. This will determine if the test rig is operating consistently and the sprag clutch is not damaged.

After these test are completed, the data must be analyzed and additional tests planned to determine the interaction between the four variables.

Chapter IX

SUMMARY

The four square test rig and sprag clutch test rig were designed and completed as required by the project schedule, which is shown in figure 37. The design that was developed meets all the initial requirements and the required minimum safety factor. The clutch engagement test cell also passed the safety review and was issued a safety permit that allowed the rig to be powered up.

The test rig was designed for ease of assembly and disassembly since the sprag clutch area is the main interest. Also the main design features of the rig were designed for a trouble free life. The main features include a set of labyrinth oil seals, a horizontally split housing, and a bronze collar lubrication supply collar.

The magnetic clutch is also a desirable feature, since the electronic control can be computer controlled. The magnetic clutch also is virtually maintenance free device. The four square test rigs circulating torque is monitored on both sides of the sprag clutch, by the Lebow transducer on one side and the strain gaged jack shaft on the other side. With this data the sprag clutch can be monitored for slippage by comparing values from the two torque transducers.

The lubrication system for the sprag clutch was also designed for several ways to lubricate the sprag clutch. The oil is feed in through either shaft using a steel collar riding on a set of bronze bushings. By changing orifices at the ends of the shafts, the amount and direction of lubricant can be controlled.

The high speed shaft line is rifled drilled to allow the instrumentation wires to be channeled to the ends of the shafts. At the ends a slip ring assembly is mounted to obtain a link to the signal conditioning equipment.

With all these features designed into the test rig, the test work on the sprag clutches should be able to carried out without problems from the mechanical equipment.

The experiments that are to be run will help identify the thermal and mechanical conditions that occur during the engagement of the sprag clutch. The primary purpose of these experiments is to verify the computer generated thermo-mechanical model for the loading and geometry on the sprag clutch and races.

Future experiments with the test rig can be done to verify optimum geometry and materials, which may improve clutch

performance. This testing will contribute in the design of future helicopter clutches and make them more reliable and have higher load carrying capacities.

REFERENCES

1. AMCP 706-201, Engineering Design Handbook Helicopter Engineering Part One Preliminary Design, 1974.

2. AMCP 706-202, Engineering Design Handbook Helicopter Engineering Part Two Detail Design, 1976.

3. American Gear Manufacturers Association. AGMA Practice for High Speed Enclosed Speed Reducers or Increasers Using Spur and Helical Gears, AGMA 421.06, 1982.

4. American Society of Metals, ASM Metals Reference Book, Second Edition, 1983.

5. Baumeister, Theodore, Standard Handbook for Mechanical Engineers, McGraw-Hill Book Company, 1967.

6. Chironis, Nicholas P., Gear Design and Application, McGraw-Hill Book Company, 1967.

7. Dally, James W. and Riley, William F., Experimental Stress Analysis, McGraw-Hill Book Company, 1965.

8. Dudley, Darle W., Handbook of Practical Gear Design, McGraw-Hill Book Company, 1984.

9. Hopkins, R. Bruce, Design Analysis of Shafts and Beams, McGraw-Hill Book Company, 1970.

10. Juvinall, Robert C., Stress, Strain, and Strength, McGraw-Hill Book Company, 1967.

11. Kish, Jules G., Helicopter Freewheel Unit Design Guide, Sikorsky Aircraft, USAAMRDL Technical Report 77-18, U.S. Army Air Mobility Research and Development Laboratory, Fort Eustis, Virginia, October 1977.

12. Kish, Jules G., Advanced Overrunning Clutch Technology, Sikorsky Aircraft, USAAMRDL Technical Report 77-16, U.S. Army Air Mobility Research and Development Laboratory, Fort Eustis, Virginia, December 1977.

13. Kish, Jules G., Advanced Overrunning Clutch Technology, Design Phase, Sikorsky Aircraft, USAAMRDL Technical Report AD/A-007815, U.S. Army Air Mobility Research and Development Laboratory, Fort Eustis, Virginia, 1974.

14. Kurniawan, Antonius S., "Generalized Eulerian-Lagrangian Finite Element Methods for Non-Linear Dynamic Problems, " Ph.D. Thesis, Case Western Reserve University, Cleveland, (1990).

15. Lynwander, P., Meyer, A.G., Chachakis, S., Sprag Overriding Aircraft Clutch, Avco Lycoming Division, USAAMRDL Technical Report 72-49, Eustis Directorate, U.S. Army Air Mobility Research and Development Laboratory, Fort Eustis, Virginia, July 1972, AD 747807.

16. Maag Gear Book, Maag Gear Wheel Company, Ltd., Zurich, Switzerland, 1963.

17. The Machinery Handbook, Industrial Press, 21st Edition.

18. Martin, George H., Kinematics and Dynamics of Machines, McGraw-Hill Book Company, 1969.

19. Perry, C.C. and Lissner, H.R., The Strain Gage Primer, McGraw-Hill Book Company, 1962.

20. Roark, Raymond J. and Young, Warren C., Formulas for Stress and Strain, McGraw-Hill Book Company, 1975.

21. Shigley, Joseph E., Mechanical Engineering Design, McGraw-Hill Book Company, 1972.

22. Standard Product Catalog, The Falk Corporation, Milwaukee, Wisconsin, 1982.

23. Thomson, William T., Theory of Vibration, Prentice-Hall, Inc., 1972.

24. Timken Engineering Journal, The Timken Company, Canton, Ohio, 1972.

25. Wilcox, Donald F., and Booser, E. Richard, Bearing Design and Application, McGraw-Hill Book Company, 1957.

Appendix 1

CHECK SHEETS

Before operating the clutch engagement test stand, the following check lists must be completed by the test engineer and engineering technician. If any step during the check fails, the reason for the failure must be determined and the appropriate action to correct the problem must be done. Then the check list is repeated from the top. The check lists are as follows.

Pre-Run Check Sheet

TEST CELL BASEMENT

1. Verify main hand valves to CTW supply manifold are open.
2. Verify hand valve to CTW return is open.
3. Verify CTW hand valve to test assembly lubrication system heat exchanger is open.
4. Verify disconnect for test assembly lubrication pump is closed.
5. Verify CTW supply mercoid is set at 40 psi.
6. Verify test assembly oil supply mercoid is set at 35 psi.
7. Verify oil level in reservoir.
8. Verify service air valve is open.

Test Cell

1. Verify panel P1207 breakers are energized.
   - BKR No. 10 Test Assembly Lube Pump and Heater
   - BKR No. 15 Control Power
   - BKR No. 17 Instrumentation Plugmolds
   - BKR No. 22 Gearboxes 1 and 2 Lube Pumps
   - BKR No. 31 Magnetic Clutch
2. DC Drive disconnect is on.
3. Verify gearboxes 1 and 2 mercoids are set at 40 psi.
4. Verify lube oil supply valve to test assembly bearings is open
5. Energize test cell vent fan.
6. Close test cell door.
7. Post sign "Keep Out Test In Progress."

Control Room

1. Verify Limits on the following meters.

	LOW	HIGH
- MR2 Gearbox 1 lube oil temperature	150F	200F
- MR4 Gearbox 2 lube oil temperature	150F	200F
- MR5 Test assembly sect. 1 oil flow	.3 GPM	.5 GPM
- MR6 Test assembly sect. 2 oil flow	.3 GPM	.5 GPM
- MR7 Test assembly lube oil temp.	200F	250F
- MR8 Test assembly lube oil reservoir temperature	150F	250F
- MR9 Test assembly bearing 1 temp.	225F	250F

- MR10 Test assembly bearing 2 temp. 225F 250F
- MR11 Test assembly bearing 3 temp. 225F 250F
- MR12 Test assembly bearing 4 temp. 225F 250F
- MR13 Lebow speed (rpm) 4044
- MR14 Lebow torque (ft/lbs) 250

3. Energize Endevco vibration units.
   - Set high limits at 10 G's
4. Turn on control panel power.
5. Acknowledge and reset annunciator.
6. Open cooling tower water valve.
   - Verify water pressure and water temperature lights on magnetic clutch panel are lit.
   - Acknowledge and reset annunciator panel.
7. Turn on gearbox 1 and gearbox 2 lube pumps.
   - Verify if gearboxes 1 and 2 lube oil pressure is adequate.
   - Acknowledge and reset annunciator panel.
8. Turn on test assembly lube pump.
   - Verify if test assembly lube oil pressure is adequate.
9. Turn on test assembly oil reservoir heater if required.

NOTE:

Circulate lube system for a sufficient amount of time so oil pressure, flow, and temperature can become stable.

10. Verify magnetic clutch control switch is in the appropriate operating mode--manual or automatic as per the test plan.
11. Energize magnetic clutch controls.
12. Verify permissive lights are lit.
13. Verify engagement/disengagement control pot voltages are correct.
14. Verify DC drive speed pot is set at zero (full CCW).
15. Verify DC drive control switch is in the appropriate operating mode--manual or automatic.
16. Verify rotation switch is in the appropriate operating mode--forward or reserve.
17. Energize DC drive control power.
18. Verify DC drive permissives are satisfied and light is lit.
19. Start DC drive.
20. Record start of run.

Shut Down Check Sheet

1. Record end of run.
2. Return DC drive speed pot to zero (full CCW).
3. Stop DC drive.
4. De-energize magnetic clutch.

NOTE:

Do not shut off cooling tower water.

5. Allow test assembly lubrication system to run for a sufficient amount of time to cool down bearings and clutch area.
6. De-energize test assembly lube pump.
7. De-energize gearbox 1 and 2 lube pumps.
8. Verify magnetic clutch has cooled down sufficiently. If so, close cooling tower water supply valve.
9. Turn off DC drive control panel.
10. Turn off control panel power.
11. De-energize Daytronics units and Endevco units.

Appendix 2

NORMAL OPERATING PROCEDURES

After successful completion of the pre-run and start up procedures, and determination that all systems are functioning properly, normal operation will include the following.

1. Varying and monitor motor speed.
2. Monitor test assembly speeds and torques.
3. Monitor all bearing temperatures.
4. Monitor all sprag clutch temperatures.
5. Monitor all Endevcos for vibrations.
6. Varying and monitor test assembly oil pressures and flows.
7. Continually man control room by engineering and technical personnel.

The following tables are a list of the various devices in the clutch engagement test rig, the location of the device, and the limit for the device.

DEVICE	LOCATION	LIMITS
PRESSURE SWITCH	GEARBOX 1	40 PSI MIN. OIL PRESSURE
PRESSURE SWITCH	GEARBOX 2	40 PSI MIN. OIL PRESSURE
THERMOCOUPLE	GEARBOX 1	200°F MAX. OIL INLET TEMP.
THERMOCOUPLE	GEARBOX 2	200°F MAX. OIL INLET TEMP.
PRESSURE SWITCH	TEST ASSEMBLY	35 PSI MIN. OIL PRESSURE
FLOWMETER	SECT. 1 TEST ASSEMBLY	.3 GPM MIN. OIL FLOW
FLOWMETER	SECT. 2 TEST ASSEMBLY	.3 GPM MIN. OIL FLOW
ACCELEROMETERS (6)	GEARBOXES & TEST ASSEMBLY HOUSING	10 G's MAX.
THERMOCOUPLES (4)	TEST ASSEMBLY SUPPORT BEARINGS	250°F MAX. BEARING TEMP.
LEVEL SWITCH	TEST ASSEMBLY OIL RESERVOIR	20 GAL. MIN.
THERMOCOUPLE	TEST ASSEMBLY INLET OIL	250°F MAX. OIL TEMP.

Table 1. Monitoring device, location, and normal operating limit.

DEVICE	LOCATION	LIMITS
SPEED PICKUP	D.C. MOTOR	2700 RPM
ROTARY TRANSFORMER	SHAFT/MAGNETIC CLUTCH TO GEARBOX 1	4044 MAX. RPM 250 FT/LBS MAX. TORQUE
TEMPERATURE SWITCH	MAGNETIC CLUTCH	80°F MAX. INLET WATER TEMP. 165°F MAX. OUTLET WATER TEMP.
PRESSURE SWITCH	MAGNETIC CLUTCH	30 PSI MIN. WATER PRESSURE 100 PSI MAX. WATER PRESSURE
D.C. DRIVE CONTROLLER - FIELD LOSS - INSTANTANEOUS OVERCURRENT - PHASE LOSS - HEATSINK THERMAL OVERLOAD - MOTOR CURRENT OVERLOAD - MOTOR CURRENT IMBALANCE - MOTOR OVERSPEED	SOUTH WALL OF TEST CELL	FACTORY SET * FINAL ADJUSTMENTS WILL BE PERFORMED DURING CHECKOUT OF DRIVE SYSTEM

Table 2. Monitoring device, location, and normal operating limit.

Appendix 3

EMERGENCY PROCEDURES

The following list contains the procedures that will be followed in the event of an emergency during a test run.

1. Press DC drive emergency stop button.
2. After rotation has stopped, de-energize test assembly lube system and gearbox 1 and 2 lube systems.
3. Visually inspect test cell through control room window.
4. In case of fire, dial 17 and evacuate control room and test cell.

The following table is a list of the various hazards that may occur during a test. The cause, effect, and recommendations are compiled for operating personal.

Table 3. Emergency conditions and responses.

ITEM	HAZARDOUS CONDITION	CAUSE	EFFECT	HAZARD LEVEL	ASSESSMENT	RECOMMENDATION
1	COLLISION	DRIVE BELT FAILURE	POTENTIAL INJURY TO PERSONNEL & EQUIPMENT	II	POSSIBLE DURING OPERATION	INSTALL SHIELDS
2	COLLISION	CLUTCH FAILURE	POTENTIAL INJURY TO PERSONNEL & EQUIPMENT	III	UNLIKELY TO OCCUR	DESIGN OUTER RACE HOUSING & TEST ASSY. HOUSING TO CONTAIN FRAGMENTS
3	COLLISION	PERSONNEL CONTACT W/ DRIVE BELTS PULLEYS, DRIVE SHAFTS & COUPLINGS	POTENTIAL INJURY TO PERSONNEL & EQUIPMENT	II	PROBABLE DURING OPERATION	INSTALL SHIELDS
4	FIRE	IGNITION OF LUBRICATION OIL	POTENTIAL INJURY TO PERSONNEL MINOR DAMAGE TO EQUIPMENT	IV	UNLIKELY TO OCCUR	MONITOR OIL TEMP-ERATURES DESIGN SUFFICIENT HI-TEMP RIG SHUT-DOWNS
5	NOISE	EQUIPMENT AND GEAR MESH OPER-ATING AT HIGH RPM	POTENTIAL INJURY TO PERSONNEL	III	POSSIBLE DURING OPERATION	REQUIRE PERSONNEL TO WEAR HEARING PROTECTION WHEN ENTERING TEST CELL POST WARNING SIGNS

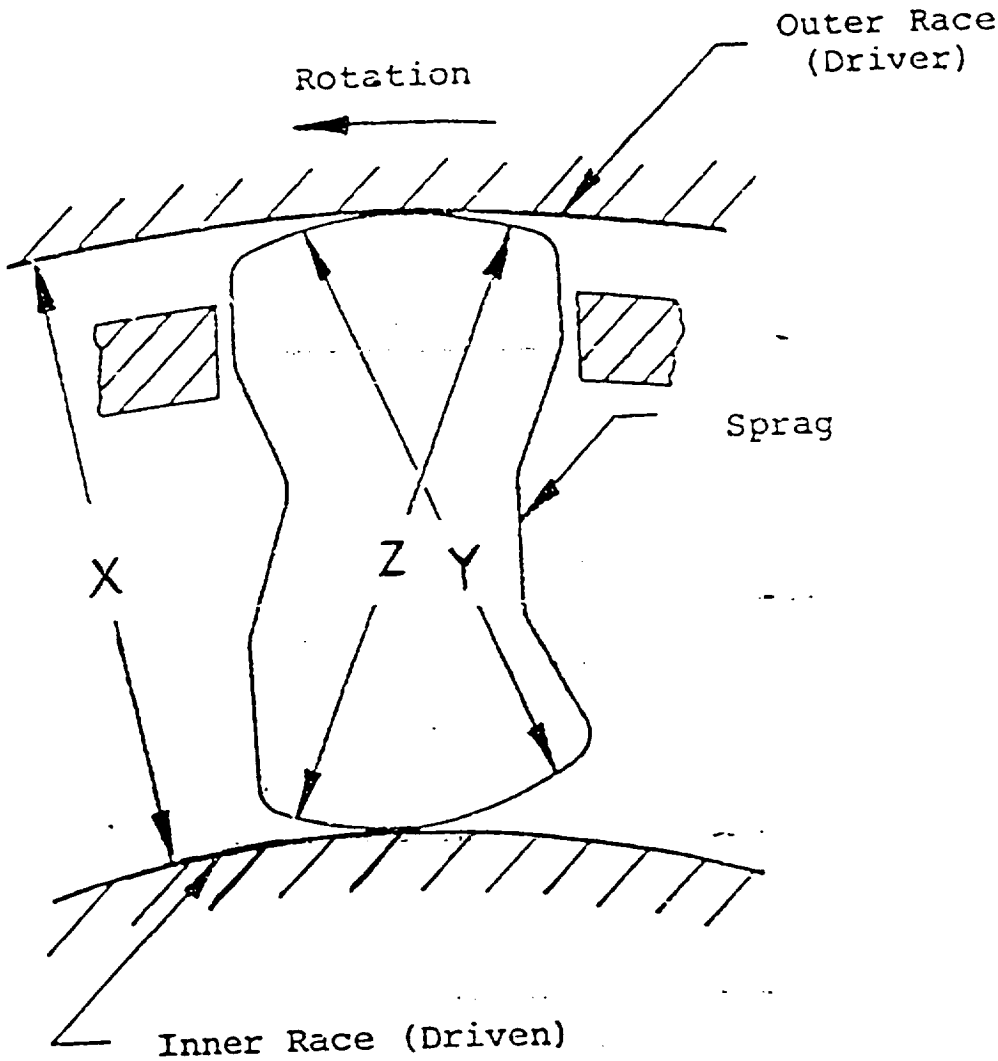

Figure 1. Typical cross section of a sprag. The dimension "Z" is greater than the "X" dimension and the "Y" dimension is smaller than the "X" dimension.

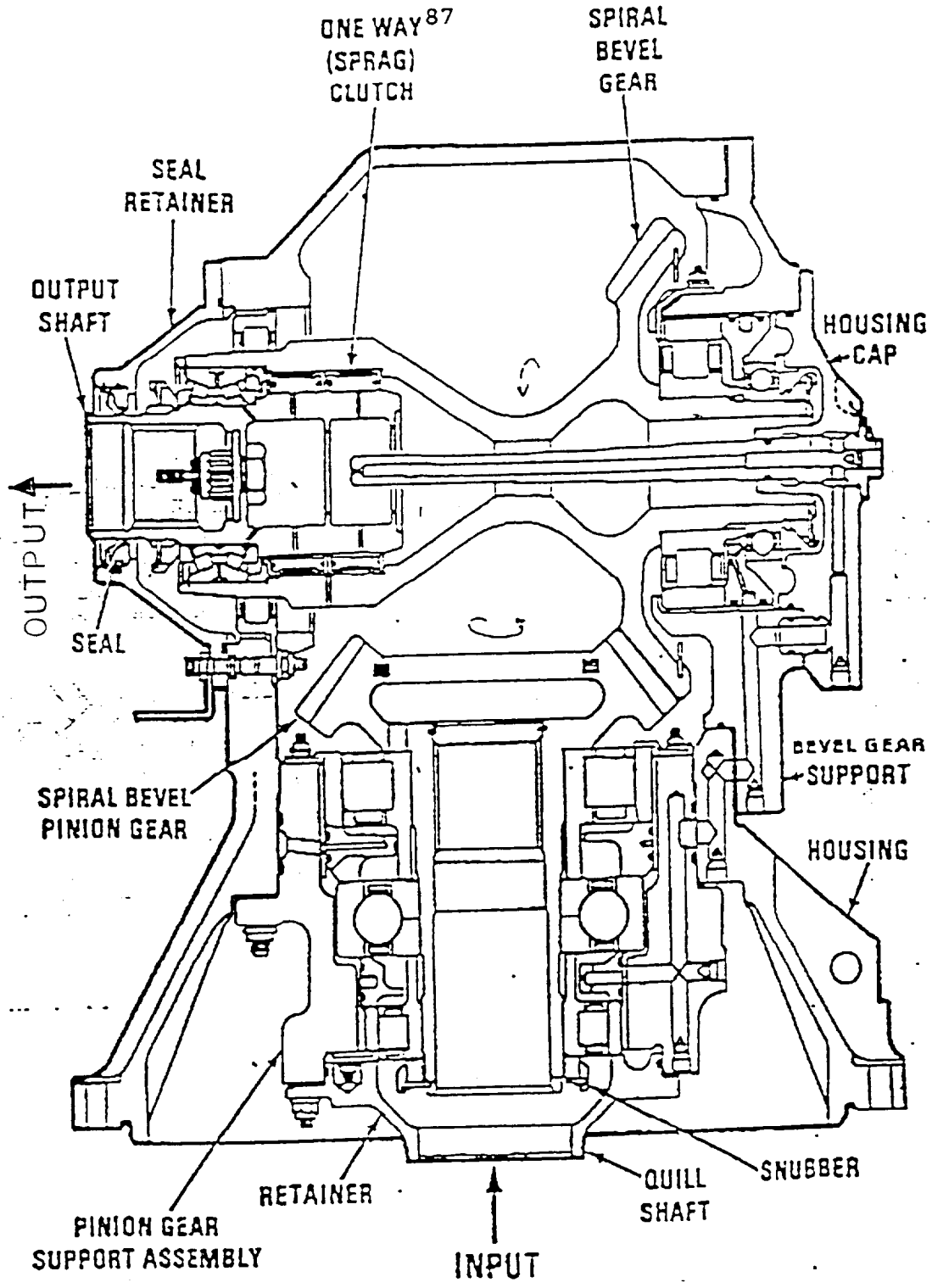

Figure 2. Cross section of a helicopter transmission.

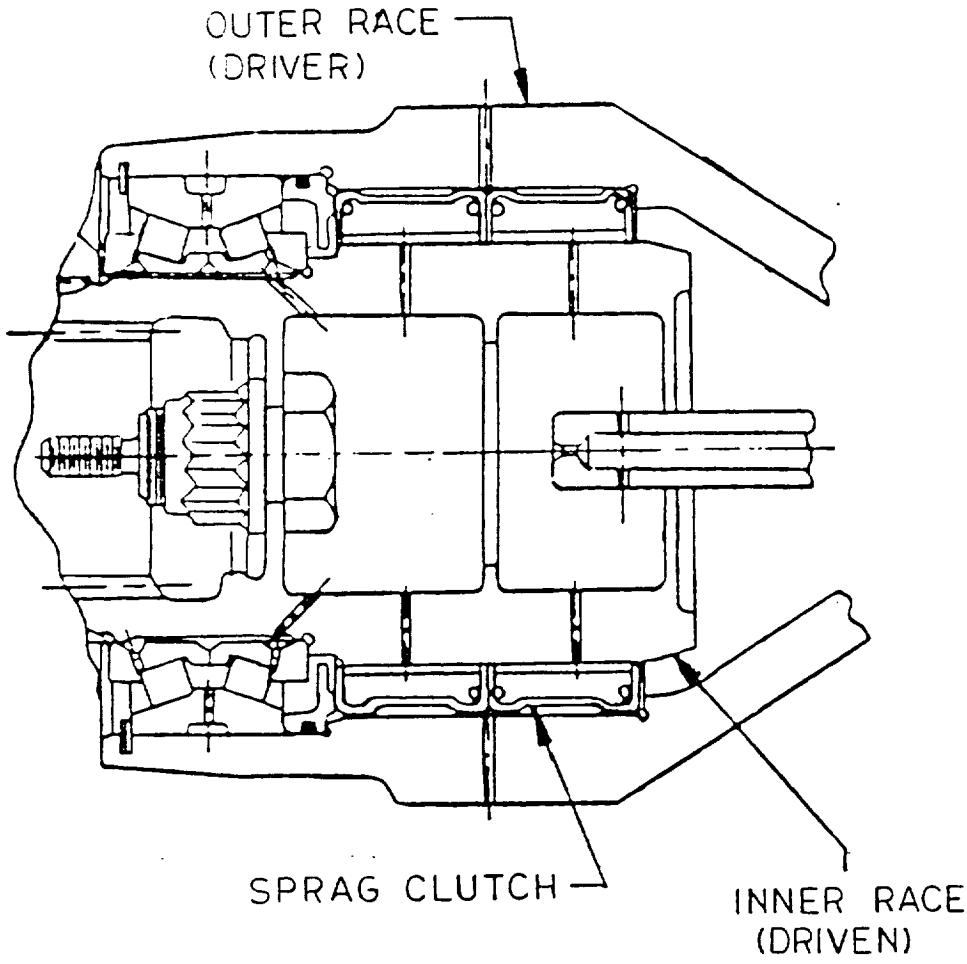

Figure 3. Enlarged view of sprag clutch assembly in the helicopter transmission. See figure 2 for an over all view.

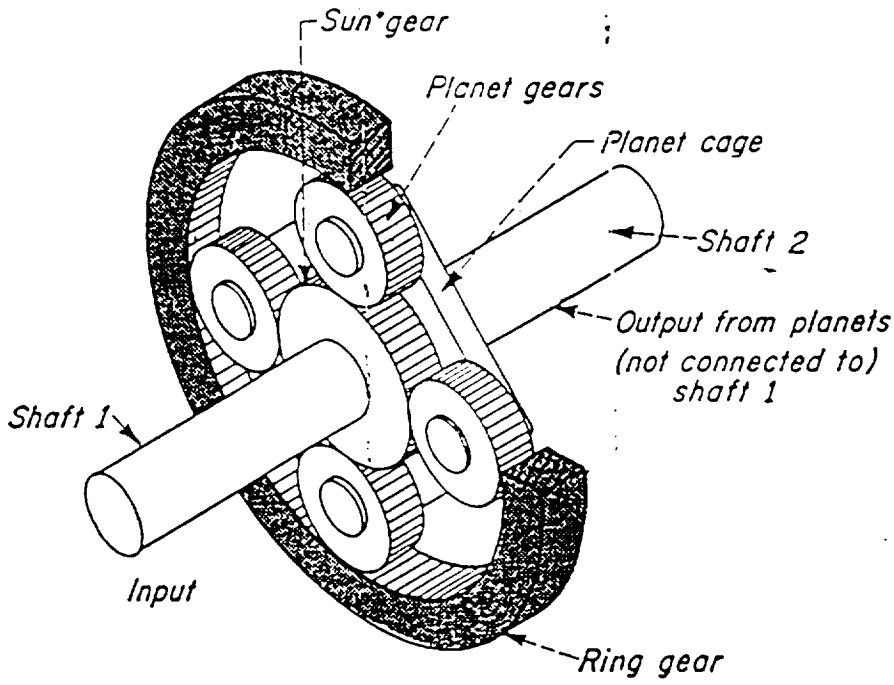

Figure 4. Planetary torque applier. Shaft 1 is connected to one set of gears and shaft 2 to the other set of gears. There is a constant ratio between shafts 1 and 2 as long as the ring gear is stationary. Rotating it introduces relative twist between the shafts. The ring gear can be accurately adjusted to give desired torque.

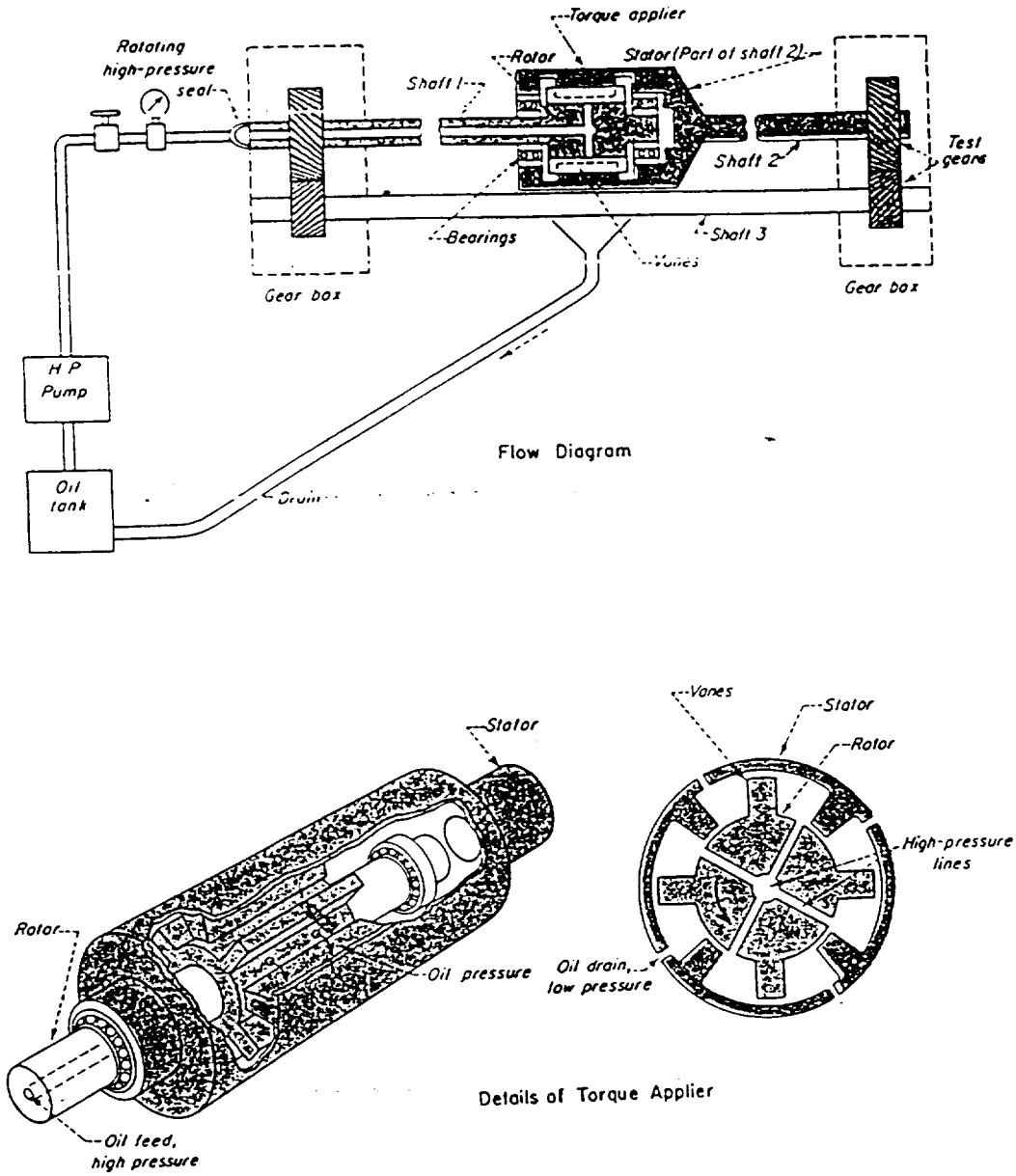

Figure 5. Hydraulic torque applier. A high pressure vane pushes oil through rotating shaft and out between the vanes of the rotor and stator. The oil forces the vanes apart, causing the twist in the shafts. Oil leakage to the low pressure side is bled off through holes in the periphery. Oil pressure is easily adjusted to give a wide range of loads.

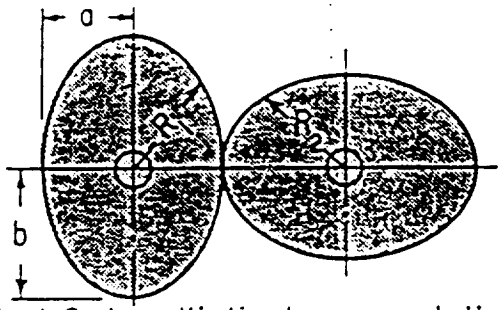

2nd Order elliptical gears rotating about their geometric centers

$$R = \frac{2ab}{(a+b) - (a-b)\cos 2\theta}$$

$C = a + b$

a = maximum radius

b = minimum radius

$$\omega_2 = \omega_1 \left[\frac{r + 1 + (r^2 - 1)\cos 2\theta_2}{2r} \right]$$

where $r = \frac{a}{b}$

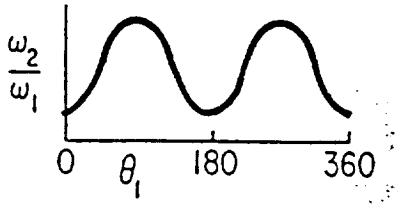

Figure 6. Elliptical gear formula and graph of relative speeds of the two gears.

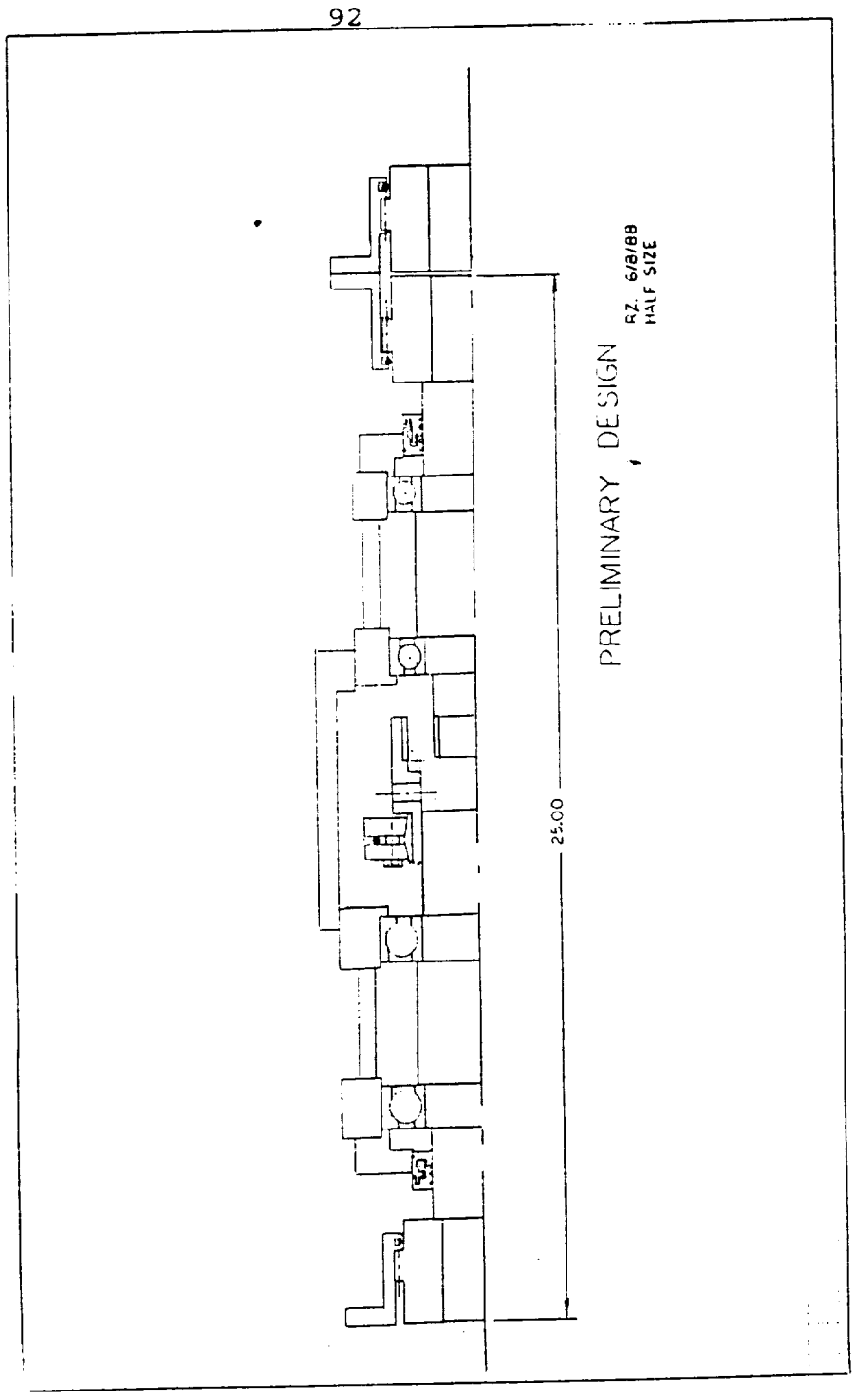

Figure 7. Preliminary design. This unit was made to replace a Lebow load cell and jack shaft on the original four square test rig.

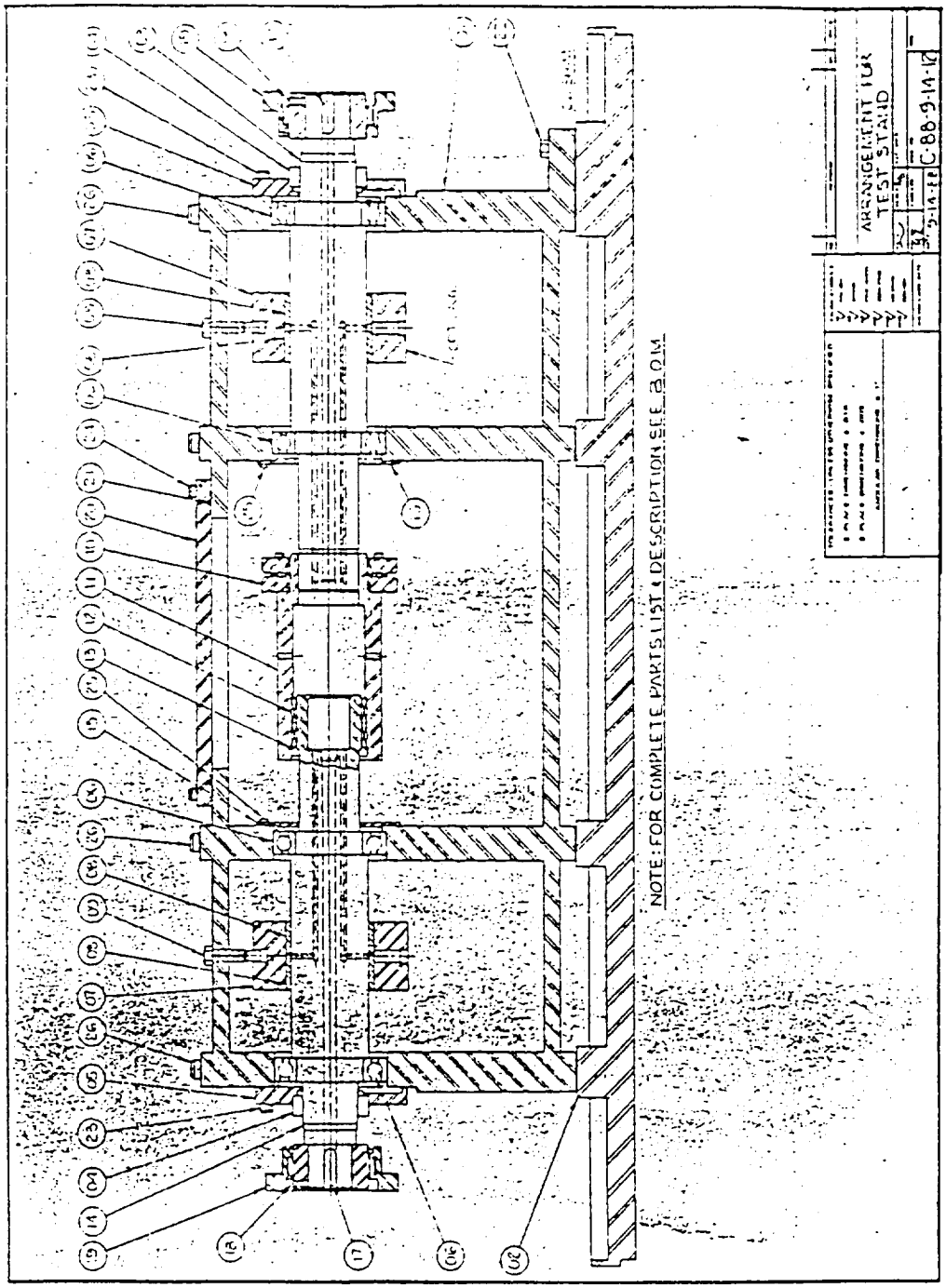

Figure 8. First design revision. Entire high speed drive line was replaced to allow for a less cramped design.

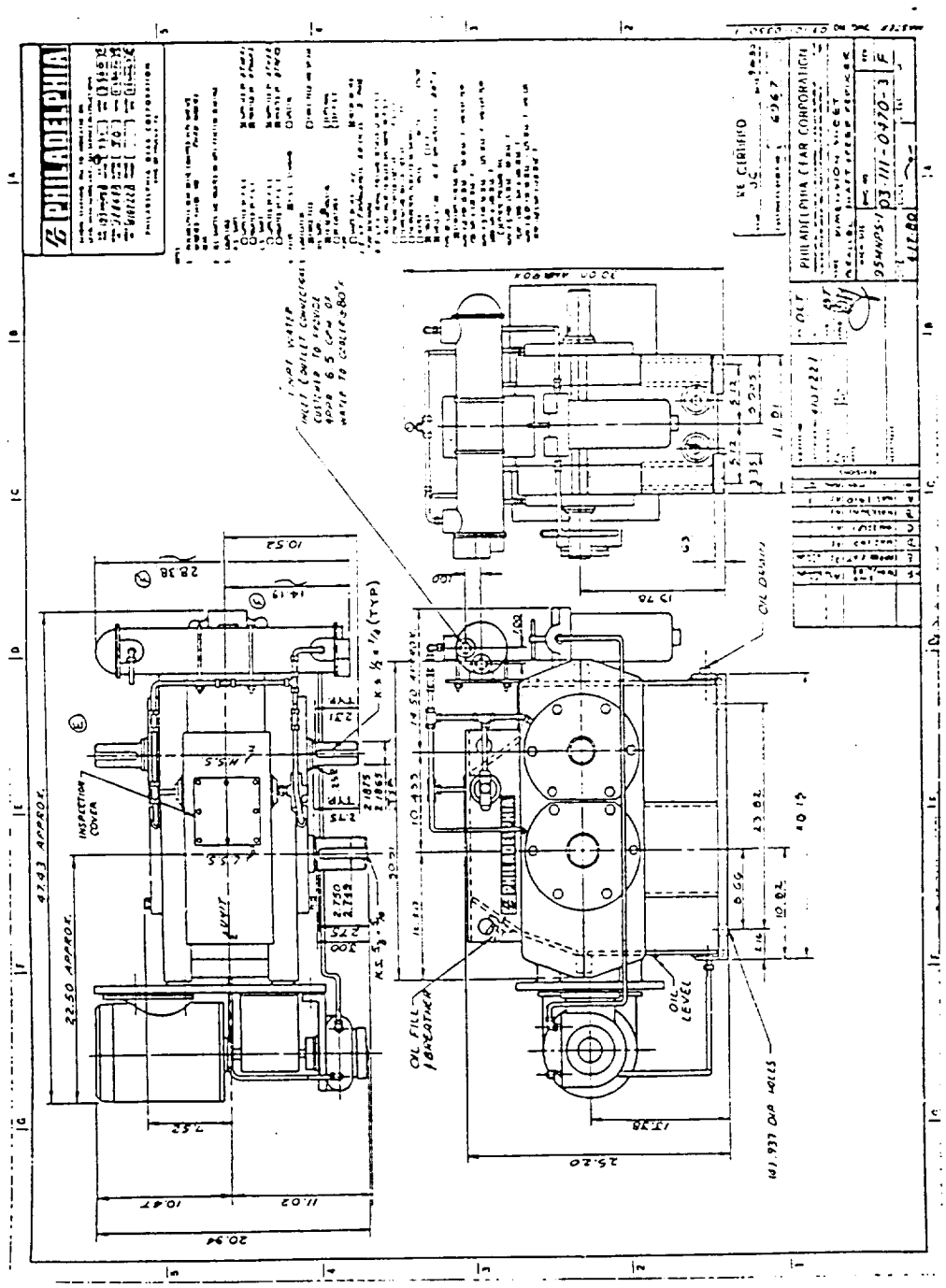

Figure 9. Certified dimension print of speed increasers.

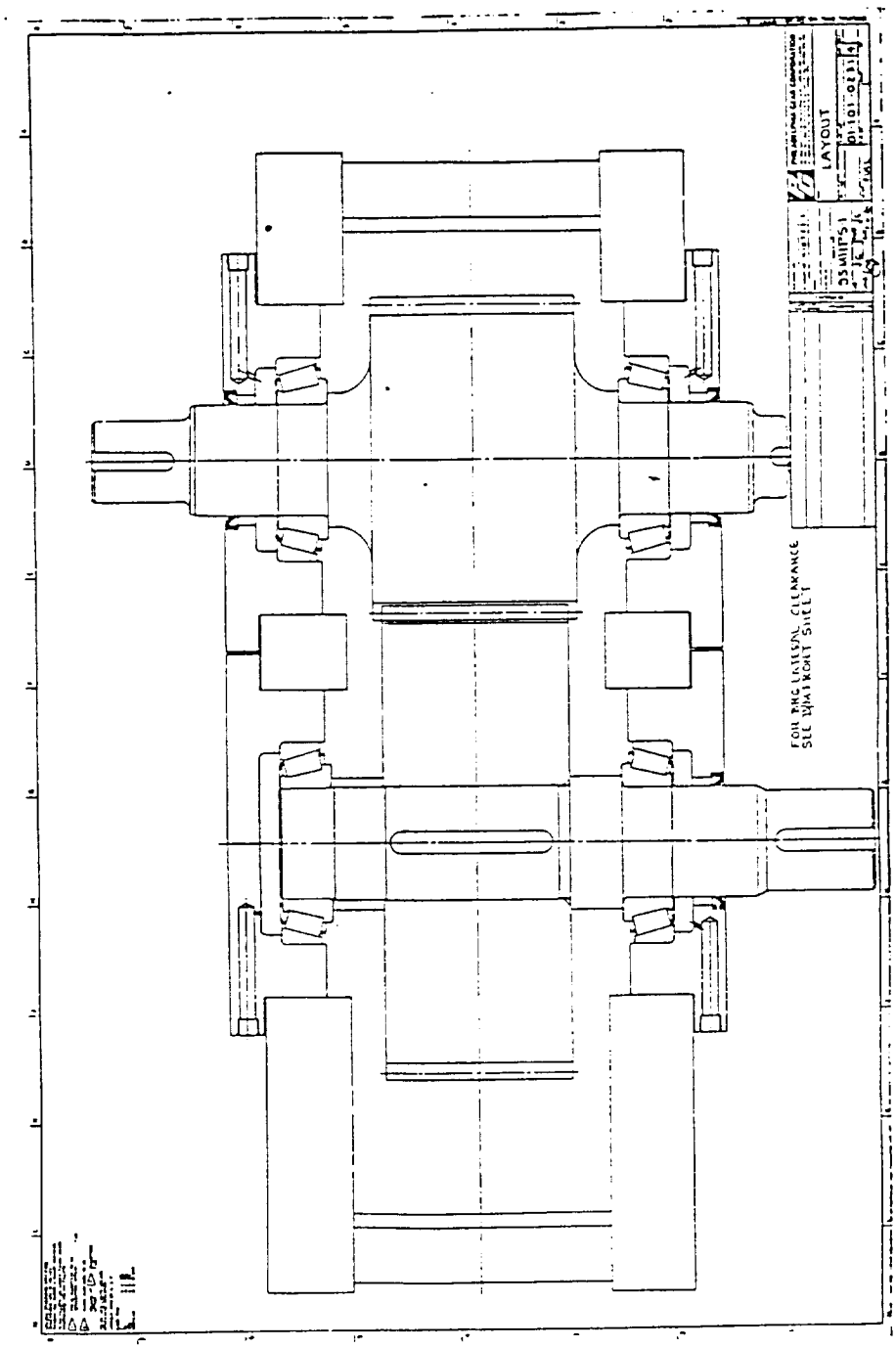

Figure 10. Arrangement drawing of speed increasers.

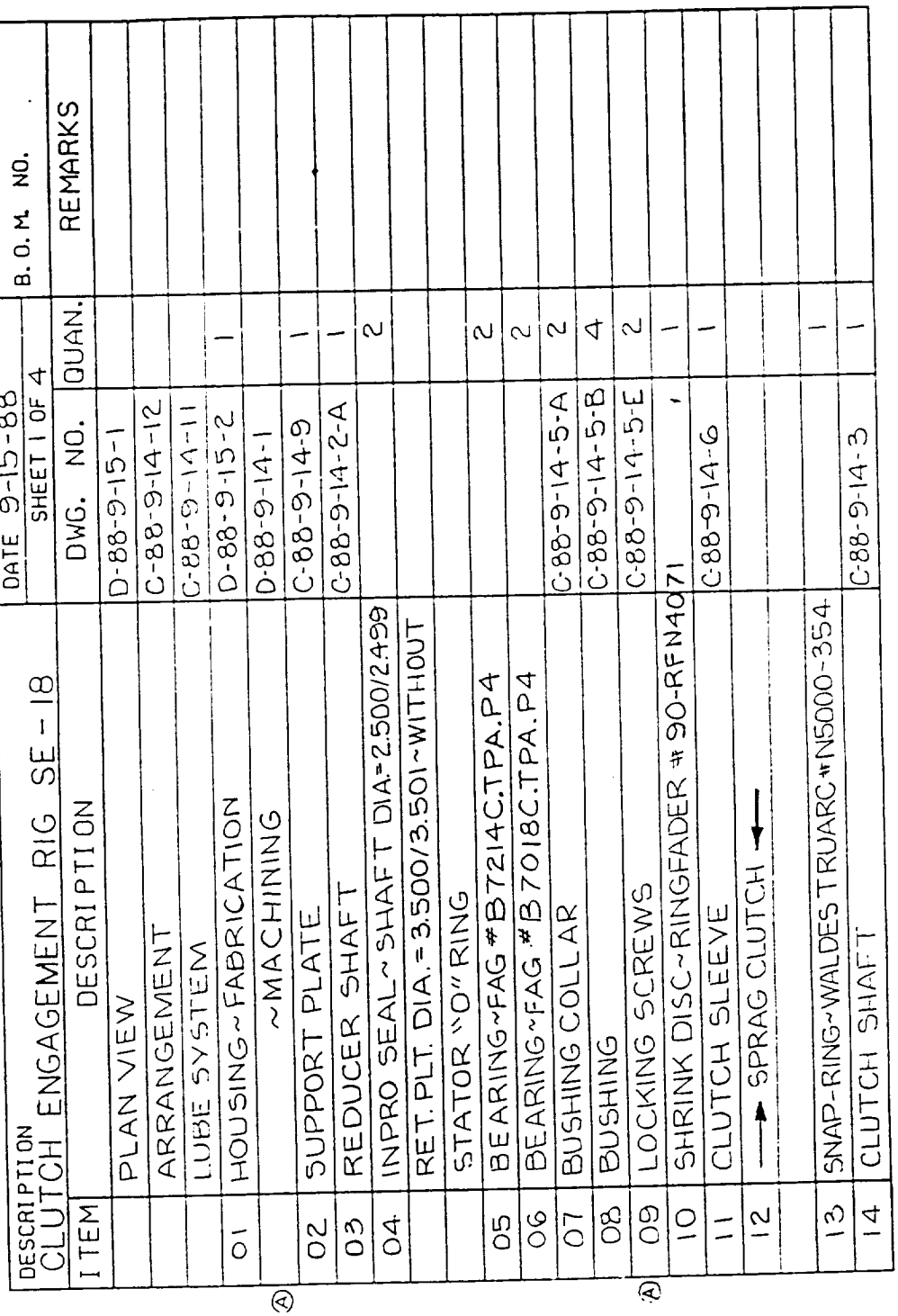

DESCRIPTION
CLUTCH ENGAGEMENT RIG SE - 18

DATE 9-15-88
SHEET 1 OF 4

B.O.M. NO.

ITEM	DESCRIPTION	DWG. NO.	QUAN.	REMARKS
	PLAN VIEW	D-88-9-15-1		
	ARRANGEMENT	C-88-9-14-12		
	LUBE SYSTEM	C-88-9-14-11		
01	HOUSING~FABRICATION	D-88-9-15-2	1	
	~MACHINING	D-88-9-14-1		
02	SUPPORT PLATE	C-88-9-14-9	1	
03	REDUCER SHAFT	C-88-9-14-2-A	1	
04	INPRO SEAL~SHAFT DIA=2.500/2.499		2	
	RET. PLT. DIA. = 3.500/3.501~WITHOUT			
	STATOR "O" RING			
05	BEARING~FAG #B7214C.TPA.P4		2	
06	BEARING~FAG #B7018C.TPA.P4		2	
07	BUSHING COLLAR	C-88-9-14-5-A	2	
08	BUSHING	C-88-9-14-5-B	4	
09	LOCKING SCREWS	C-88-9-14-5-E	2	
10	SHRINK DISC~RINGFADER # 90-RFN4071		1	
11	CLUTCH SLEEVE	C-88-9-14-6	1	
12	⟵ SPRAG CLUTCH ⟶			
13	SNAP-RING~WALDES TRUARC #N5000-354		1	
14	CLUTCH SHAFT	C-88-9-14-3	1	

Figure 11A. Bill of material for the four square test rig.

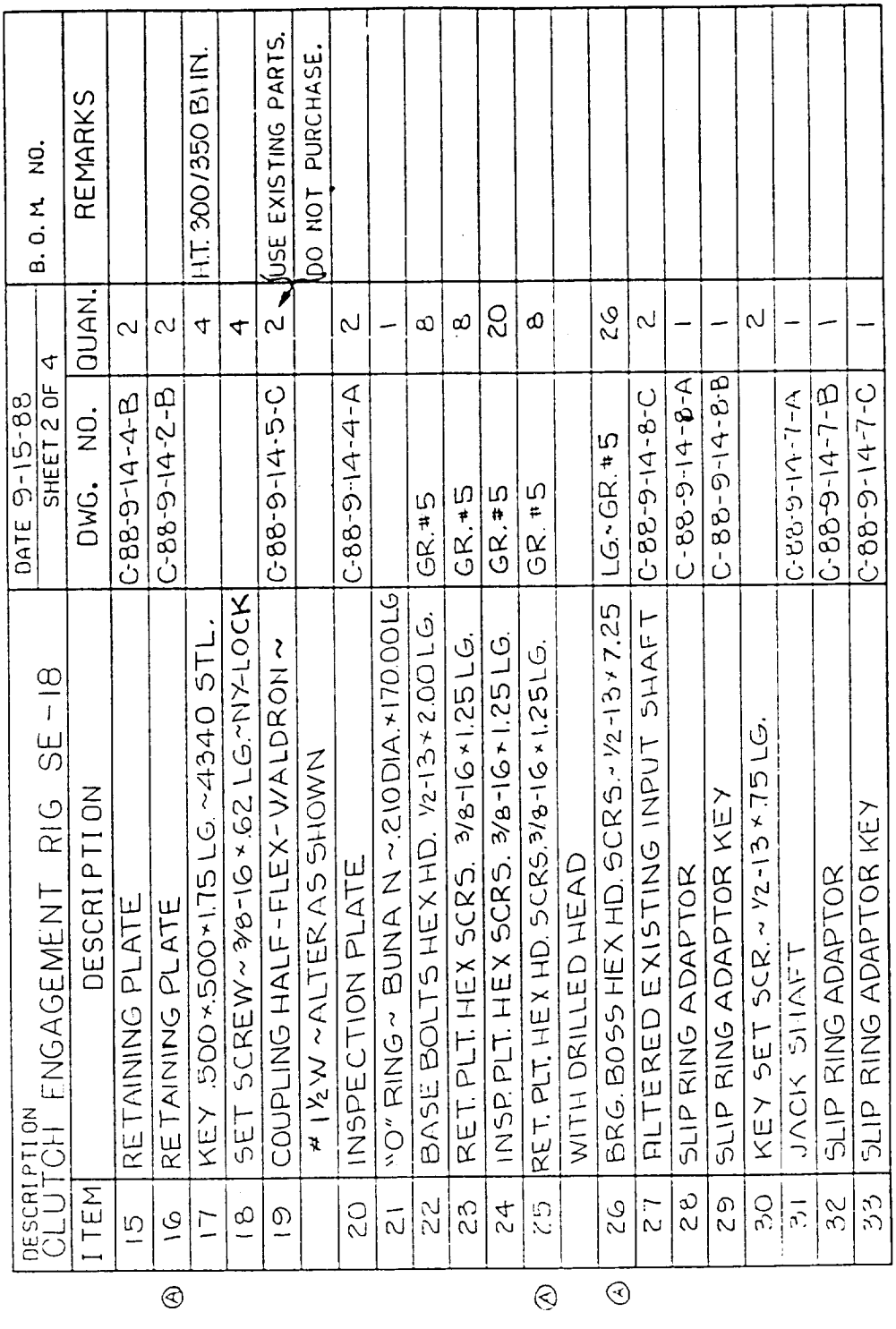

DESCRIPTION
CLUTCH ENGAGEMENT RIG SE-18

DATE 9-15-88
SHEET 2 OF 4

B. O. M. NO.

ITEM	DESCRIPTION	DWG. NO.	QUAN.	REMARKS
15	RETAINING PLATE	C-88-9-14-4-B	2	
16	RETAINING PLATE	C-88-9-14-2-B	2	
17	KEY .500×.500×1.75 LG.~4340 STL.		4	H.T. 300/350 BHN.
18	SET SCREW~ 3/8-16×.62 LG.~NY-LOCK		4	
19	COUPLING HALF-FLEX-V/ALDRON~	C-88-9-14-5-C	2	USE EXISTING PARTS.
	#1½W ~ALTER AS SHOWN			DO NOT PURCHASE.
20	INSPECTION PLATE	C-88-9-14-4-A	2	
21	"O" RING~ BUNA N ~.210 DIA.×170.00 LG		1	
22	BASE BOLTS HEX HD. ½-13×2.00 LG.	GR.#5	8	
23	RET. PLT. HEX SCRS. 3/8-16×1.25 LG.	GR.#5	8	
24	INSP. PLT. HEX SCRS. 3/8-16×1.25 LG.	GR.#5	20	
25	RET. PLT. HEX HD. SCRS. 3/8-16×1.25 LG.	GR.#5	8	
	WITH DRILLED HEAD			
26	BRG. BOSS HEX HD. SCRS.~ ½-13×7.25	LG.~GR.#5	26	
27	ALTERED EXISTING INPUT SHAFT	C-88-9-14-8-C	2	
28	SLIP RING ADAPTOR	C-88-9-14-8-A	1	
29	SLIP RING ADAPTOR KEY	C-88-9-14-8-B	1	
30	KEY SET SCR.~ ½-13×.75 LG.		2	
31	JACK SHAFT	C-88-9-14-7-A	1	
32	SLIP RING ADAPTOR	C-88-9-14-7-B	1	
33	SLIP RING ADAPTOR KEY	C-88-9-14-7-C	1	

Figure 11B. Bill of material for the four square test rig.

DESCRIPTION
CLUTCH ENGAGEMENT RIG SE-18

DATE 9-15-88
SHEET 3 OF 4

B. O. M. NO.

ITEM	DESCRIPTION	DWG. NO.	QUAN.	REMARKS
34	MOTOR BRACKET	C-88-9-14-10	1	
35	COUPLING~FALK TYPE 20 #1025G		1	
	MOTOR HALF=3.2485/3.2495DIA.~KEY .750×.375			
	RED. HALF=2.7485/2.7495DIA.~KEY .625×.312			
36	REDUCER KEY .625×.625×2.75LG.~	4340 STEEL	1	H.T. 300/350 BHN.
37	MOTOR KEY .750×.750×5.25LG. ~	4340 STEEL	1	H.T. 300/350 BHN.
38	MOTOR HEX HD. SCRS. 1.12"×2.75LG.		4	
39	COUNTER SUNK PIPE PLUG 3/8" N.P.T.		2	
40	COUPLING HALF~RIGID~WALDRON~	C-88-9-14-5-D	1	USE EXISTING PARTS.
	#1½W~ ALTER AS SHOWN			DO NOT PURCHASE.
41	COUPLING HALF~FLEX~WALDRON~#2W	C-88-9-14-5-C	1	ALTER AS SHOWN
42	MICHIGAN SCIENTIFIC SLIP RING		2	
	#SR20M/EXTENDED LIFE CONTACTS			
43	SLIP RING SOC. HD. SCRS. 8-32×.50LG.		6	
44	STRAIN GAGES~EA-06-125TL-350-SE		2	(10 GAGES)
45	LOCKNUT~SPIETH #MSR 90×12; R-501		2	
46	CLUTCH SHAFT ADAPTOR	C-88-9-14-13	1	
47	SHOULDER SCRS. HEX SOC. HD.		2	
	.375 DIA. SIZE×1.00LG.~5/16-18 THD.	GR. #8		
48	CLUTCH SHAFT ADAPTOR HEX HD.		6	
	SCRS. 3/8-16×1.00LG. W/DR. HDS.	GR. #5		

Figure 11C. Bill of material for the four square test rig.

DESCRIPTION CLUTCH ENGAGEMENT RIG SE-18

DATE 9-15-88

SHEET 4 OF 4

B. O. M. NO.

ITEM	DESCRIPTION	DWG. NO.	QUAN.	REMARKS
49	SET SCR. HEX SOC. NY-LOCK ~ 1/4-20	.50 LG.	12	
50	"O" RING ~ APR-568-018 ~ 70 DURO		1	
51	"O" RING ~ APR-568-032 ~ 70 DURO		1	
52	EYE BOLTS SH'RD. 1/2-13		4	
53	PIPE PLUG 1" N.P.T.		8	
54	PIPE PLUG 3/8" N.P.T.		6	
55	DRILL ROD ~ 1/2 DIA. x .75 LG.		2	
56	BEARING SLEEVE	C-88-9-14-14	2	

Figure 11D. Bill of material for the four square test rig.

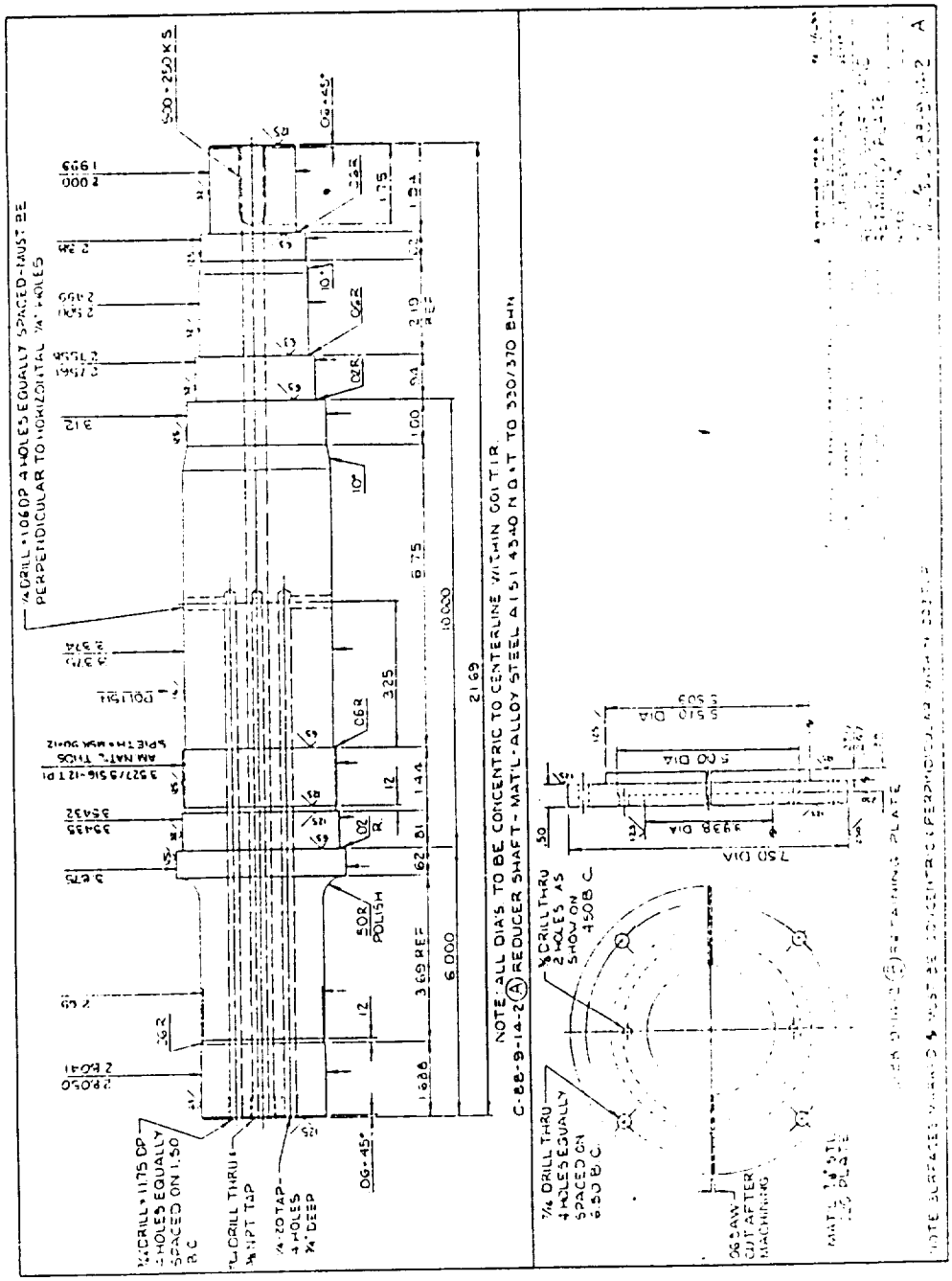

Figure 12. Drawing C-88-9-12-2. Outer sprag clutch shaft and inner bearing retaining plate.

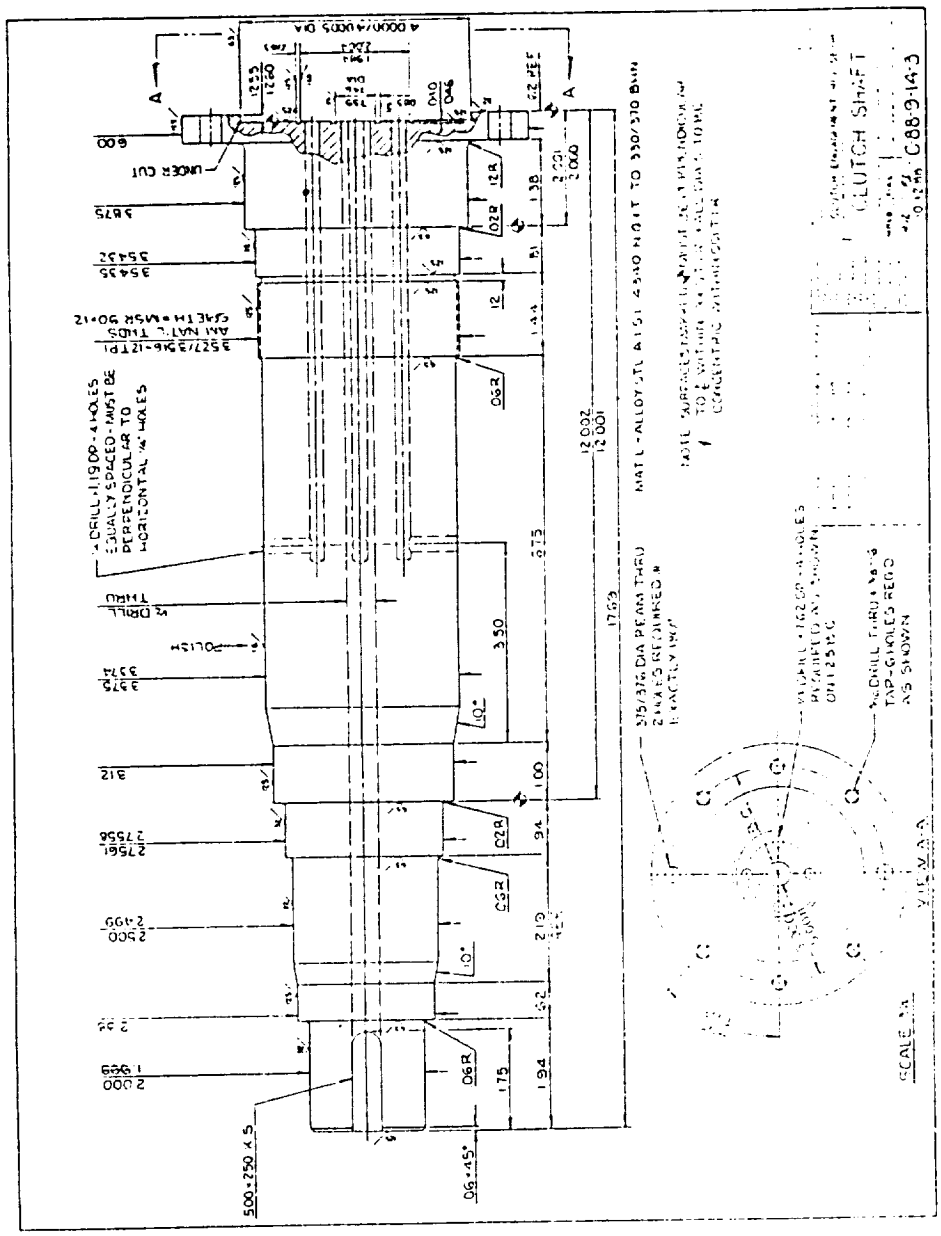

Figure 13. Drawing C-88-9-14-3. Inner clutch shaft with flange connection.

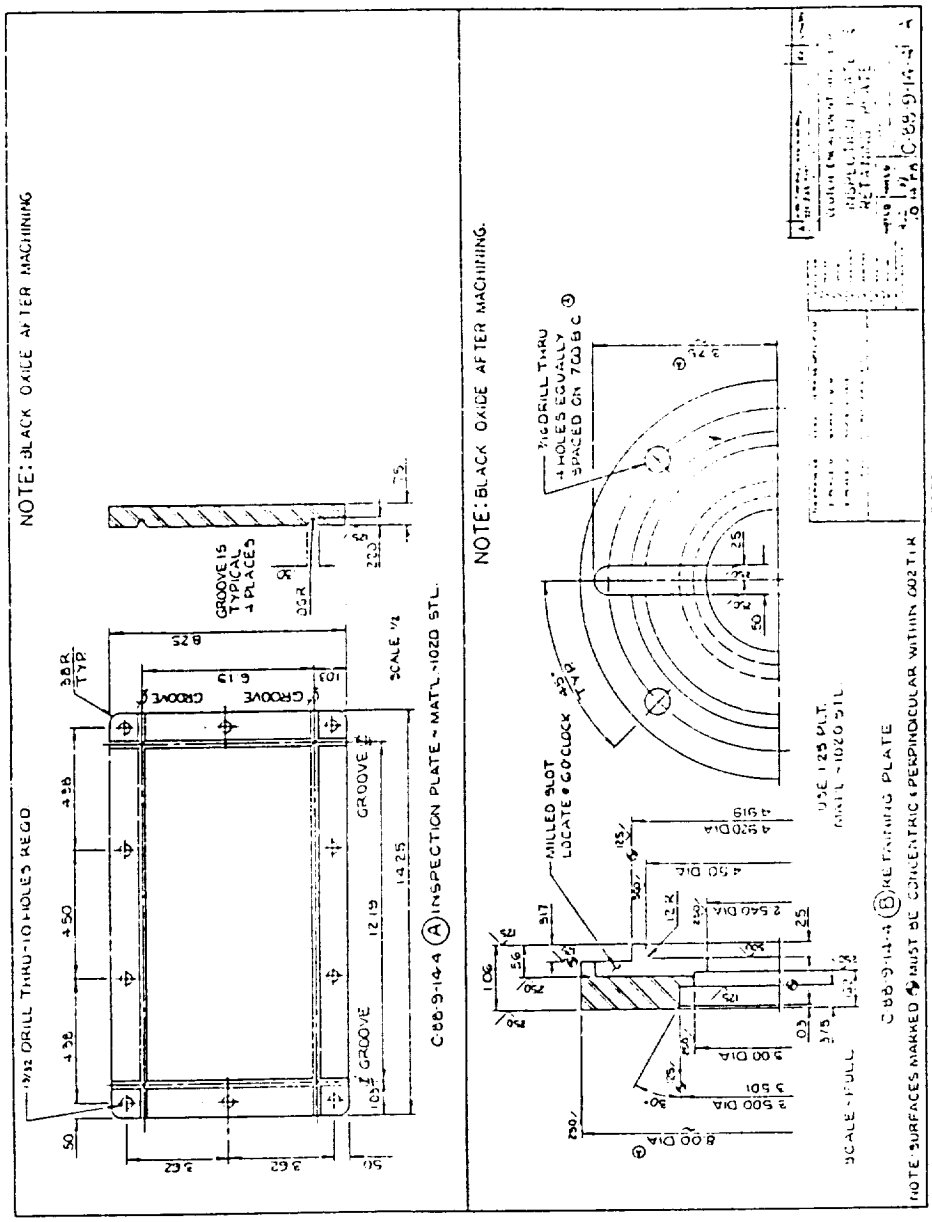

Figure 14. Drawing C-88-9-14-4. Test rig inspection plate and outer bearing retaining plate.

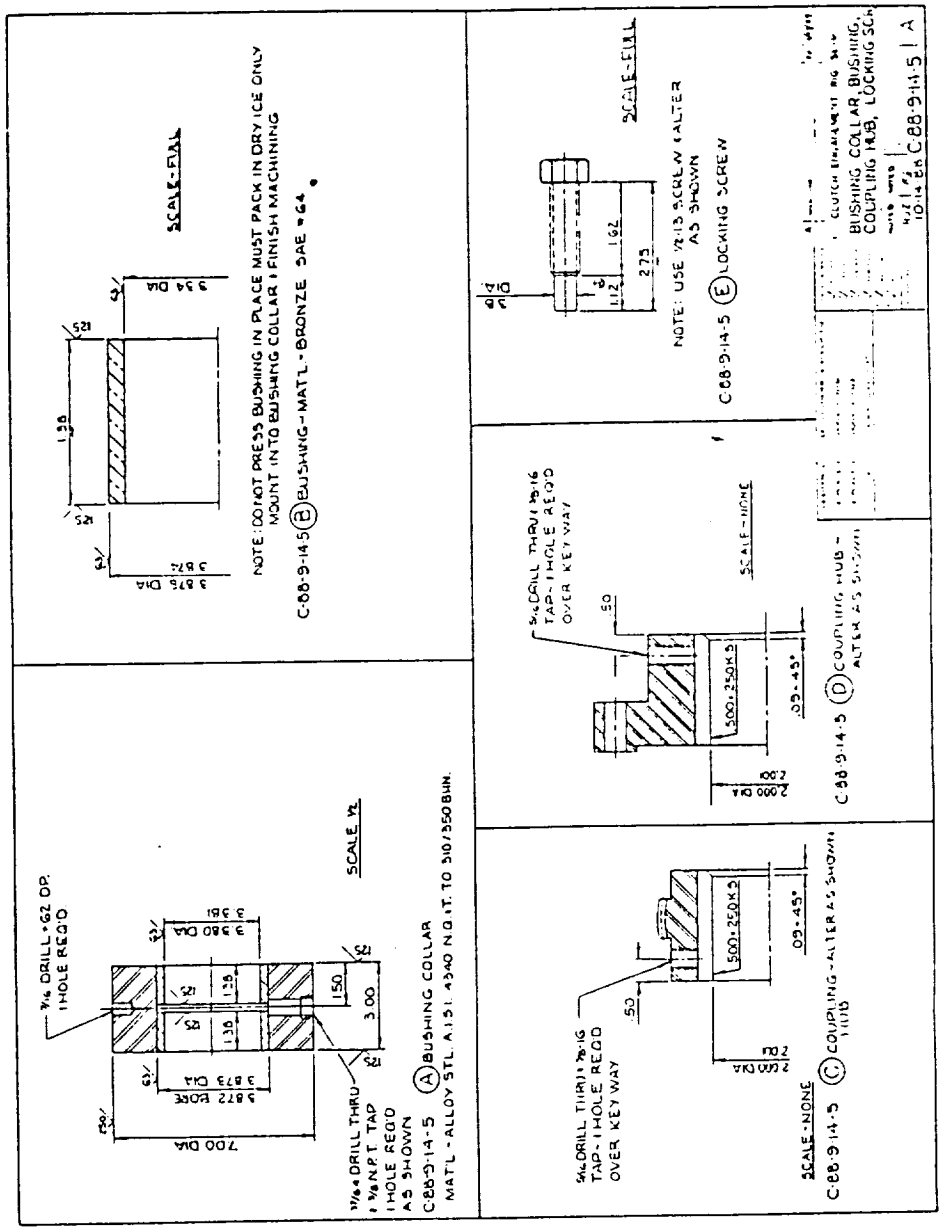

Figure 15. Drawing C-88-9-14-5. Lubrication bushing collar, bronze bushing, coupling hubs, and locking screw.

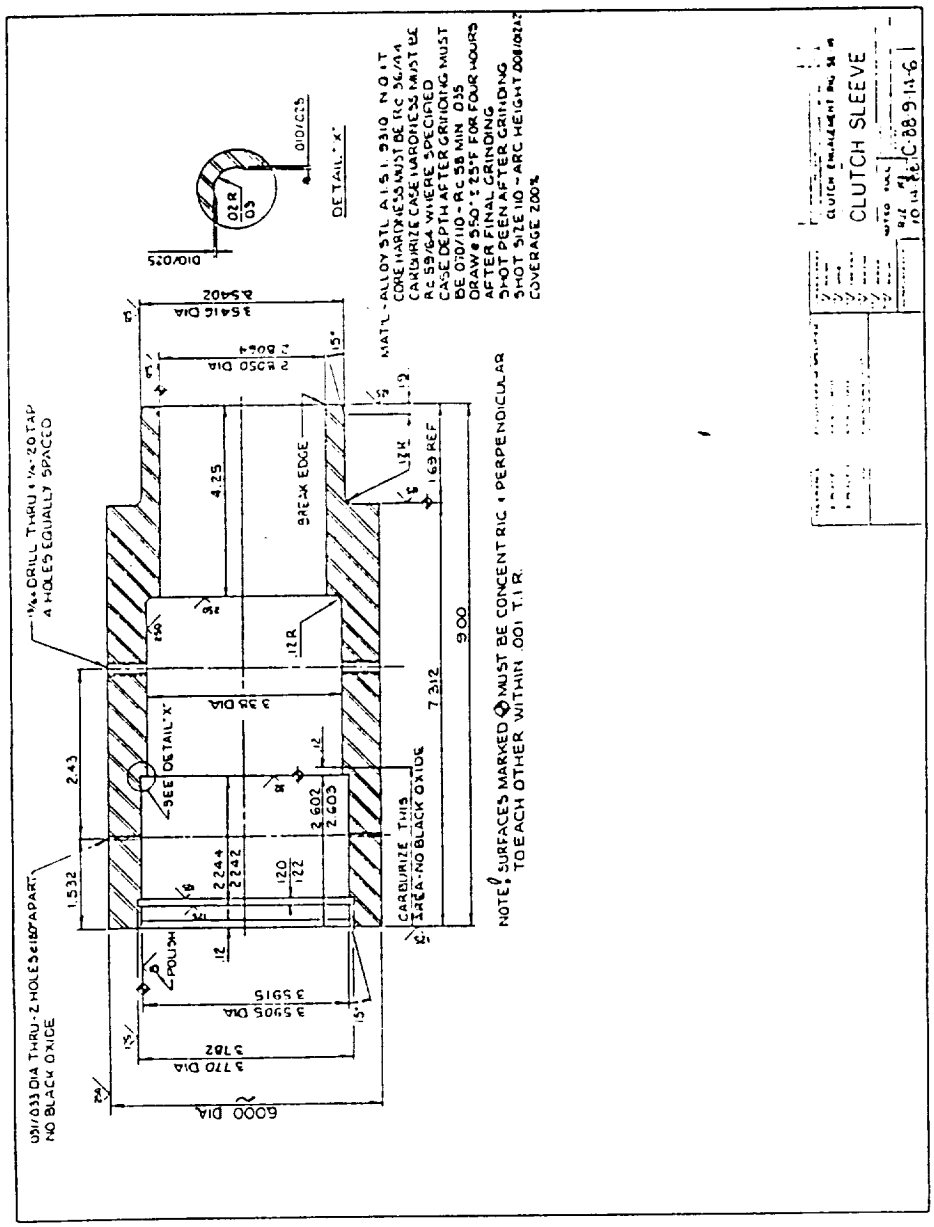

Figure 16. Drawing C-88-9-14-6. Outer sprag clutch sleeve.

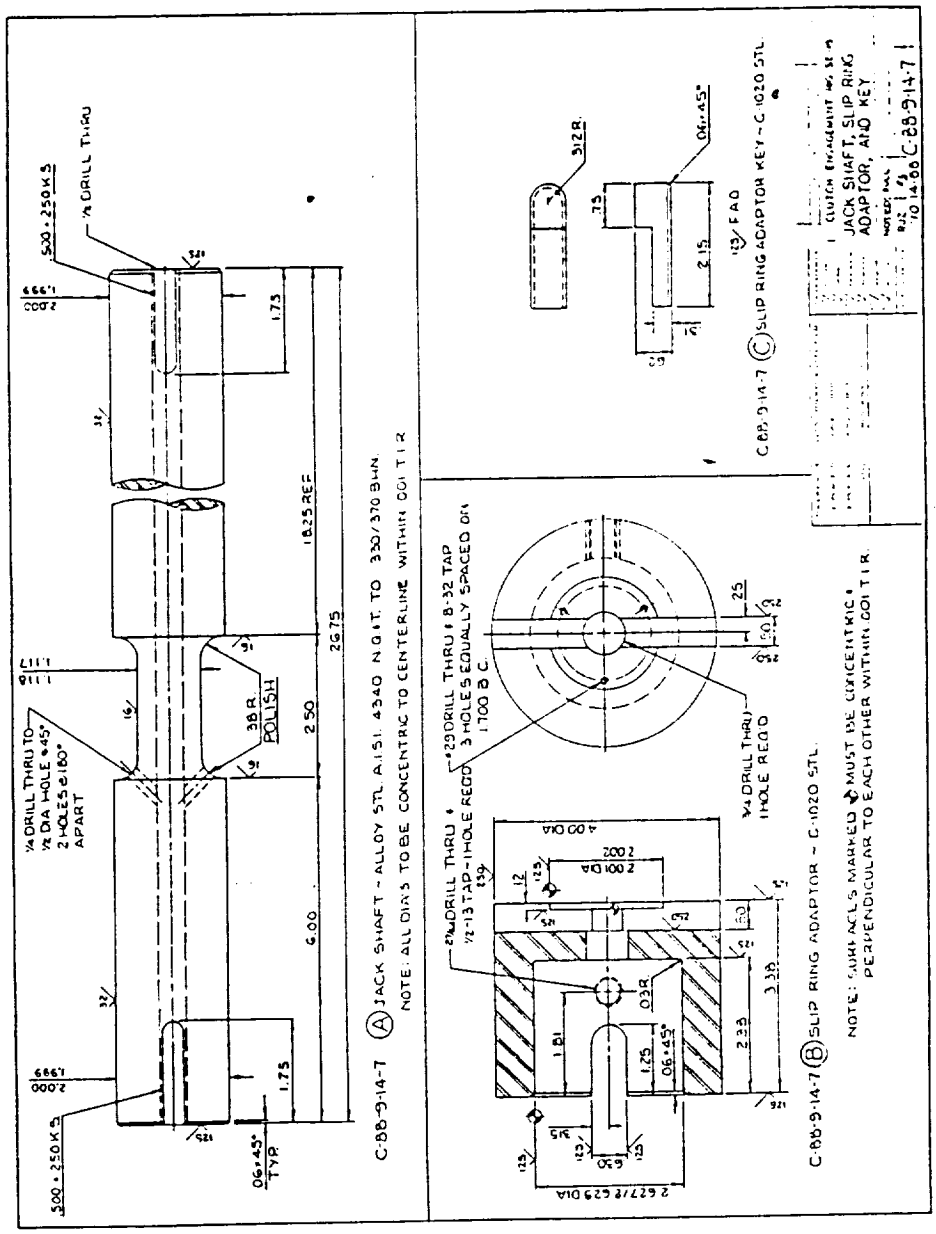

Figure 17. Drawing C-88-9-14-7. Torque transducer jack shaft, slip ring adaptor, and drive key.

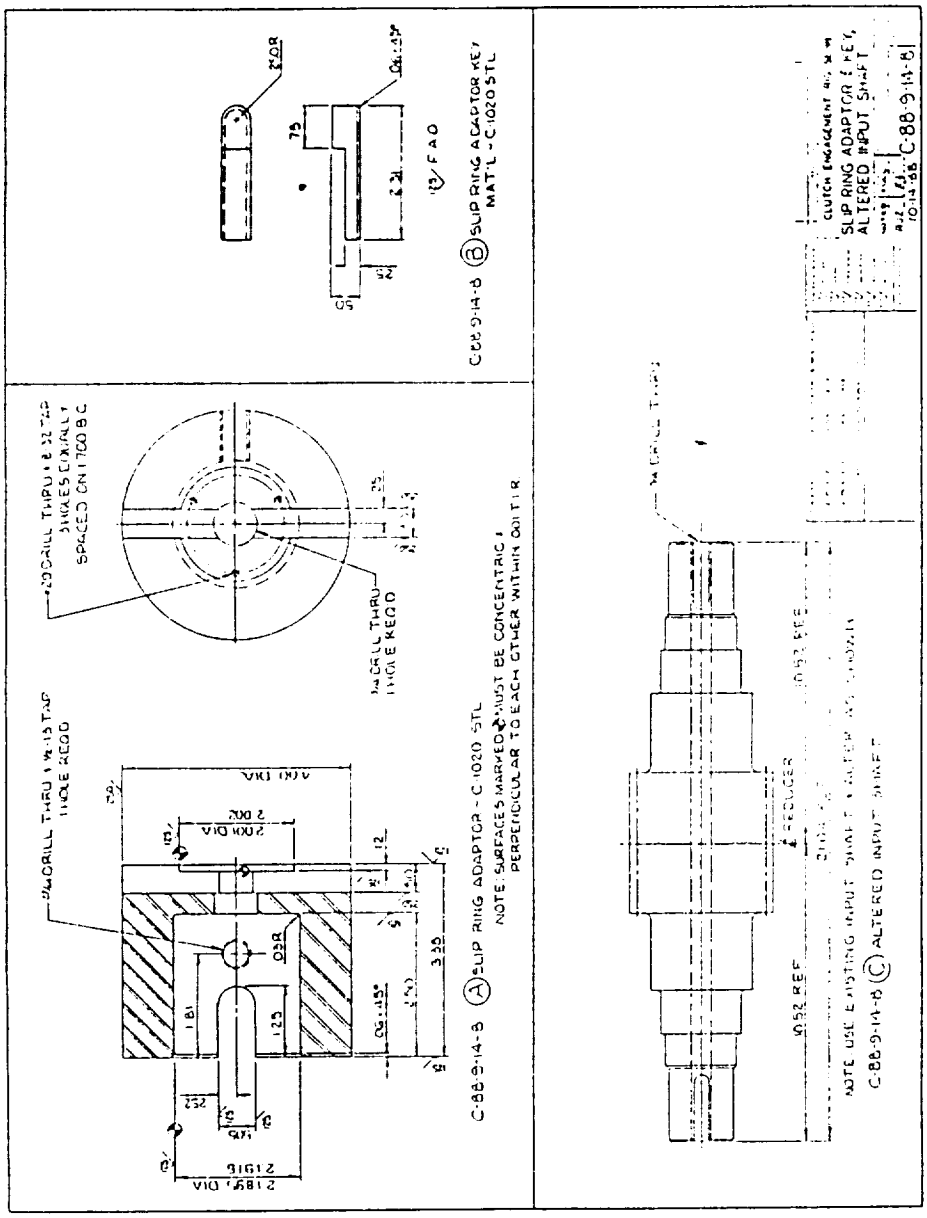

Figure 18. Drawing C-88-9-14-8. Slip ring adaptor, drive key, and increaser high speed shaft modifications.

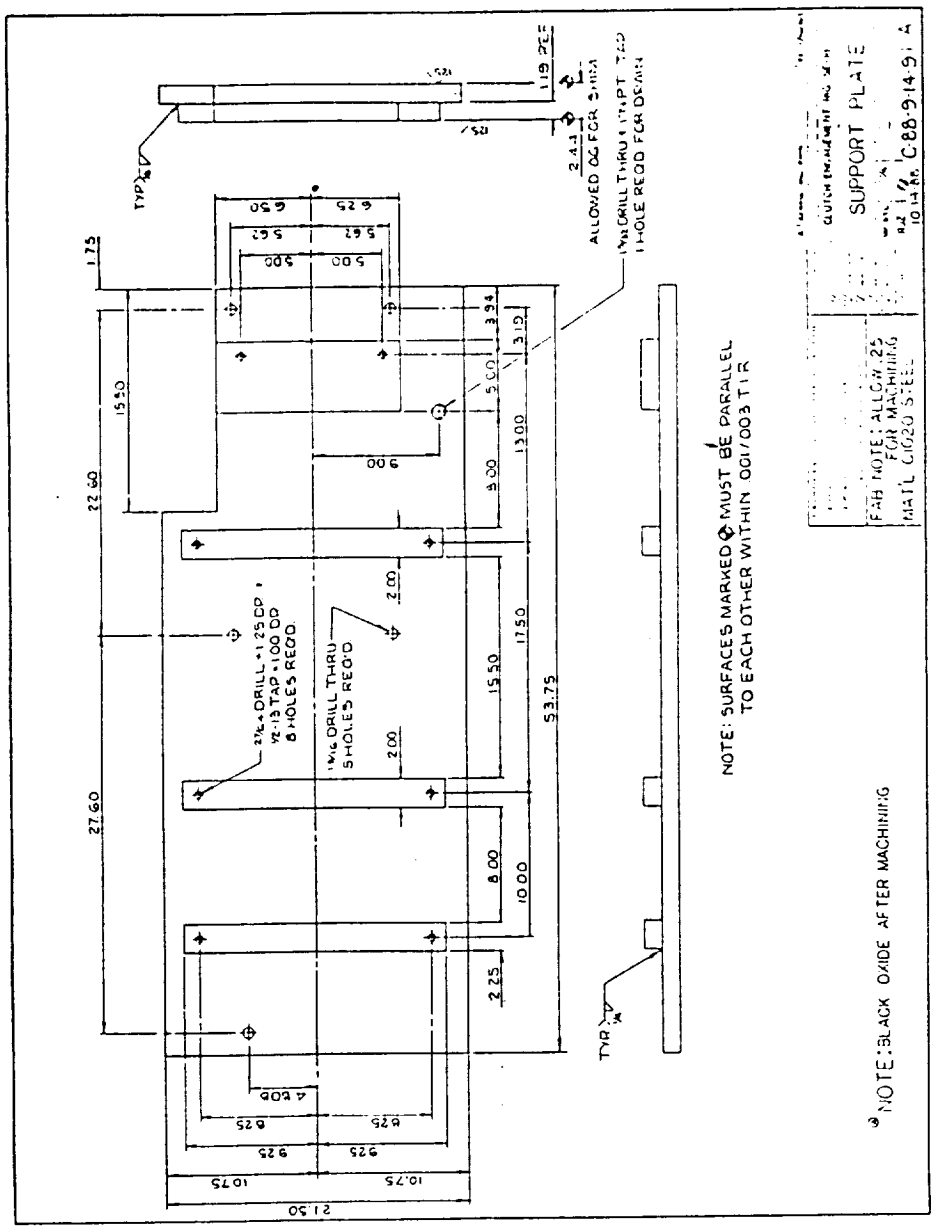

Figure 19. Drawing C-88-9-14-9. Test rig support plate.

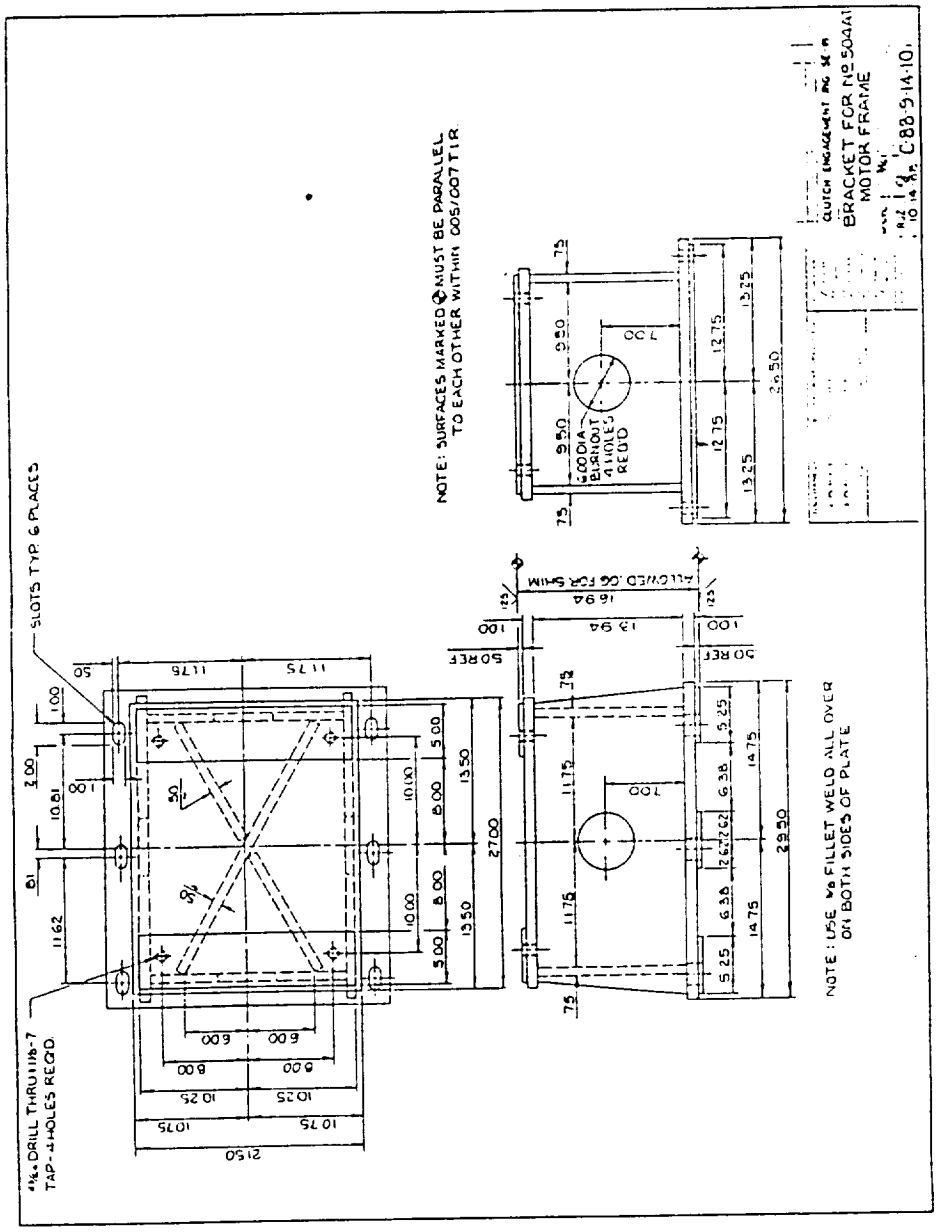

Figure 20. Drawing C-88-9-14-10. Motor stand for 200 hp DC motor with frame number 504AT.

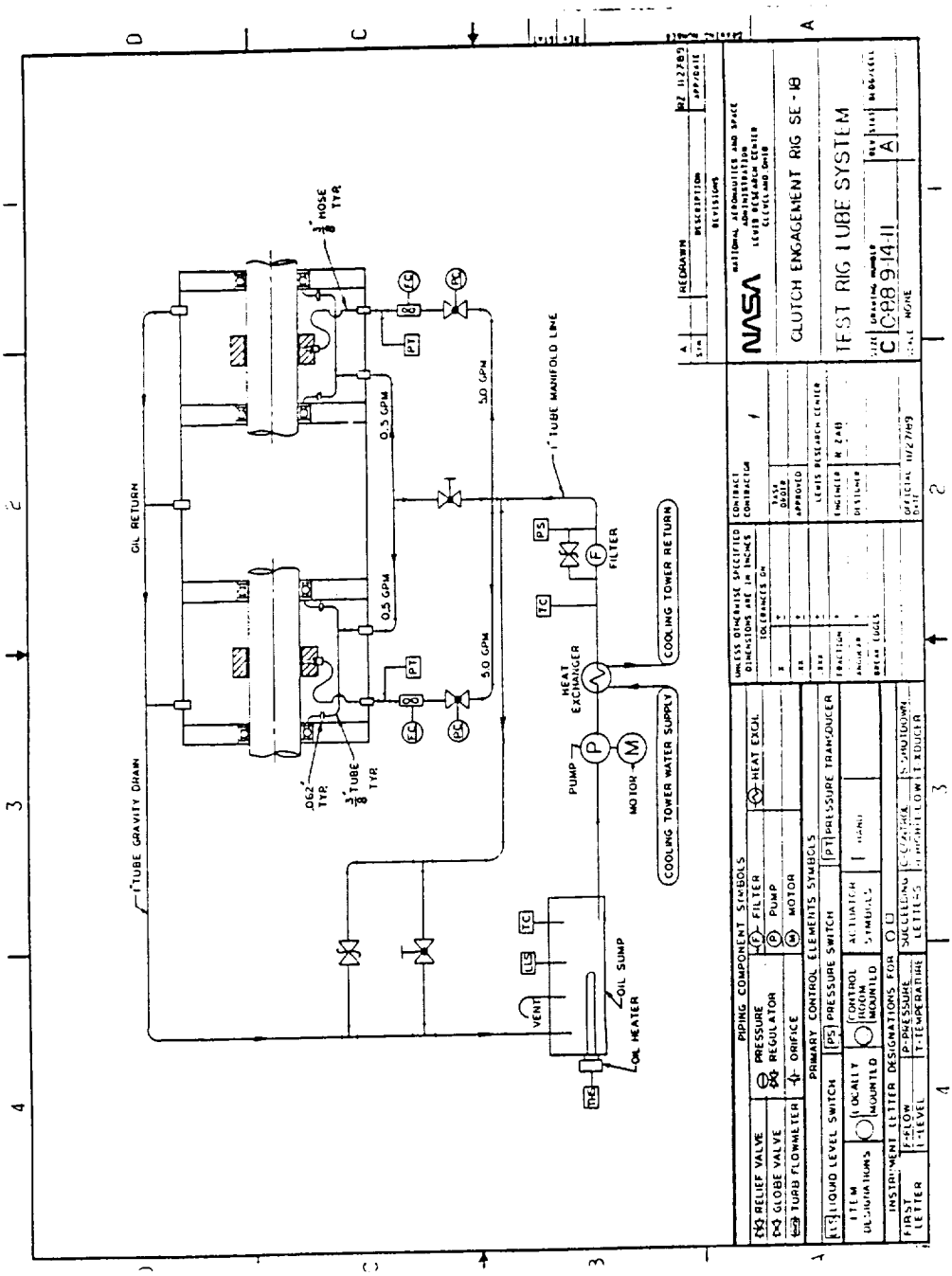

Figure 21. Drawing C-88-9-14-11. Test rig lubrication schematic.

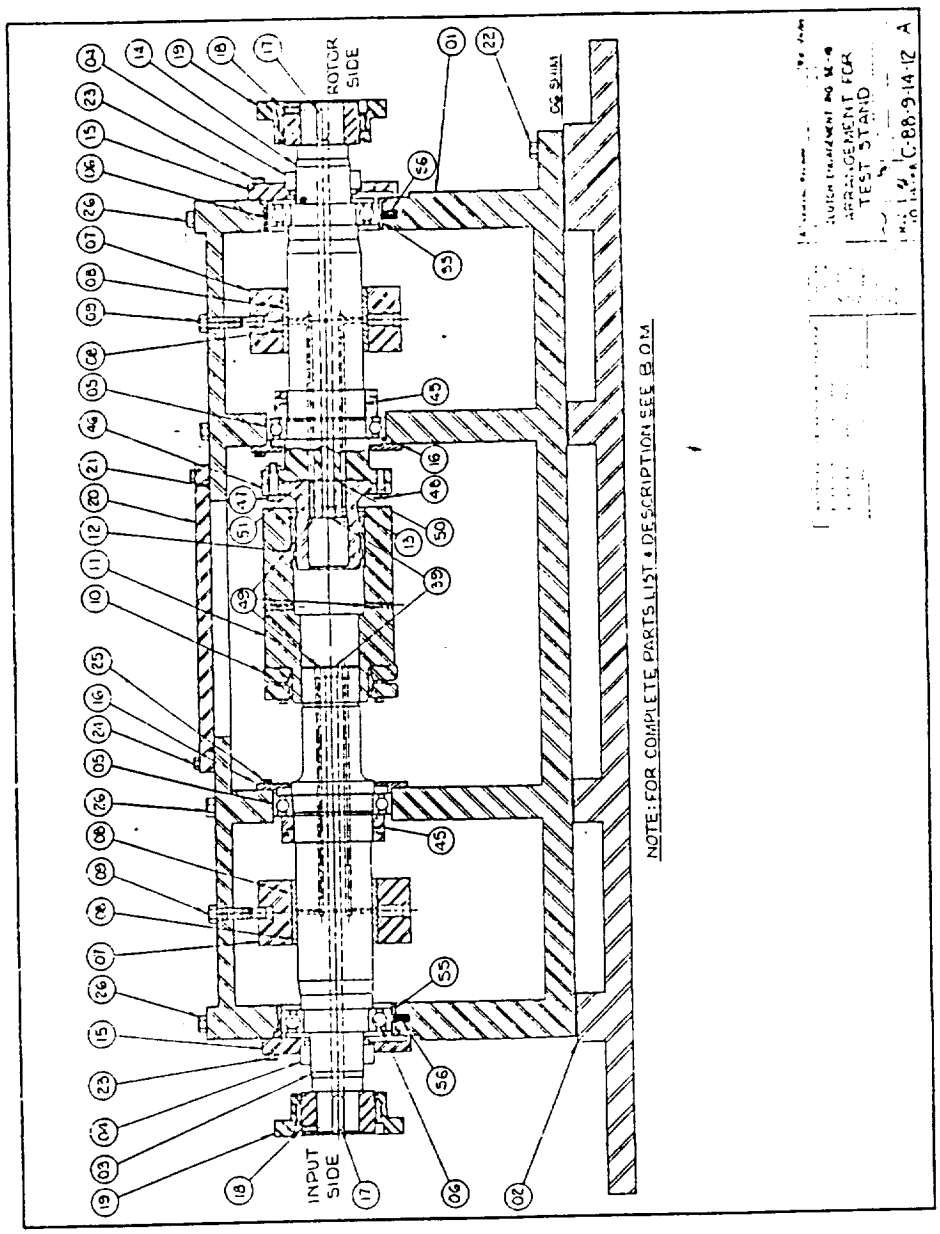

Figure 22. Drawing C-88-9-14-12. Arrangement for the final design of the test rig.

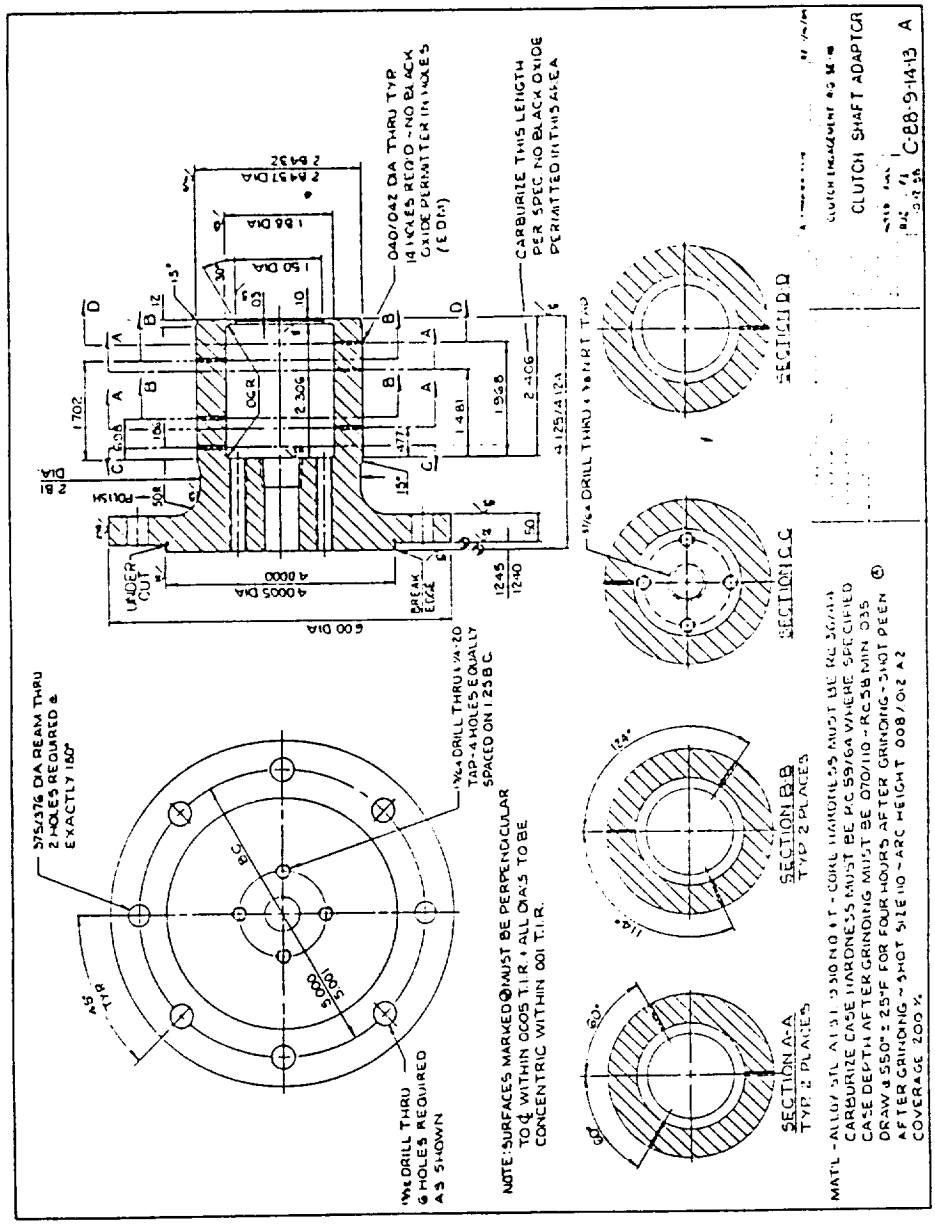

Figure 23. Drawing C-88-9-14-13. Sprag clutch inner race adaptor.

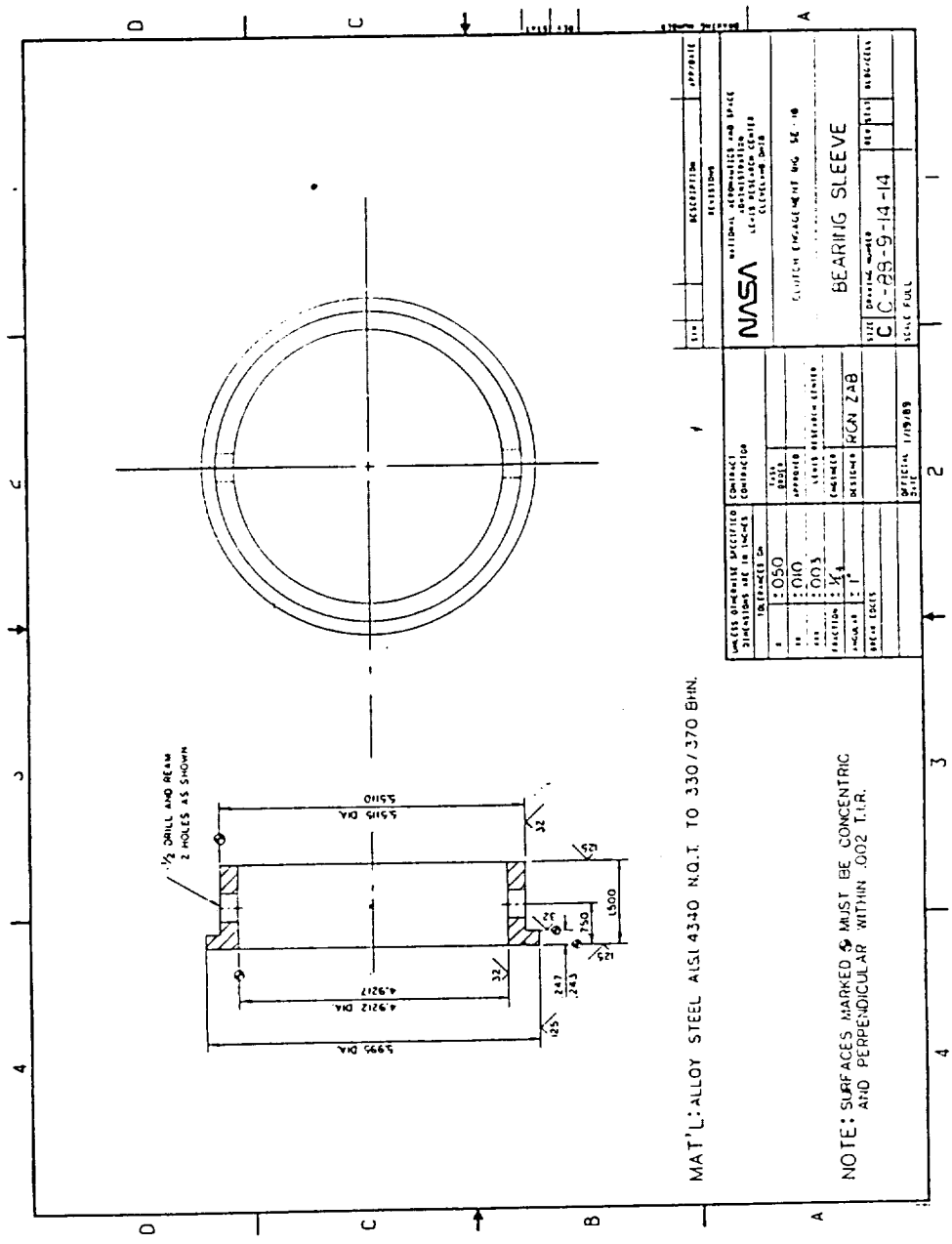

Figure 24. Drawing C-88-9-14-14. Outer bearing sleeve.

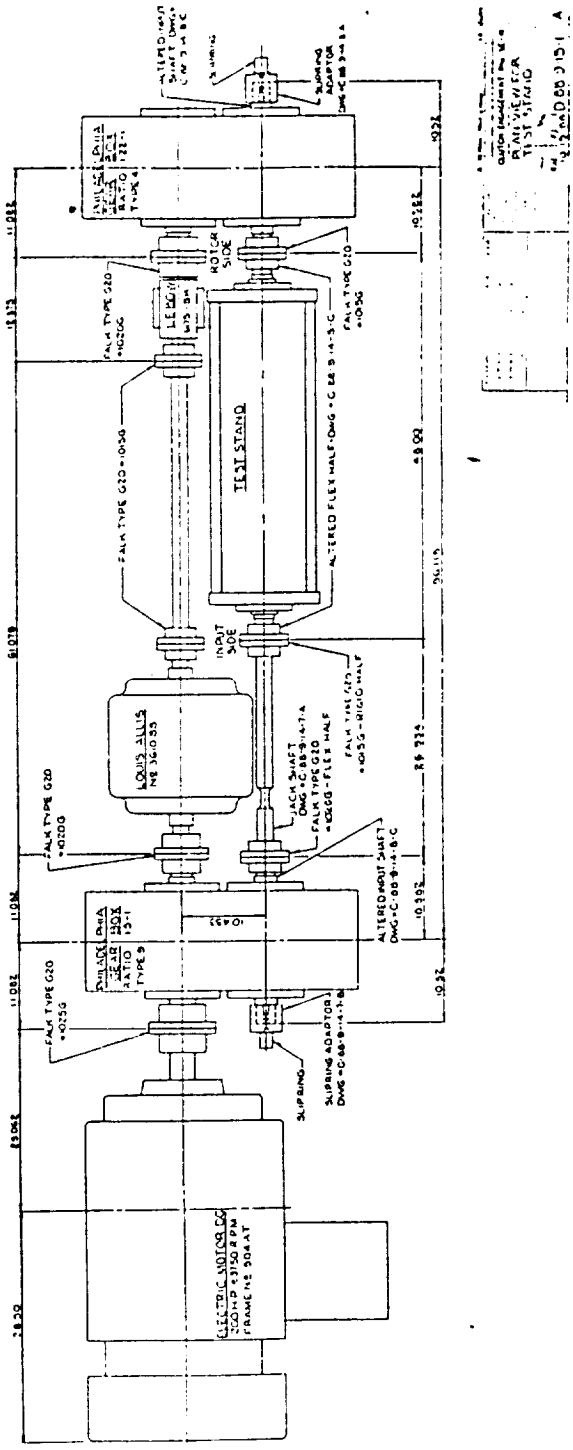

Figure 25. Drawing D-88-9-15-1. Plan view for the four square test rig.

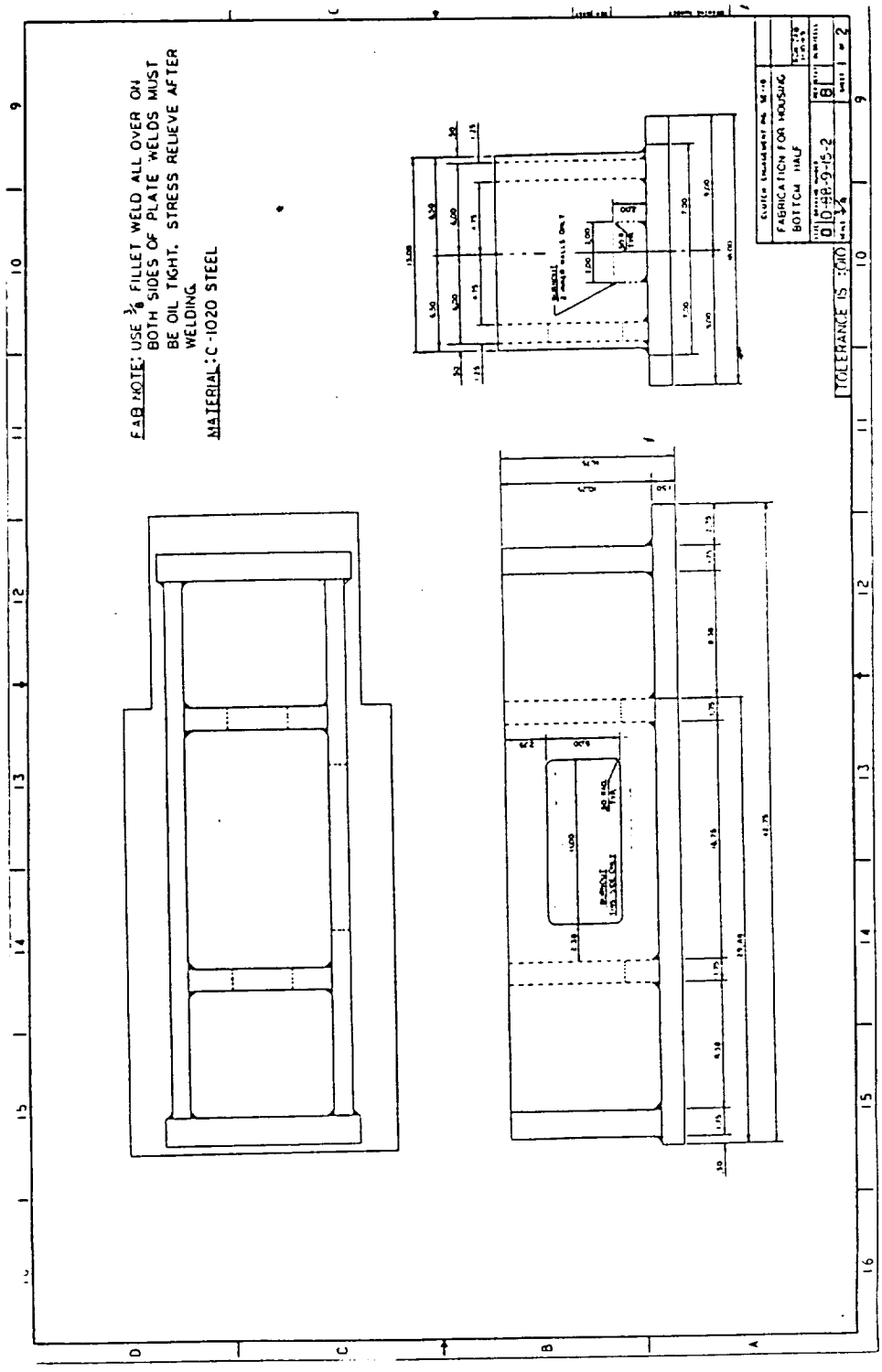

Figure 26. Drawing D-88-9-15-2. Weldment drawing for bottom half of test rig housing.

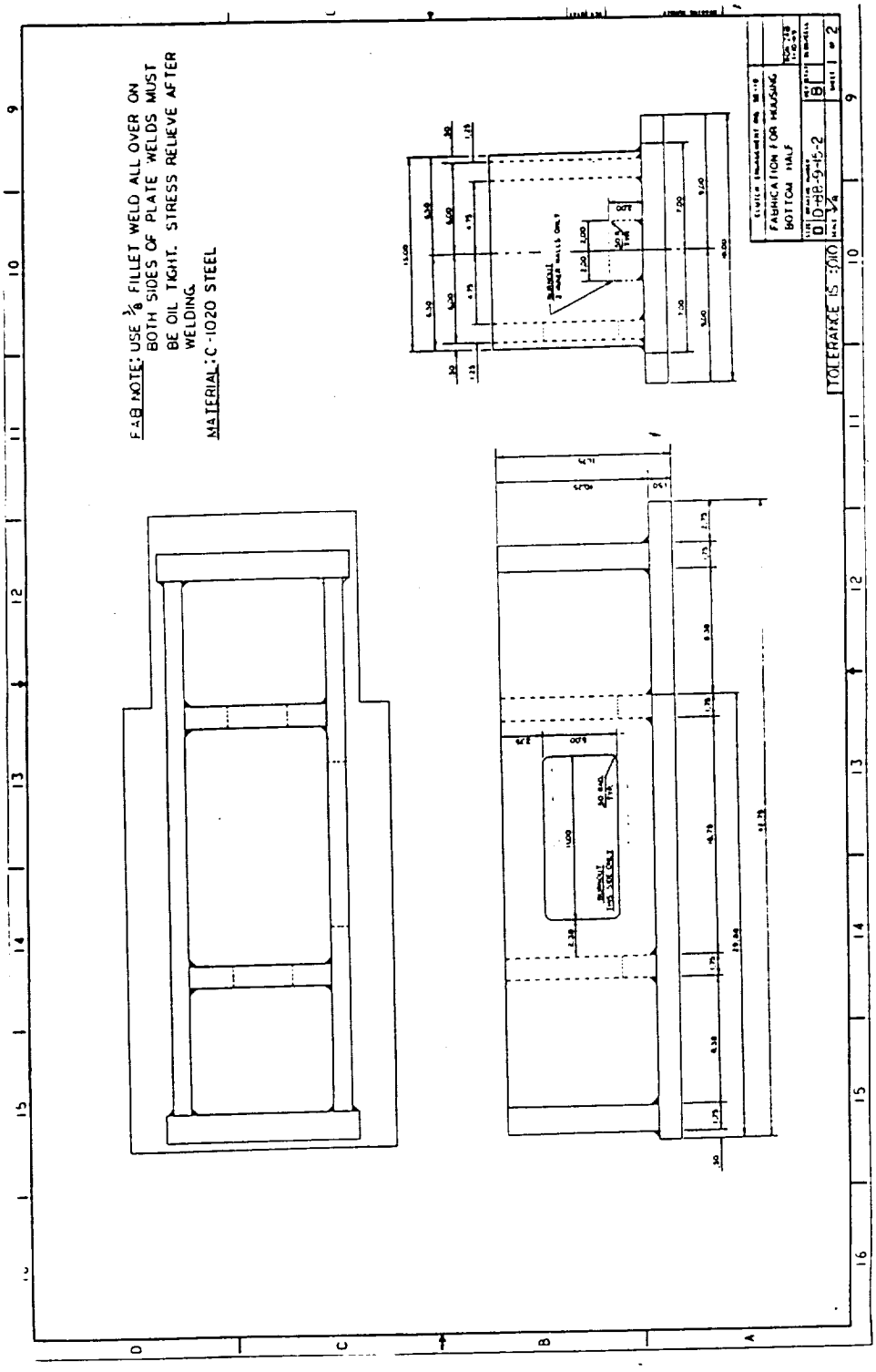

Figure 27. Drawing D-88-9-15-2. Weldment drawing for top half of test rig housing.

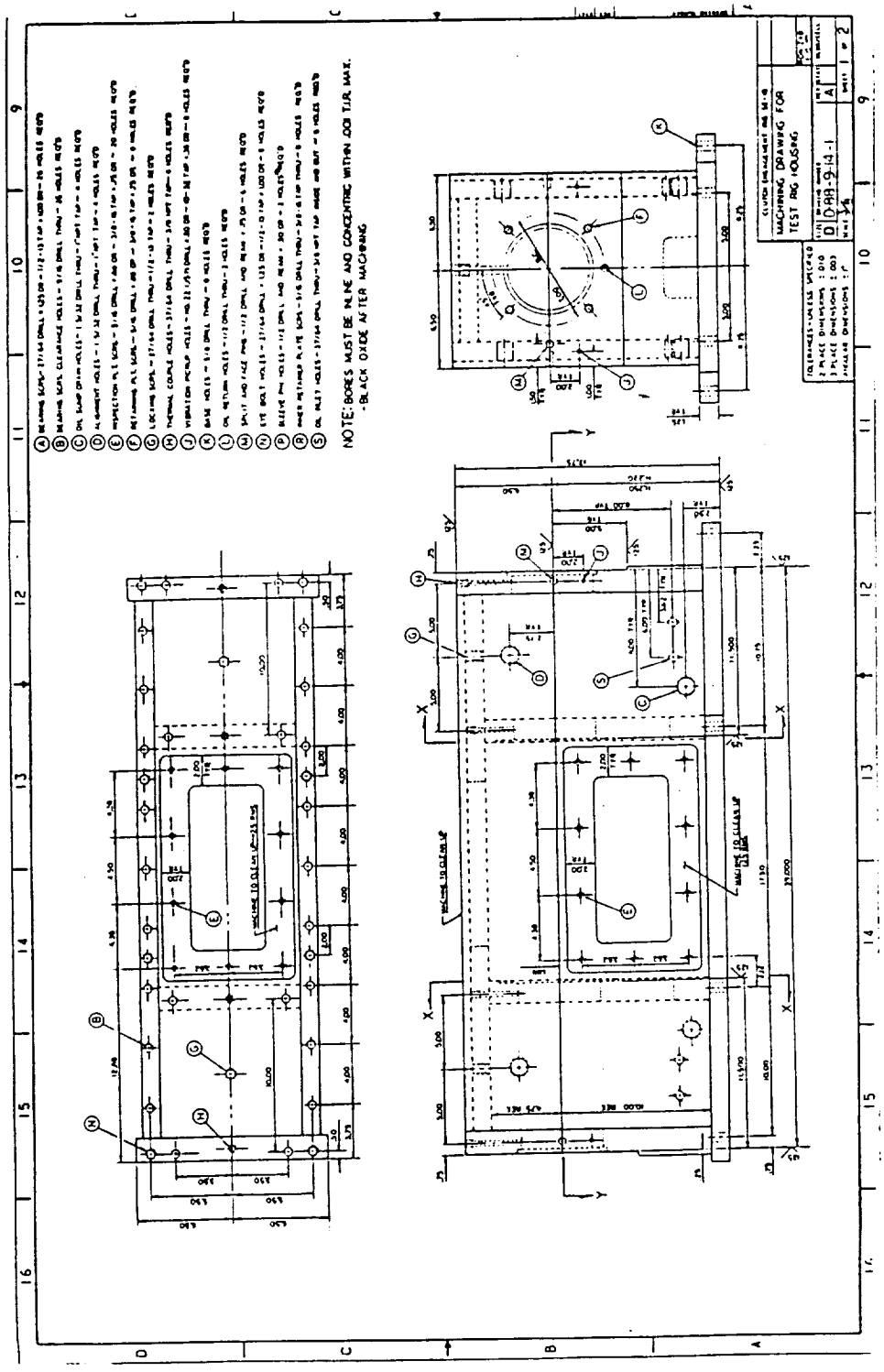

Figure 28. Drawing D-88-9-15-1. Machining drawing for the test rig housing. Sheet 1.

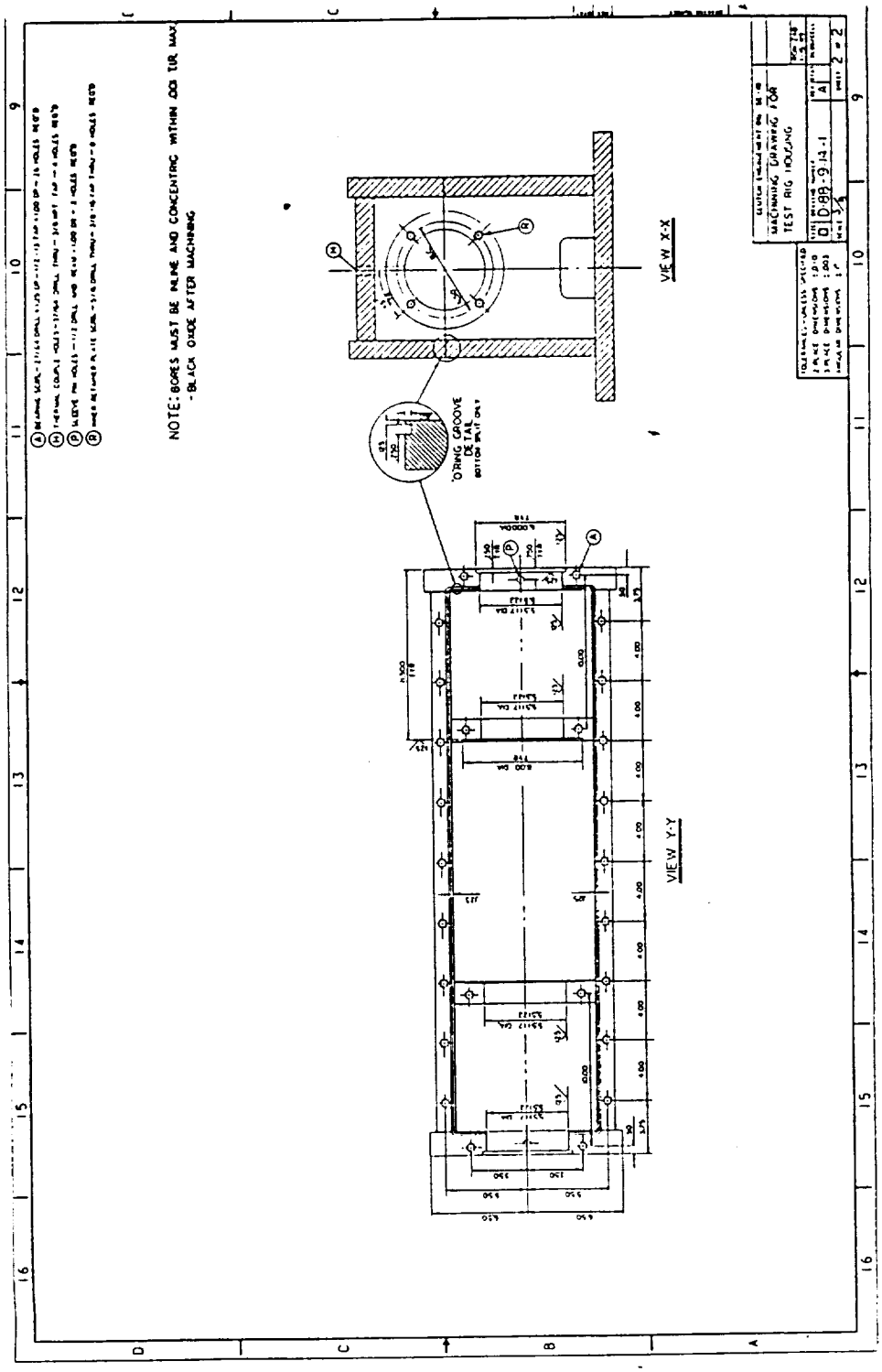

Figure 29. Drawing D-88-9-15-1. Machining drawing for the test rig housing. Sheet 2.

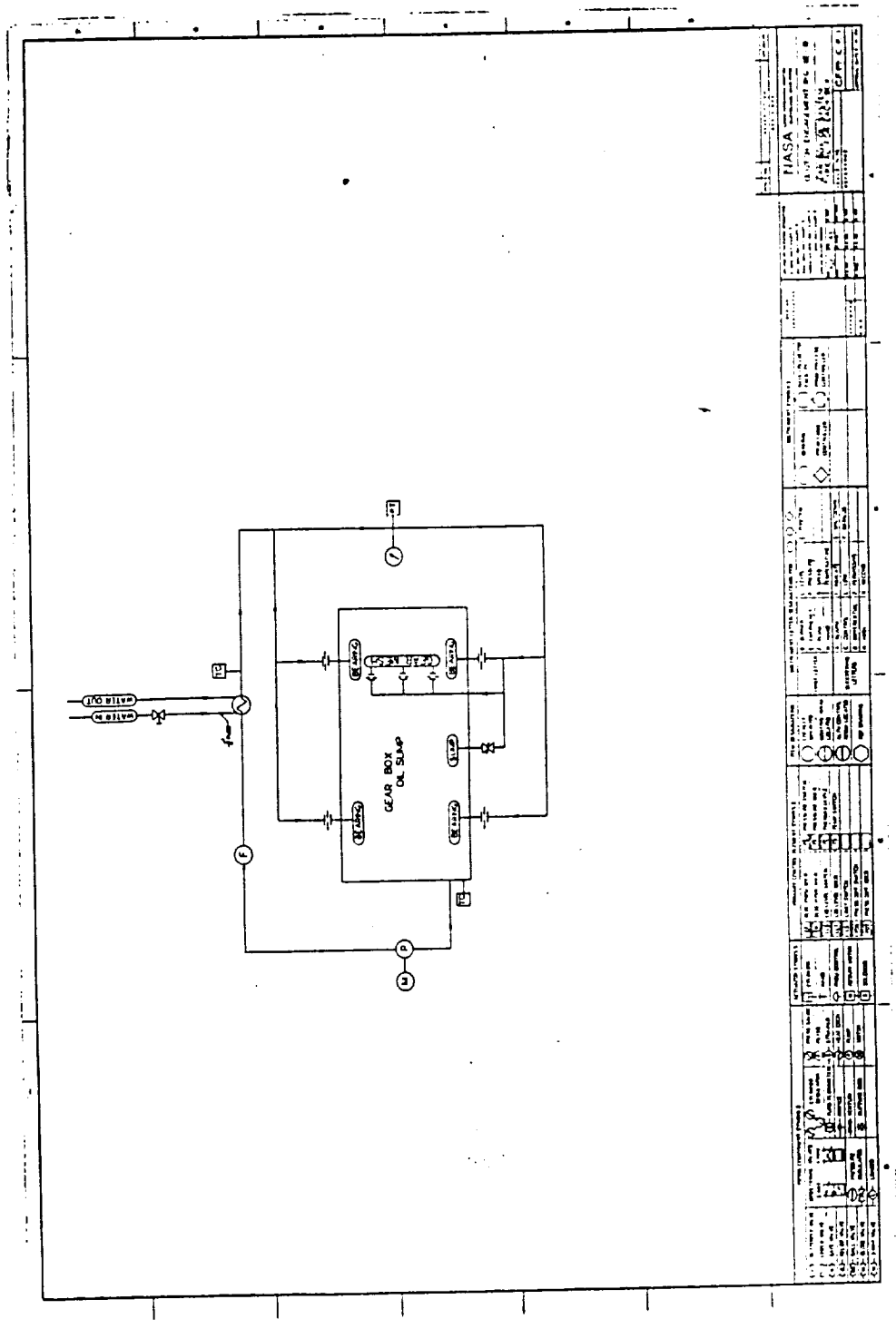

Figure 30. Drawing CF-88-10-16-1. Typical gear box oil system schematic.

Note: Gages to be placed 180 degrees apart on the necked down portion of the torque jack shaft. See figure 17.

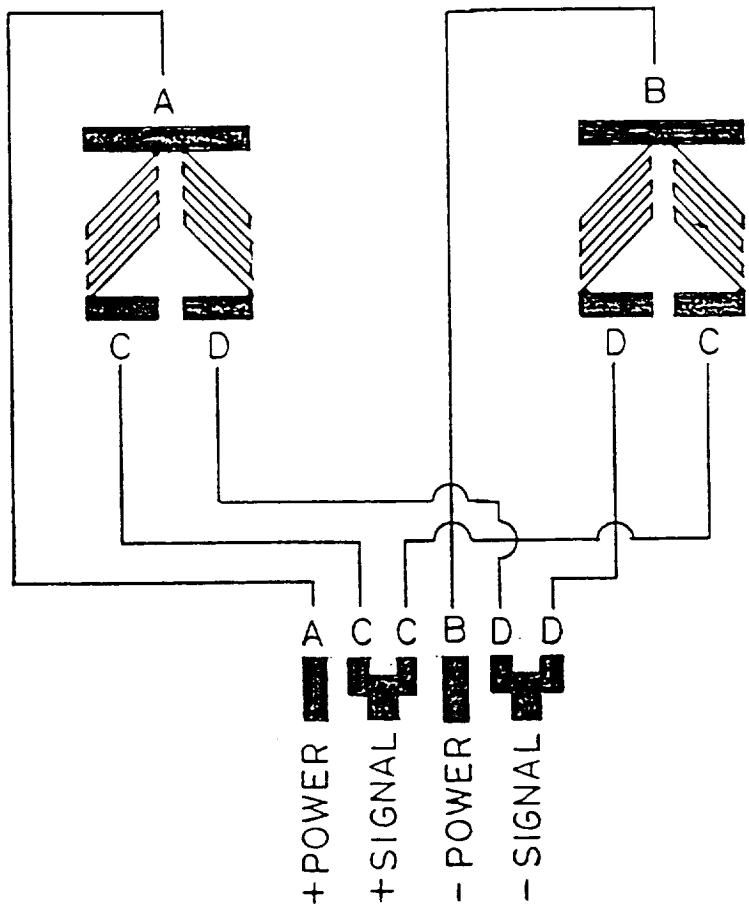

Figure 31. Torsional strain gage bridge wiring diagram.

---------- Generating Hob Parameters ----------

Factor for addendum of Gear		1.0000
Factor for addendum of Generating Hob		1.4000
Factor for D+F - Generating Hob		2.4000
Basic helix angle - Generating Hob		0.0000
Normal press. angle of Generating Hob		20.0000
Factor for top corner radius		0.3939
Generating Hob tip radius		0.0985
Hob D+F	(TDF/TDP)	0.6000
Hob addendum		0.3500
Hob code number		7

HELICAL GEAR SET on STANDARD CENTERS with 0/DP modified addendum

	NORMAL	TRANSVERSE
DIAMETRAL PITCH	4.0000	3.8340
CIRCULAR PITCH	0.7854	0.8194
BASE PITCH	0.7380	0.7660
PRESSURE ANGLE	20.000 (20 0' 0")	20.793 (20 47' 36")
HELIX ANGLE	16.565 (16 33' 54")	
REFERENCE CENTER DISTANCE	10.4330	
FACE WIDTH	5.1130	
F/D RATIO OF PINION	0.5601	
GEAR RATIO	1.2857	
AXIAL PITCH	2.7548	
TOOL PITCH	4.0000	

	PINION	GEAR
NUMBER OF TEETH	35	45
BASE DIAMETER	8.5343	10.9727
ROOT DIAMETER	8.4143	11.0225
REFERENCE PITCH DIAMETER	9.1289	11.7371
OUTSIDE DIAMETER	9.6289	12.2371
WHOLE TOOTH	0.6073	0.6073
TRANS. TIP TOOTH THICKNESS	0.1934	0.1976
CLEARANCE	0.1073	0.1073
PINION CUTTER WITHDRAWAL	-0.0073	-0.0073
COEFF. OF PROFILE SHIFT	-0.0292	-0.0292
TOOTH SLIDING PARAMETER	0.4857	0.5277
MINIMUM HOB LENGTH	2.0430	2.0748
TT REDUCTION	0.0050 / 0.0080	0.0050/ 0.0080
TRANS. TT AT REFER. PD	0.4042 / 0.4012	0.4042/ 0.4012
SPAN MEASUREMENT	3.4544 / 3.4514	4.2320/ 4.2290
MEASURED OVER	5 TEETH	6 TEETH

Figure 32A. General gear geometry for the 1.2857 ratio gear increaser.

---------- AGMA RATING (421.06) ----------

TRANS. CONTACT RATIO	MP	1.611
FACE CONTACT RATIO	MF	1.856
TOTAL CONTACT RATIO	MT	3.467
MIN. LENGTH OF CONTACT	LMIN	8.392
CONTACT LINE ANGLE	NV	5.809
LENGTH OF ACTION	Z	1.234
NUMBER GROUND OR SKIVED		2
BLANK TEMPERATURE		125
AGMA OIL GRADE NUMBER		6
CRITICAL SCORING NUMBER		12500

		PINION	GEAR
SURFACE FINISH	RMS	32.0000	32.0000
MINIMUM CASE DEPTH	IN.	0.0434	0.0434
MAXIMUM CASE DEPTH	IN.	0.1043	0.1043
SCORING NUMBER		14881.6034	13124.3406

REDUCTION SET NUMBER		1
NOMINAL DIAMETRAL PITCH	PD	3.834
ELASTIC COEFFICIENT	CP	2300.000
HARDNESS RATIO FACTOR	CH	1.000
SURFACE CONDITION FACTOR	CF	1.000

		DURABILITY	STRENGTH
LOAD DIST. FACTOR	CM,KM	1.3924	1.3702
DYNAMIC FACTOR	CV,KV	0.4850	0.6950
LIFE FACTOR PINION	CL,KL	1.0000	1.0000
LIFE FACTOR GEAR	CL,KL	1.0000	1.0000

		PINION	GEAR
LOAD ANGLE	ALPHA	25.5208	24.4565
TT AT CRIT SECTION	T	0.5068	0.5229
TH TO CRIT SECTION	H	0.4719	0.4743
X TO CRIT SECTION	X	0.1361	0.1441
HELICAL FACTOR	Ch	1.3053	1.3053
STRESS CORR. FACTOR	KF	1.473	1.5027
FORM FACTOR	Y	0.5552	0.5812
GEOM. FACTOR DURABILITY	I	0.1532	0.1532
GEOM. FACTOR STRENGTH	J	0.5670	0.5832
PITCH LINE VELOCITY	VT	11949.67 FPM	11949.67 FPM
BRINELL NUMBER		555 BHN	555 BHN
AGMA QUALITY LEVEL		12	12
ALLOW. CONTACT STRESS	Sac	146900 PSI	146900 PSI
ALLOW. BENDING STRESS	Sat	47100 PSI	50400 PSI
APPLIED SPEED	NP	5000.00 RPM	3888.89 RPM
ALLOW. POWER DURABILTY	Pac	3681.00 HP	3681.00 HP
ALLOW. POWER STRENGTH	Pat	7060.00 HP	7770.00 HP

Figure 32B. AGMA horsepower rating for the 1.2857 ratio gear increaser.

---------- Generating Hob Parameters ----------

Factor for addendum of Gear	1.0000
Factor for addendum of Generating Hob	1.4000
Factor for D+F - Generating Hob	2.4000
Basic helix angle - Generating Hob	0.0000
Normal press. angle of Generating Hob	20.0000
Factor for top corner radius	0.3939
Generating Hob tip radius	0.0788
Hob D+F (TDF/TDP)	0.4800
Hob addendum	0.2800
Hob code number	7

HELICAL GEAR SET on STANDARD CENTERS with 0/DP modified addendum

	NORMAL	TRANSVERSE
DIAMETRAL PITCH	5.0000	4.7925
CIRCULAR PITCH	0.6283	0.6555
BASE PITCH	0.5904	0.6128
PRESSURE ANGLE	20.000 (20 0' 0")	20.793 (20 47' 36")
HELIX ANGLE		16.565 (16 33' 54")
REFERENCE CENTER DISTANCE		10.4330
FACE WIDTH		5.1130
F/D RATIO OF PINION		0.6126
GEAR RATIO		1.5000
AXIAL PITCH		2.2038
TOOL PITCH		5.0000

	PINION	GEAR
NUMBER OF TEETH	40	60
BASE DIAMETER	7.8028	11.7042
ROOT DIAMETER	7.7747	11.9479
REFERENCE PITCH DIAMETER	8.346	12.5196
OUTSIDE DIAMETER	8.7464	12.9196
WHOLE TOOTH	0.4858	0.4858
TRANS. TIP TOOTH THICKNESS	0.1566	0.1611
CLEARANCE	0.0858	0.0858
PINION CUTTER WITHDRAWAL	-0.0058	-0.0058
COEFF. OF PROFILE SHIFT	-0.0292	-0.0292
TOOTH SLIDING PARAMETER	0.4170	0.4690
MINIMUM HOB LENGTH	1.6483	1.6849
TT REDUCTION	0.0040 / 0.0060	0.0040/ 0.0060
TRANS. TT AT REFER. PD	0.3233 / 0.3213	0.3233/ 0.3213
SPAN MEASUREMENT	3.3698 / 3.3678	4.6139/ 4.6119
MEASURED OVER	6 TEETH	8 TEETH

Figure 32C. General gear geometry for the 1.5000 ratio gear increaser.

---------- AGMA RATING (421.06) ----------

TRANS. CONTACT RATIO	MP	1.644
FACE CONTACT RATIO	MF	2.320
TOTAL CONTACT RATIO	MT	3.964
MIN. LENGTH OF CONTACT	LMIN	8.254
CONTACT LINE ANGLE	NV	5.809
LENGTH OF ACTION	Z	1.008

NUMBER GROUND OR SKIVED	2
BLANK TEMPERATURE	125
AGMA OIL GRADE NUMBER	6
CRITICAL SCORING NUMBER	12500

		PINION	GEAR
SURFACE FINISH	RMS	32.0000	32.0000
MINIMUM CASE DEPTH	IN.	0.0424	0.0424
MAXIMUM CASE DEPTH	IN.	0.0835	0.0835
SCORING NUMBER		13684.3981	11173.2642

REDUCTION SET NUMBER		1
NOMINAL DIAMETRAL PITCH	PD	4.792
ELASTIC COEFFICIENT	CP	2300.000
HARDNESS RATIO FACTOR	CH	1.000
SURFACE CONDITION FACTOR	CF	1.000

		DURABILITY	STRENGTH
LOAD DIST. FACTOR	CM,KM	1.3924	1.2702
DYNAMIC FACTOR	CV,KV	0.4850	0.6950
LIFE FACTOR PINION	CL,KL	1.0000	1.0000
LIFE FACTOR GEAR	CL,KL	1.0000	1.0000

		PINION	GEAR
LOAD ANGLE	ALPHA	24.9309	23.4622
TT AT CRIT SECTION	T	0.4125	0.4306
TH TO CRIT SECTION	H	0.3784	0.3822
X TO CRIT SECTION	X	0.1124	0.1213
HELICAL FACTOR	Ch	1.3053	1.3053
STRESS CORR. FACTOR	KF	1.4911	1.5261
FORM FACTOR	Y	0.5697	0.6049
GEOM. FACTOR DURABILITY	I	0.1614	0.1614
GEOM. FACTOR STRENGTH	J	0.5690	0.5904
PITCH LINE VELOCITY	VT	10925.41 FPM	10925.41 FPM
BRINELL NUMBER		555 BHN	555 BHN
AGMA QUALITY LEVEL		12	12
ALLOW. CONTACT STRESS	Sac	146900 PSI	146900 PSI
ALLOW. BENDING STRESS	Sat	47100 PSI	50400 PSI
APPLIED SPEED	NP	5000.00 RPM	3333.33 RPM
ALLOW. POWER DURABILTY	Pac	3242.00 HP	3242.00 HP
ALLOW. POWER STRENGTH	Pat	5182.00 HP	5753.00 HP

Figure 32D. AGMA horsepower rating for the 1.5000 ratio gear increaser.

Shaft Load Analysis

Right Hand Pinion, Type 3

Teeth	35	TDP	3.834	NDP	4.000	HA. 16.563
Loca.	4.063	Ang	180.000	NPA	20.000	TPA 20.793
HP	200.000	RPM	5000.000	Torque (in-lbs)		2521.000
Tang. force			552.319	Sep force		209.730
Thrust for.			164.265	Pitch rad.		4.564

Resultant force 591 lbs at 290.8 degs (CW) or 69.2 degs (CCW)

---------- Sum of Forces on 8.1250 bearing spread ----------

Clockwise

Bearing A force is	276.45 lbs	at angle	272.61 degs
Bearing B force is	339.31 lbs	at angle	305.52 degs
Thrust reaction is	164.27 lbs	towards	bearing B

Counter clockwise

Bearing A force is	339.31 lbs	at angle	54.48 degs
Bearing B force is	276.45 lbs	at angle	87.39 degs
Thrust reaction is	164.27 lbs	towards	bearing A

Single Row Timkens Standard Mount Type No. 1

Bearing A	575 572	Bearing B	575 572
K Factor A	1.450	K Factor B	1.450
Rating 1 Row A	11200	Rating 1 Row B	11200
Lub life adj fac A	1.000	Lub life adj fac B	1.000
Oper. Temperature	170.0 F	Lub. Viscosity	1000. SUS

Clockwise

Eq. load on bearing A	276.45 lbs	
Thrust induced by bearing A	89.61 lbs	
Bearing A life	> 500000.00	hrs
Eq. load on bearing B	503.84 lbs	
Thrust induced by bearng B	253.87 lbs	
Bearing B life	> 500000.00	hrs

Counter clockwise

Eq. load on bearing A	503.84 lbs	
Thrust induced by bearing A	253.87 lbs	
Bearing A life	> 500000.00	hrs
Eq. load on bearing B	276.45 lbs	
Thrust induced by bearing B	89.61 lbs	
Bearing B life	> 500000.00	hrs

Figure 33A. Bearing load analysis and bearing life calculations for high speed shaft of 1.2857 ratio increaser.

Shaft Load Analysis

Left Hand Gear, Type 2

Teeth	45	TDP	3.834	NDP 4.000	HA. 16.563
Loca.	4.063	Ang	0.000	NPA 20.000	TPA 20.793
HP	200.000	RPM	3888.000	Torque (in-lbs)	3242.027
Tang. force			552.445	Sep. force	209.778
Thrust for.			164.303	Pitch rad.	5.869

Resultant force 591 lbs at 249.2 degs (CW) or 110.8 degs (CCW)

---------- Sum of Forces on 8.1250 earing spread ----------

Clockwise

Bearing A force is	276.57 lbs	at angle 272.86 degs
Bearing B force is	355.36 lbs	at angle 231.01 degs
Thrust reaction is	164.30 lbs	towards bearing B

Counter clockwise

Bearing A force is	355.36 lbs	at angle 128.99 degs
Bearing B force is	276.57 lbs	at angle 87.14 degs
Thrust reaction is	164.30 lbs	towards bearing A

Single Row Timkens Standard Mount Type No. 1

Bearing A	780 772	Bearing B	780 772
K Factor A	1.510	K Factor B	1.510
Rating 1 Row A	18700	Rating 1 Row B	18700
Lub life adj fac A	1.000	Lub life adj fac B	1.000
Oper. Temperature	170.0 F	Lub. Viscosity	1000. SUS

Clockwise

Eq. load on bearing A	276.57 lbs	
Thrust induced by bearing A	86.08 lbs	
Bearing A life	> 500000.00	hrs
Eq. load on bearing B	520.23 lbs	
Thrust induced by bearing B	250.39 lbs	
Bearing B life	> 500000.00	hrs

Counter clockwise

Eq. load on bearing A	520.23 lbs	
Thrust induced by bearing A	250.39 lbs	
Bearing A life	> 500000.00	hrs
Eq. load on bearing B	276.57 lbs	
Thrust induced by bearing B	86.08 lbs	
Bearing B life	> 500000.00	hrs

Figure 33B. Bearing load analysis and bearing life calculations for low speed shaft of 1.2857 ratio increaser.

Shaft Load Analysis

Right Hand Pinion, Type 3

Teeth	40	TDP	4.793	NDP 5.000	HA. 16.563
Loca.	4.063	Ang	180.000	NPA 20.000	TPA 20.793
HP	200.000	RPM	500.000	Torque (in-lbs)	2521.000
Tang. force			604.099	Sep. force	229.392
Thrust for.			179.665	Pith rad.	4.173

Resultant force 646 lbs at 290.8 degs (CW) or 69.2 degs (CCW)

---------- Sum of Forces on 8.1250 bearing spread ----------

Clockwise

Bearing A force is	302.88 lbs	at angle	274.24 degs
Bearing B force is	366.16 lbs	at angle	304.42 degs
Thrust reaction is	179.67 lbs	towards bearing B	

Counter clockwise

Bearing A force is	366.16 lbs	at angle	55.58 degs
Bearing B force is	302.88 lbs	at angle	85.76 degs
Thrust reaction is	179.67 lbs	towards bearing A	

Single Row Timkens Standard Mount Type No. 1

Bearing A	575 572	Bearing B	575 572
K Factor A	1.450	K Factor B	1.450
Rating 1 Row A	11200	Rating 1 Row B	11200
Lub life adj fac A	1.000	Lub life adj fac B	1.000
Oper. Temperature	170.0 F	Lub. Viscosity	1000. SUS

Clockwise

Eq. load on bearing A	302.88 lbs	
Thrust induced by bearing A	98.17 lbs	
Bearing A life	> 500000.00 hrs	
Eq. load on bearing B	549.33 lbs	
Thrust induced by bearing B	277.84 lbs	
Bearing B life	> 500000.00 hrs	

Counter clockwise

Eq. load on bearing A	549.33 lbs	
Thrust induced by bearing A	277.84 lbs	
Bearing A life	> 500000.00 hrs	
Eq. load on bearing B	02.88 lbs	
Thrust induced by bearing B	98.17 lbs	
Bearing B life	> 500000.00 hrs	

Figure 33C. Bearing load analysis and bearing life calculations for high speed shaft of 1.5000 ratio increaser.

Shaft Load Analysis

Left Hand Gear, Type 2

Teeth	60	TDP	4.793	NDP	5.000	HA. 16.563
Loca.	4.063	Ang	0.00	NPA	20.000	TPA 20.793
HP	200.000	RPM	3333.330	Torque (in-lbs)		3781.504
Tang. force			604.100	Sep. force		22.392
Thrust for.			179.665	Pitch rad.		6.260

Resutant force 646 lbs at 249.2 degs (CW) or 110.8 degs (CCW)

---------- Sum of Forces on 8.1250 bearing spread ----------

Clockwise

Bearing A force is	302.98 lbs	at angle 274.49 degs
Bearing B force is	394.08 lbs	at angle 230.04 degs
Thrust reaction is	179.67 lbs	towards bearing B

Counter clockwise

Bearing A force is	394.08 lbs	at angle 129.96 degs
Bearing B force is	302.98 lbs	at angle 85.51 degs
Thrust reaction is	179.67 lbs	towards bearing A

Single Row Timkens Standard Mount Type No. 1

Bearing A	780 772	Bearing B	780 772
K Factor A	1.510	K Factor B	1.510
Rating 1 Row A	18700	Rating 1 Row B	18700
Lub life adj fac A	1.000	Lub life adj fac B	1.000
Oper. Temperature	170.0 F	Lub. Viscosity	1000. SUS

Clockwise

Eq. load on bearing A	302.98 lbs	
Thrust induced by bearing A	94.31 lbs	
Bearing A life	> 500000.00 hrs	
Eq. load on bearing B	571.33 lbs	
Thrust induced by bearing B	273.97 ls	
Bearing B life	> 500000.00 hrs	

Counter clockwise

Eq. load on bearing A	571.33 lbs	
Thrust induced by bearing A	273.97 lbs	
Bearing A lite	> 500000.00 hrs	
Eq. load on bearing B	302.98 lbs	
Thrust induced by bearing B	94.31 lbs	
Bearing B life	> 500000.00 hrs	

Figure 33D. Bearing load analysis and bearing life calculations for low speed shaft of 1.5000 ratio increaser.

Shaft Load Analysis

Outer Sprag Clutch Bearing Analysis

---------- Sum of Forces on 9.190 bearing spread ----------

Clockwise and Counter clockwise
Bearing A force is 15.00 lbs at angle 270.00 degs
Bearing B force is 28.00 lbs at angle 270.00 degs

Single Row Ball Bearing

Bearing A FAG#B7214C.TPA.P4 Bearing B FAG#B7018C.TPA.P4
Rating 1 Row A 17000 Rating 1 Row B 16000

Clockwise and Counter Clockwise

Bearing A life > 100000.00 hrs
Bearing B life > 100000.00 hrs

==========

Shaft Load Analysis

Inner Sprag Clutch Bearing Analysis

---------- Sum of Forces on 9.190 bearing spread ----------

Clockwise and Counter clockwise
Bearing A force is 19.00 lbs at angle 270.00 degs
Bearing B force is 31.00 lbs at angle 270.00 degs

Single Row Ball Bearing

Bearing A FAG#B7214C.TPA.P4 Bearing B FAG#B7018C.TPA.P4
Rating 1 Row A 17000 Rating 1 Row B 16000

Clockwise and Counter Clockwise

Bearing A life > 100000.00 hrs
Bearing B life > 100000.00 hrs

Figure 34. Bearing load analysis and bearing life calculations for inner and outer sprag clutch shafts.

Location	Size & Type	Torque Capacity (inch-pounds)	Safety Factor
Motor to Reducer	2.5W Flex	47257	12.50
Reducer to Motor	2.5W Flex	73844	19.53
Reducer to Clutch	2.0W Flex	41922	11.09
Clutch to Reducer	2.0W Flex	25918	6.86
Clutch to Jack Shaft	1.5W Flex	20607	6.36
Jack Shaft to Clutch	1.5W Rigid	13646	4.21
Jack Shaft to Lebow	1.5W Flex	8332	2.57
Lebow to Jack Shaft	1.5W Rigid	10234	3.16
Lebow to Reducer	2.0W Flex	13720	4.23
Reducer to Lebow	2.0W Flex	41922	12.93
Reducer to Test Rig	2.0W Flex	40023	15.88
Test Rig to Reducer	2.0W Flex	19390	7.69
Test Rig to Jack Shaft	1.5W Flex	19390	7.69
Jack Shaft to Test Rig	1.5W Rigid	18190	7.22
Jack Shaft to Reducer	2.0W Flex	24387	9.67
Reducer to Jack Shaft	2.0W Rigid	25150	9.98

Figure 35. Torque capacity and safety factors for all the gear couplings on the four square rig.

Hub or gear material		Steel
Modulus of elasticity	(psi)	30.0E+06
Poisson's ratio		0.292
Coefficient of expansion		66.0E-07
Shaft or bushing material		Steel
Modulus of elasticity	(psi)	30.0E+06
Poisson's ratio		0.292
Coefficient of expansion		66.0E-07
Length of hub		1.94
Motor torque	(in-lbs)	3242.00
Service factor		1.00
Torque transmitted	(in-lbs)	3242.00
Type of key		Rectangular
Number of keys		1
Brinell hardness		310-360
Key length		1.94
Key width		0.31
Key depth		0.31

		Minimum	Maximum
O.D. of hub or gear	(in)	3.40000	3.40000
I.D. of hub or gear	(in)	1.37450	1.37500
O.D. of shaft or bushing	(in)	1.37450	1.37500
I.D. of shaft or bushing	(in)	0.00000	0.00000
Clearance fit	(in)	0.00050	-0.00050
Shaft strength (7000 allow)	(in-lb)	3569.13	3569.13
Press force required	(lb)	0.00	4588.31
Temp. required to sweat on gear	(F)	70.00	125.12
Torque carried by press fit	(in-lb)	0.00	3154.13
Key shear stress	(psi)	210.91	7781.20
Key compressive stress	(psi)	421.82	15562.40
Torque carried by key	(in-lb)	8332.91	8332.91
Tor. carried by key & press	(in-lb)	8332.91	11487.03
Safety factor		2.57	3.54

Figure 36. Typical press fit and key load analysis. This run is for the coupling between the jack shaft to Lebow torque transducer.

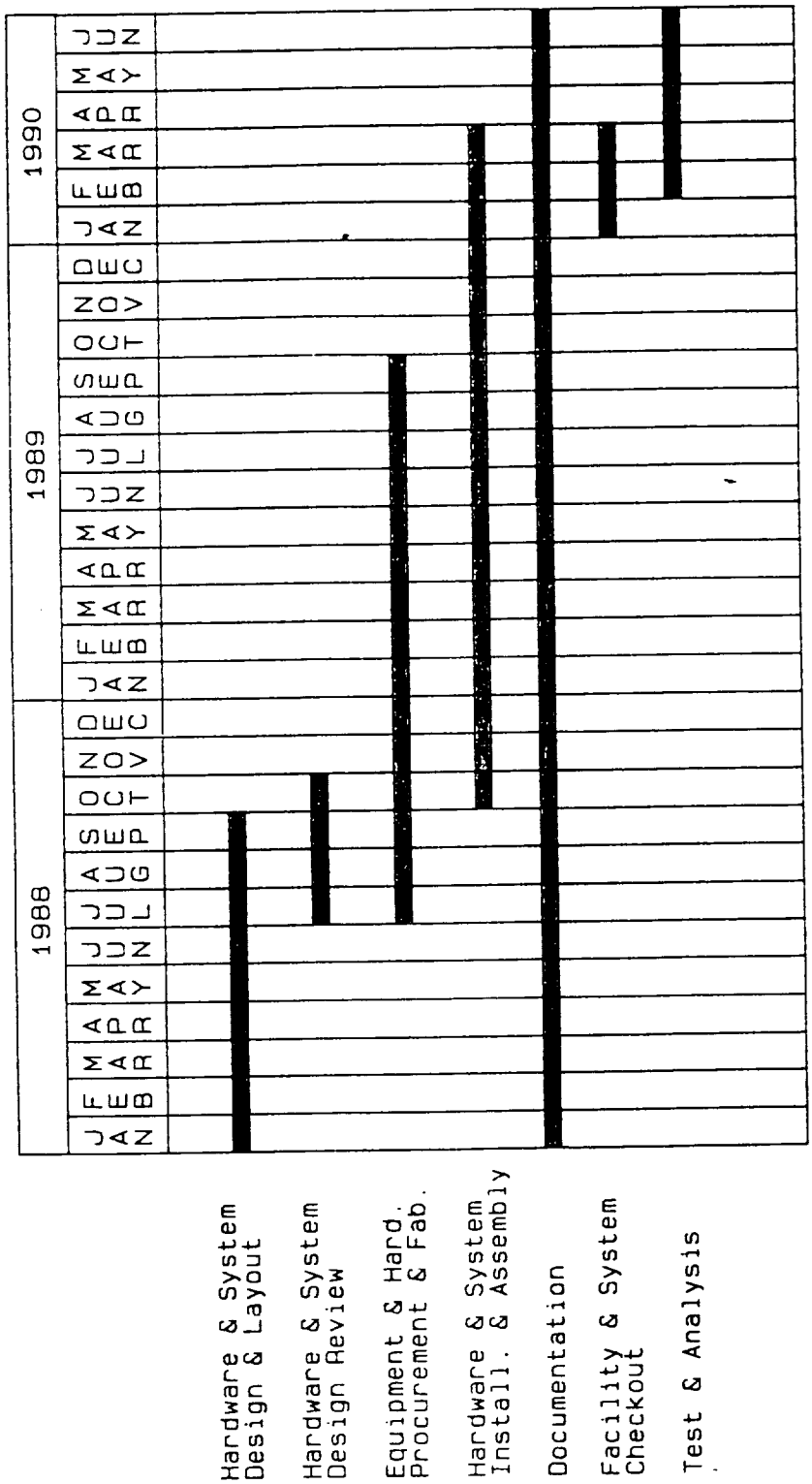

Figure 37. Clutch engagement rig project schedule.

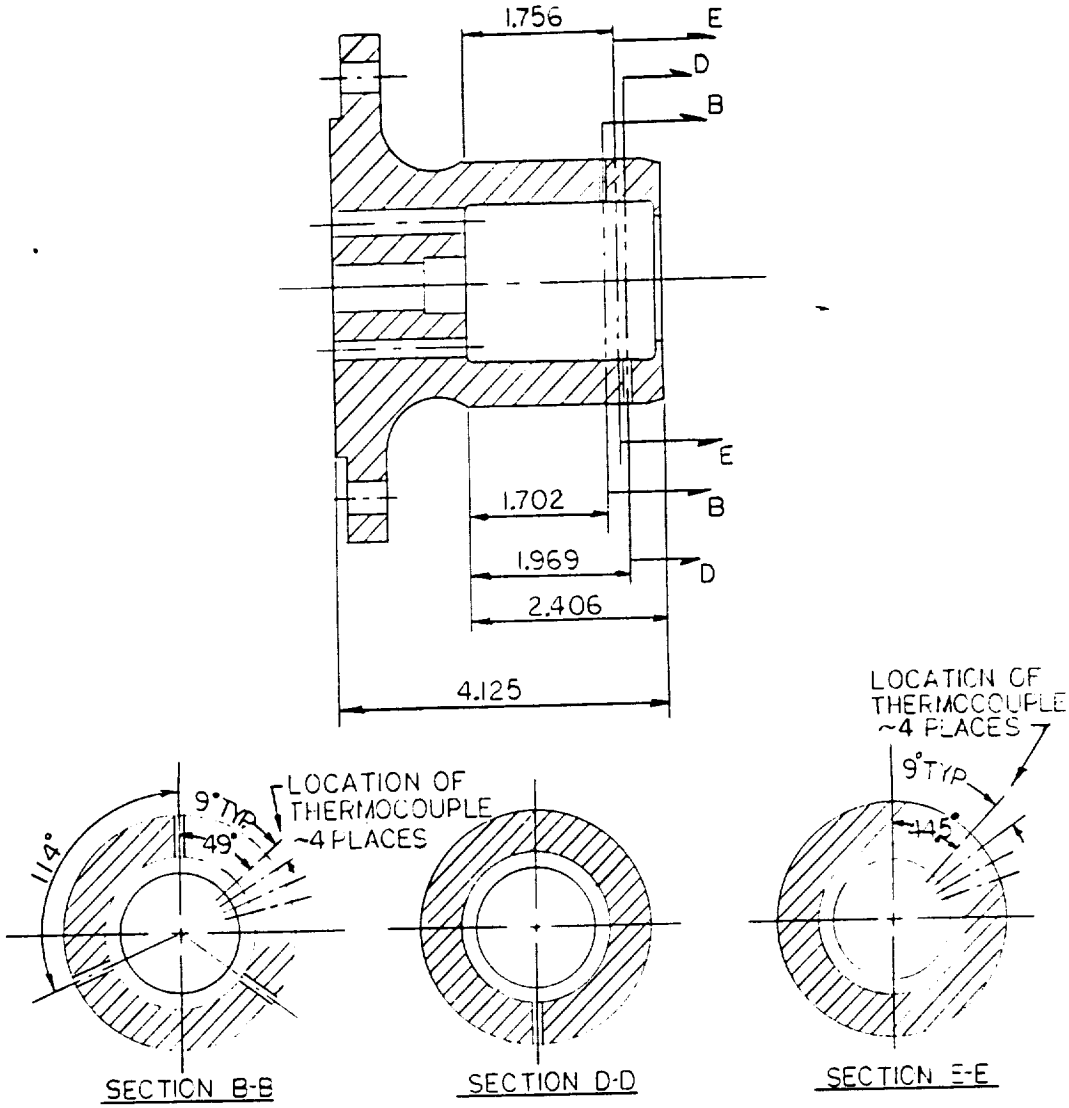

Figure 38. Location of thermocouples on the inner clutch race.

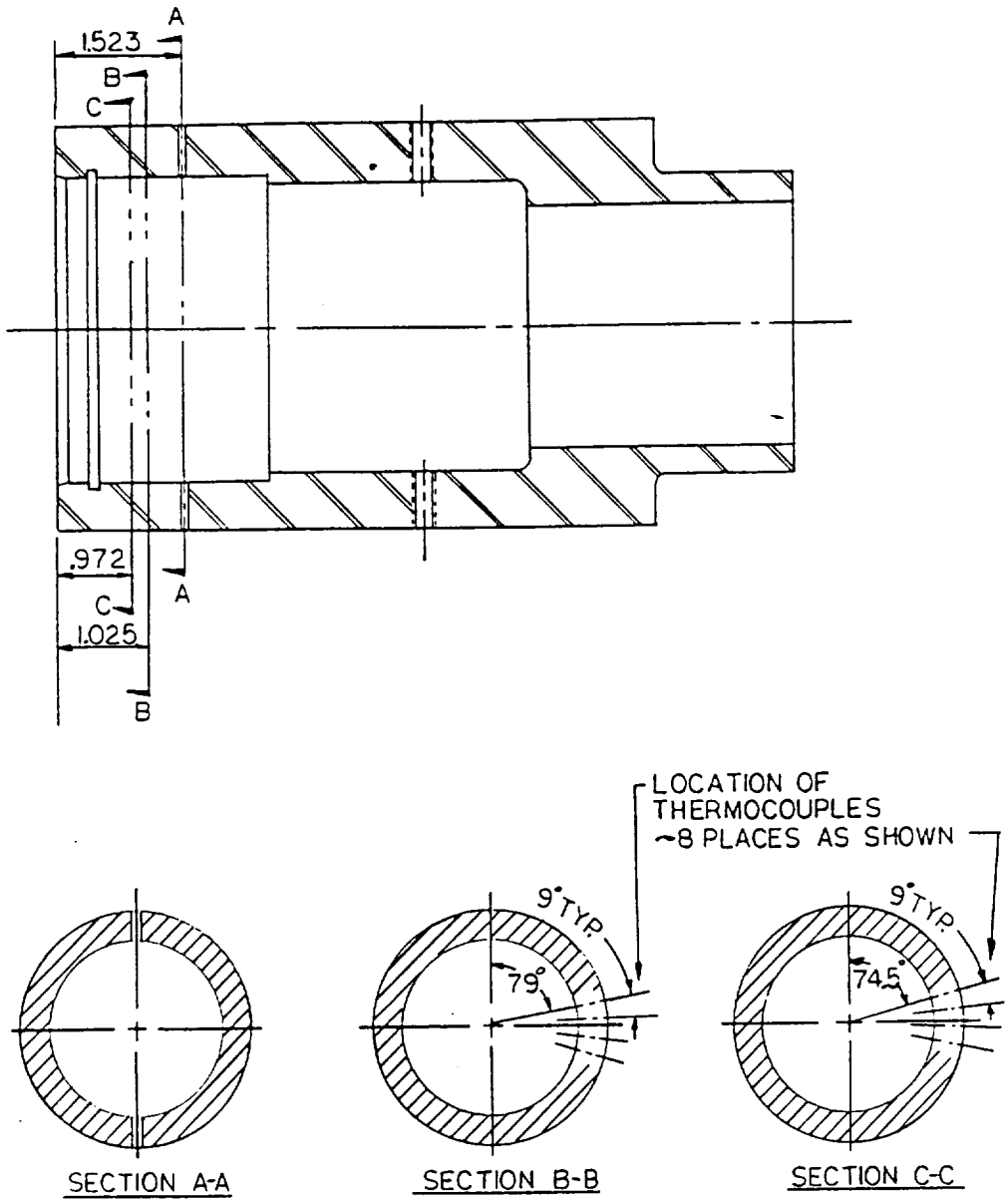

NOTE: REFER TO DRAWING C-88-9-14-6 FOR LOCATION OF LUBRICATION HOLES.

Figure 39. Location of thermocouples on outer clutch race.

PART TWO

NOTATION

$\mathcal{B}, B$	Body or bodies
$\mathcal{P}, P$	Part of body
χ	Total motion
K	Eulerian motion
Ω	Lagrangian motion
$\mathcal{E}$	Euclidian space
T	Trajectory of motion χ
N	Set of all unit vector
t	Time parameter
V	Vector space
$\mathbf{s}$	Surface traction
$\mathbf{b}$	Body forces
$\mathbf{T}$	Cauchy stress
ρ	Density
$\mathbf{x}^r$	Spatial coordinate
$\mathbf{x}$	Current configuration coordinate
$\mathbf{X}$	Material coordinate
$\mathbf{E}$	Green-Lagrange strain tensor
$\mathbf{I}$	Unit matrix
$\mathbf{S}$	Second Piola - Kirchhoff stress tensor
$\bar{\mathbf{u}}$	Increment of motion K
$\hat{\mathbf{u}}$	Increment of motion Ω

Δu	Increment of total motion
$\mathcal{S}$	Trial solution space
$\mathcal{V}$	Variation space
$\cdot$	Material time derivative
$\circ$	Time derivative holding $\mathbf{x}^r$ constant
$'$	Spatial time derivative

CHAPTER I

INTRODUCTION

I.1. BACKGROUND

In many mechanical systems, there are bodies that come in contact or slip along an interface. In most engineering simulations of such systems, one assumes that the bodies are perfectly joined or that the bodies are free to slide. This is especially true when modeling a problem using the finite element method. The modeling of sliding contact boundary conditions in finite element problems is a difficult task; the contact boundary conditions are often enforced on the discrete system using such methods as "contact" elements or "gap" elements [1]. Gap elements are non-linear springs which have zero stiffness when the distance between nodal point is positive and a large stiffness when a nodal point penetrate a body. The large stiffness value is used to enforce a displacement constraint between contacting nodes to prevent penetration of one body into another. The uses of gap elements also requires that the contacting nodal points aline making mesh construction difficult.

While the contact element approach will sometimes produce accurate results in static problems, the method represents an ad hoc modification of the discrete approximation of the original continuum problem. Such modifications often results in an

approximation to the original system that may destroy the convergence behavior of the finite element method. The use of gap elements has sometimes been justified by calling the gap element stiffness a penalty parameter. However, the use of penalty methods requires a two step convergence sequence to be used. The limit of the solutions as the penalty parameter becomes unbounded and the limit as the element size approaches zero must both be studied to insure a good solution.

In dynamic problems, the use of gap elements is even more problematic. The sudden change in the boundary conditions associated with a node will produce shock waves that propagate from the contacting nodes. These waves are artifices of the discretization of contact boundary conditions. In the continuum problem the contact area maybe growing continuously; however, the discrete problem, modeled using gap elements, will replace this continuous growth in the contact region with point impacts at each node.

Also, in dynamic problems, the area of contact may change as bodies slide from one point to another. In order to solve such a problem using finite elements, the mesh must be rezoned to keep a high concentration of elements around the contacting boundaries where large stress gradients are expected. The frequent use of mesh rezoning is computationally demanding and will artificially smooth the stress field.

In summary, finite element modelling of sliding contact

problems is usually performed using ad-hoc methods that may violate some of the basic mechanical laws and which require great skill in producing good result.

I.2. MOTIVATION

The basis for the project is to provide a rational method for finite element modeling of sliding contact problems. Specifically we seek an understanding of the behavior of helicopter transmission components which rely on sliding contact for their operation. One such component is a sprag clutch. A sprag clutch is a device that will allow power to be transmitted when rotated in one direction and freewheels (no power transmission) in the opposite direction. The principle of sprag clutch operation is illustrated in figure I.2.1. The sprag component is designed with cross-corner dimensions such that a>b. Assuming that an engine is driving counterclockwise through the outer race, the wedging action of the sprag (contact through dimension a) will drive a gearbox through the inner race. If the engine is shut down and the gearbox continues to rotate, the clutch will overrun (sprags rotate clockwise toward dimension b), thus achieving the desired effect of disengaging the engine and its associated drag torque from the drive system.

The clutch problem is characterized by large rotation and possibly large deformation of the two (or possibly more) moving bodies. When the bodies are in relative motion in the region of

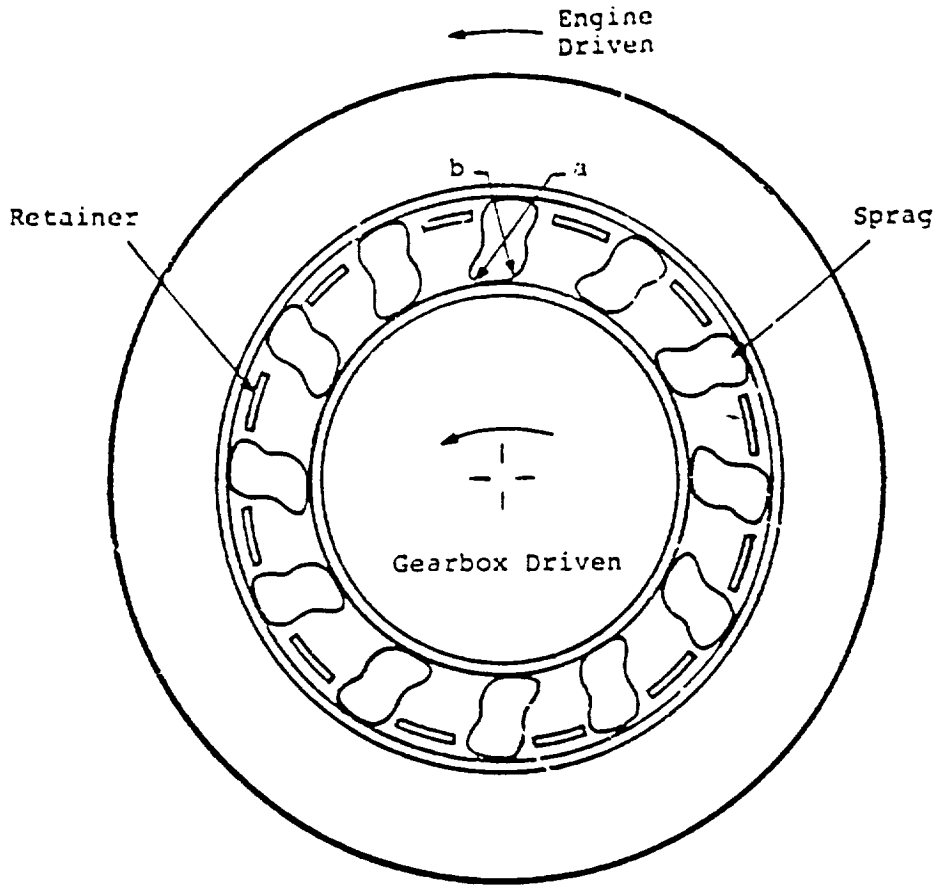

Figure I.2.1

Operation of the sprag clutch

contact, we have to look at a different set of material points at each time. If we use a Lagrangian description and Finite Elements as numerical vehicle, we must look at the same set of material points in each element at each time. Consequently, in the region of contact we have to look at different elements at different times. This forces us to use a fine discretization in all regions that will be in contact. Another way to avoid excessive discretization is to do remeshing, at frequent time intervals. Since the nature of remeshing itself does not involve any conservation laws, we will loose accuracy each time this is done. These difficulties together with those mentioned in I.1, limit the availability of analytical tools that can be used to quantify the problem. Designs of clutches to date rely heavily on experimental results and only simplified static analysis [2].

I.3. APPROACH & OBJECTIVE

The approach to this problem is to develop a formulation, in which we can focus our attention only upon the domain in which we are interested (the domain could be for example, the contact domain), without having to put extra mesh outside that domain, and without having to do remeshing. This domain is regarded as a reference configuration not necessarily part of the motion.

Instead of following the same set of material points, the material is allowed to move accross element boundaries. Consequently, we will have different set of material points in an element at

different times. The objective of this study is to derive such formulation as a basic tool to build a solution for the problem at hand.

As Hilbert once mentioned: "If we do not succeed in solving mathematical problem, it is often because we have failed to recognize the more general standpoint from which the problem before us appears.....This way to find general methods is certainly the most practicable and the surest..... ". This is our starting point. We approach the formulation as general as possible. The tools to achieve this are all available. Truesdell once mentioned: "The classical nature of mechanics reflects its greatness: Ever old and ever new, it continues to pour out for us understanding and application, linking a changing world to unchanged law... . What the foundation of mechanics need is not more people to do research on them but instead more people to learn and absorb and master and apply what has been done" [17]. It is in this light and spirit we pursue our objective.

We will therefore review the basic concepts, laws, and axioms of mechanics to serve as our groundwork. Our formulation will rest upon them. Then we develop programs to put the formulation into a format that can be used and tested.

I.4. LITERATURE REVIEW

Often when the domain of an engineering problem undergoes large motions, the problem is recast in terms of an alternate moving

coordinate system. Early applications of these ideas include the work of Coriolis [11], who introduced a transformation allowing an equation of motion to be written in terms of a coordinate system fixed on a rotating sphere. Numerous other examples of the use of a moving coordinate system included the work of Cole and Hut [9] who solved the problem of a moving line load on a half spaces and the work of Mathews [20] who solved the problem of a beam on an elastic foundation subjected to a moving load. In all the above cited work, the governing equations use a single moving coordinate system. The use of a single moving coordinate system allows rigid body motion to be accounted for in a convenient manner.

When the motion of the domain become more complex, the use of a single moving coordinate system does not result in a simplified formulation of the problem. A second approach that has been used is the use of multiple (but countable) independently prescribed moving coordinate systems. While such description have not been used for analytical solution, such techniques are the basis for most large displacement, small strain finite element formulations. Such work included the convected coordinate formulation of Belytschko and Hsieh [4] and the moving coordinate system of Belytschko, Chiapetta, and Bartell [5]. In the convected coordinate methods, the equation of motion for an element is written in terms of a coordinate system attached at the element. This allows the solution of problems with large rigid body motion of an element without using a large strain formulation.

The use of multiple moving coordinate systems, while enlarging the class of problems that can be solved, still has its limitations. The deformation of an element must still be small. The use of a purely Lagrangian description (moving the coordinate system with a material point) requires a fixed set of material points to be considered. In addition, the nodal points are fixed to the material points; any refinement of the mesh is done independently of the original governing equations.

All the difficulties and limitations cited above prompted another approach. Instead of using a convected coordinate in each element, a reference configuration which can be independently moved is used. These method are often called Arbitrary Lagrangian - Eulerian (ALE) Formulations.

The earliest use of ALE approach is the work of Frank and Lazarus [12]. They solved free surface fluid flow problems using an Eulerian description in one direction and a Lagrangian description in the other direction of the reference frame. Noh [22] as well as Hirt [15] presented the ALE formulations by using a finite difference method. The novel aspect of their formulation is that the finite difference grid can be moved arbitrarily in Eulerian or Lagrangian fashion.

In 1977, Donea, Fasoli-Stella and Giuliani [10] described the use of a mixed Eulerian-Lagrangian technique for solving transient Fluid-Structure interaction problems. The formulation was focused on the fluid domain. The idea of the formulation is to look at a

reference volume whose surface may be moving with a prescribed velocity, and express the balance laws in this reference volume. Their formulation allows an element to be moved with fluid in Lagrangian fashion or to be held fixed in Eulerian fashion. In 1980, Hughes, Liu and Zimmermann [16] using the same idea as Donea et al, formulated a mixed Eulerian-Lagrangian Finite Element formulation for incompressible viscous flows. Their procedures are appropriate for modeling the fluid subdomain of fluid-solid interaction, and free-surface problems.

Similar approaches using Finite Element method have been reported by Mullen [21]. All of the above works used the ALE description for a Newtonian fluid.

The use of mixed Eulerian-Lagrangian for solid mechanics was first done in 1984 by Haber [14]. He formulated a mixed Eulerian-Lagrangian technique for large deformation analysis in solid mechanics. He considered only the static problem.

In 1986, Koh and Haber [19] formulate an Elastodynamic Mixed Eulerian-Lagrangian description. In this work, only small deformation behavior was considered.

To summarize, there are two aspects that were lacking from previous works. First, no Non-Linear Dynamic formulations have been considered. Second, the ALE formulations from previous works were derived under the assumption that the reference frame was inertial. Under this assumption, an unnecessary body force may be generated when we move the reference configuration.

The problem that we have requires a more general formulation. In this thesis we will develop a formulation suitable for Non-Linear Dynamic problems. The reference frame considered is a moving frame described by a change in observer [13] [26].

Our formulation will be implemented through Finite Element method. Since the nature of our governing equation is non-linear, a suitable solution algorithm for non-linear equation must be used. Bogner, Mallet and Minich [6] use the "energy search" method. This approach is based on the fact that solving n simultaneous non linear equations is equivalent to the problem of finding critical points of a scalar-valued function of n variables. Bathe [3] used a different approach. The non-linear governing equation is decomposed incrementally at the continuum level. The discretization is applied after proper decomposition is introduced. He shows that this approach leads to a Newton type of algorithm. We will follow the method described by Bathe [3].

Since our formulation is time dependent, discretization in time variable is needed. Bathe [3] gives a description of various temporal integration schemes. We chose to use a Newmark integration scheme. Hughes [17] gives a rigorous analysis of the convergence of a Newmark family of temporal integrations.

CHAPTER II

FORMULATION

II.1 BASIC CONCEPTS

The primitive elements of mechanics are

1. Bodies.
2. Motions.
3. Forces.

Body B is a diffeomorph of the closure of a regular region of $\mathcal{E}$.

Motion of a body B is a class C^3 function

$$\chi : B \times R \longrightarrow \mathcal{E}$$

with $\chi(.,t)$, for each fixed t, a deformation of B.

Force is a description of mechanical interactions between body B and its environment during a motion.

These elements are governed by axioms or laws which describe mechanics as a whole. The axioms abstract the common features of all mechanical phenomena. The general principles are then illustrated by constitutive equations, which abstract the differences among bodies.

The basic axioms connecting motion and force are the **momentum balance laws.** The following definition will be useful before stating the laws themselves. Let N be the set of all unit vectors. By a system of forces for B during a motion (with trajectory T) we

mean a pair $(\mathbf{s}, \mathbf{b})$ of functions

$$\mathbf{s}: N \times T \longrightarrow V, \qquad \mathbf{b}: T \longrightarrow V$$

with

(i) $\mathbf{s}(\mathbf{n}, \mathbf{x}, t)$, for each $\mathbf{n} \in N$ and t, a smooth function of $\mathbf{x}$ on B_t;

(ii) $\mathbf{b}(\mathbf{x}, t)$, for each t, a continuous function of $\mathbf{x}$ on B_t.

We call $\mathbf{s}$ the surface force and $\mathbf{b}$ the body force; and we define the force $\mathbf{f}(P, t)$ and moment $\mathbf{m}(P, t)$ (about $\mathbf{o}$) on part P at time t by

$$\mathbf{f}(P, t) = \int_{\partial P_t} \mathbf{s}(\mathbf{n})\, dA + \int_{P_t} \mathbf{b}\, dV, \tag{1}$$

$$\mathbf{m}(P, t) = \int_{\partial P_t} \mathbf{r} \times \mathbf{s}(\mathbf{n})\, dA + \int_{P_t} \mathbf{r} \times \mathbf{b}\, dV. \tag{2}$$

Here $\mathbf{n}$ is the outward unit normal to ∂P_t and $\mathbf{r}$ is the position vector.

Let χ be a motion of B. Given a part P of B, the linear momentum $\mathbf{l}(P, t)$ and the angular momentum $\mathbf{a}(P, t)$ (about the origin $\mathbf{o}$) of P at time t are defined by

$$\mathbf{l}(P, t) = \int_{P_t} \mathbf{v}\rho\, dV, \tag{3}$$

$$\mathbf{a}(P, t) = \int_{P_t} \mathbf{r} \times \mathbf{v}\rho\, dV, \tag{4}$$

where $\mathbf{r}: E \longrightarrow V$ is the position vector.

With this definition, the momentum balance laws can be stated as follows:

For every part P and time t,

$$\mathbf{f}(P,t) = \dot{\mathbf{l}}(P,t) \tag{5}$$

$$\mathbf{m}(P,t) = \dot{\mathbf{a}}(P,t) \quad . \tag{6}$$

Tacit in the statement of this axiom is the existence of an observer relative to which the motion and forces are measured. Observers relative to which the axioms hold are called inertial. Note also that the axioms were laid on the part P of the body B. As it was stated in the introduction, our interest is balance of momentum in the spatial region R. To do that we make use of the work due to Cauchy, stated in this following theorem.

Cauchy's Theorem.

Let $(\mathbf{s},\mathbf{b})$ be a system of forces for B during a motion. Then a necessary and sufficient condition that the momentum balance laws be satisfied is that there exist a spatial tensor field T (called the Cauchy stress) such that

(a) for each unit vector $\mathbf{n}$

$$\mathbf{s}(\mathbf{n}) = \mathbf{T}\,\mathbf{n};$$

(b) $\mathbf{T}$ is symmetric; (6a)

(c) $\mathbf{T}$ satisfies the equation of motion

$$\operatorname{div}\mathbf{T} + \mathbf{b} = \rho\,\dot{\mathbf{v}}$$

A proof of this theorem can be found in Gurtin [13]. This theorem gives the local momentum balance. The momentum balance for region R of interest can be obtained by integrating this equation over the region R. Gurtin [13] give derivation of momentum balance for fixed region R as follows.

Let R be a control volume at time t. Then at that time

$$\int_{\partial R} \mathbf{s}(\mathbf{n})\, dA + \int_{R} \mathbf{b}\, dV = \frac{d}{dt} \int_{R} \mathbf{v}\, \rho\, dV + \int_{\partial R} (\rho \mathbf{v}) \mathbf{v} \cdot \mathbf{n}\, dA , \qquad (7)$$

$$\int_{\partial R} \mathbf{r} \times \mathbf{s}(\mathbf{n})\, dA + \int_{R} \mathbf{r} \times \mathbf{b}\, dV = \frac{d}{dt} \int_{R} \mathbf{r} \times \mathbf{v}\, \rho\, dV + \int_{\partial R} \mathbf{r} \times (\rho \mathbf{v}) \mathbf{v} \cdot \mathbf{n}\, dA . \qquad (8)$$

However, if region R is a funtion of time, the balance of momentum will take the form as follows (the proof is given in Appendix 1)

$$\int_{\partial R} \mathbf{s}(\mathbf{n})\, dA + \int_{R} \mathbf{b}\, dV = \int_{R} \dot{\mathbf{v}}\, \rho\, dV , \qquad (9)$$

$$\int_{\partial R} \mathbf{r} \times \mathbf{s}(\mathbf{n})\, dA + \int_{R} \mathbf{r} \times \mathbf{b}\, dV = \int_{R} \mathbf{r} \times \dot{\mathbf{v}} \rho\, dV \qquad (10)$$

This can be expressed in a more compact form in the following theorem(The proof is given in Appendix 2)

Theorem of virtual work

Let $(\mathbf{s}, \mathbf{b})$ be a system of forces for B during a motion. Then a necessary and sufficient condition that the momentum balance laws are satisfied is that given any region R and time t,

$$\int_{\partial R} \mathbf{s}(\mathbf{n}) \cdot \mathbf{w}\, dA + \int_{R} \mathbf{b}_{*} \cdot \mathbf{w}\, dV = 0 \qquad (11)$$

for every infinitesimal rigid displacement $\mathbf{w}$, where $\mathbf{b}_{*}$is given by

$$\mathbf{b}_* = \mathbf{b} - \rho\dot{\mathbf{v}}, \tag{12}$$

and $\mathbf{w}$ is defined by following definition:

An **infinitesimal rigid displacement** of B is a vector field $\mathbf{w}$ on B with $\nabla\mathbf{w}$ constant and skew, or equivalently, a vector field $\mathbf{w}$ that admits the representation

$$\mathbf{w}(p) = \mathbf{w}(q) + \nabla\mathbf{w}\,(p-q) \tag{13}$$

for all $p, q \in B$.

It can be proved that the virtual work equation can also be written as (The proof is given in Appendix 3)

$$\int_{\partial R} \mathbf{s}(\mathbf{n})\cdot\mathbf{w}\, dA + \int_{R} \mathbf{b}_*\cdot\mathbf{w}\, dV = \int_{R} \mathbf{T}\cdot\text{grad}\ \mathbf{w}\, dV \tag{14}$$

where $\mathbf{w}$ here is admissible virtual displacement.

The formulation above then motivate the following section.

II.2 KINEMATICS

Let B be the initial configuration of a body, and B_t be the current configuration of the body in the motion χ . The motion χ, can be decomposed into two motion, K and Ω. Let B_r be the configuration of B at time t in the motion K. We can focus our attention in the spatial region V_r, measured from seperate coordinate system $\mathbf{e}_1$. In the meantime we can think that V_r is a fixed region of space. Later we will consider general case where V_r is a function of time. We require that V_r be such that :

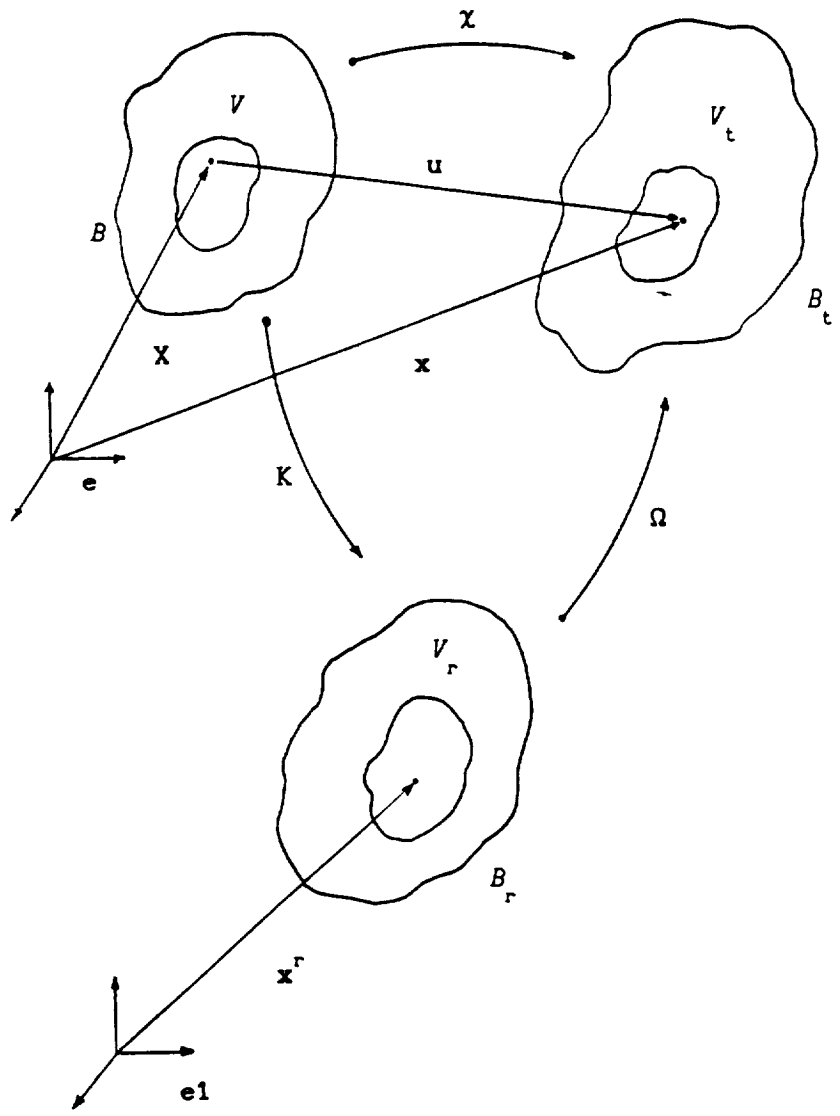

Fig II.2.1

Kinematics of Mixed Eulerian-Lagrangian model

$$V_r = \{(x^r) \mid x^r \in B_r\}. \tag{1}$$

In the motions that we study, we will choose V_r as our reference configuration. The initial configuration will serve as state of zero strain, but not necessarily as the state of zero stress. V is the set material points that occupy V_r at time t. Precisely,
$V = K^{-1}(V_r, t)$, at each time t. And similarly, V_t can be tought as : $V_t = \chi(V, t)$ or $V_t = \Omega(V_r, t)$.
Here V_t is equivalent with R in section II.1.

We choose Green - Lagrange strain tensor as the strain measure. Precisely,

$$E = 1/2\,[J^T J - I] \tag{2}$$

$$J = \nabla \chi \tag{3}$$

And since we decompose the motion,

$$\chi = \Omega \circ K \tag{4}$$

Consequently,

$$\nabla \chi = \nabla \Omega \;\; \nabla K \tag{5}$$

and if we define

$$\nabla \Omega = \hat{J} = \frac{\partial x_i}{\partial x^r_j} \tag{6}$$

$$\nabla K = \bar{J} = \frac{\partial x^r_i}{\partial X_j} \tag{7}$$

we have $J = \hat{J}\ \bar{J}$ (8)

Then the expression for Green - Lagrange strain will become

$$E = 1/2\ [\bar{J}^T\ \hat{J}^T\ \hat{J}\ \bar{J} - I\ ] \tag{9}$$

II.3 VIRTUAL WORK, STATIC CASE

Let T be the Cauchy stress at time t, and let w be an admissible virtual displacement. Assume that the body forces present are due only to inertial effects. Under that condition, the virtual work expressed in the current configuration is

$$\int_{V_t} [T \cdot \text{grad } w]\ dV_t = R \tag{1}$$

$$R = \int_{\partial V_t} [T\ n \cdot w]\ dA \tag{2}$$

Let
$$J = \det (\ J\ )$$
$$\hat{J} = \det (\ \hat{J}\ ) \tag{3}$$
$$\bar{J} = \det (\ \bar{J}\ )$$

Let
$$\tilde{J} = [\ \bar{J}\ ]^{-1}$$
$$\tilde{J} = \det (\ \tilde{J}\ ) \tag{4}$$

Since we want to refer everything to the reference configuration, we must convert the virtual work equation accordingly. Bringing the L.H.S. of the virtual work equation into the initial configuration first, we get :

$$\int_V [\ T \cdot \text{grad } w\ ]\ dV_t \quad = \quad \int_V [\ T \cdot \text{grad } w\ ]_i\ J^t\ dV =$$

$$\int_V [\ T_i \cdot (\text{grad } w)_i\ ]\ J^t\ dV \quad =$$

$$\int_V [\ T_i\ J^{-T} \cdot \nabla_X\ w_i\ ]\ J^t\ dV \quad =$$

Premultiplying the integrand with $J\ J^{-1}$,

$$\int_V [\ J\ S \cdot \nabla_X\ w\ ]\ dV \tag{5}$$

where $S = J^t\ J^{-1}\ T_i\ J^{-T}$ is the second Piola - Kirchhoff stress.

The subscript "i" means the initial (in this case material) description of the corresponding spatial field. ∇_X means the gradient with respect to **X** and " grad " means the gradient with respect to **x** , equivalently ∇_x .

Continuing to bring the virtual work into reference configuration,

$$\int_{V_r} [\ J^t\ S \cdot \nabla_X\ w_i\ ]_r\ \tilde{J}^t\ dV_r \quad =$$

$$\int_{V_r} [\ (\ J^t S^t)_r \cdot \nabla_{X^r}\ w_r\ \bar{J}^t\ ]\ \tilde{J}^t\ dV_r \tag{6}$$

Similarly we can bring the R.H.S into reference configuration,

$$\int_{\partial V_r} [\ T_r\ \hat{J}\ \underline{\hat{J}}^{-T}\ \mathbf{m} \cdot \mathbf{w}_r\ ]\ dA \qquad (7)$$

where $\mathbf{m}$ is the outward unit normal vector to the surface of the reference configuration. We can drop the subscript r without any danger of confusion, since everything will we expressed and refered to the reference configuration. We also drop the subscript for gradient, ∇ meant to be ∇_{X^r} unless specifically stated.

II.4 INCREMENTAL DECOMPOSITION

Since the nature of the equation

$$\int_{V_r} [\ (\ J^t S^t)\ \cdot \nabla_{X^r}\ w\ \bar{J}^t\ ]\ \tilde{J}^t\ dV_r\ = R^t \qquad (1)$$

is non-linear, we seek an incremental decomposition. Bathe [3] show that this incremental decomposition will lead to the Newton type of algorithm. Focusing on the integrand above, letting

$$W_1^t = [\ (\ J^t S^t)\ \cdot \nabla\ w\ \bar{J}^t\ ]\ \tilde{J}^t \qquad (2)$$

W_1 can be expanded at the neighbourhood time $t+\Delta t$,

$$W_1^{t+\Delta t} = [\ J^{t+\Delta t}\ S^{t+\Delta t} \cdot \nabla\ w^{t+\Delta t}\ J^{t+\Delta t}\ ]\ \tilde{J}^{\ t+\Delta t} \qquad (3)$$

letting

$$J^{t+\Delta t} = J^t + \Delta\ J \qquad (4)$$

$$S^{t+\Delta t} = S^t + \Delta\ S \qquad (5)$$

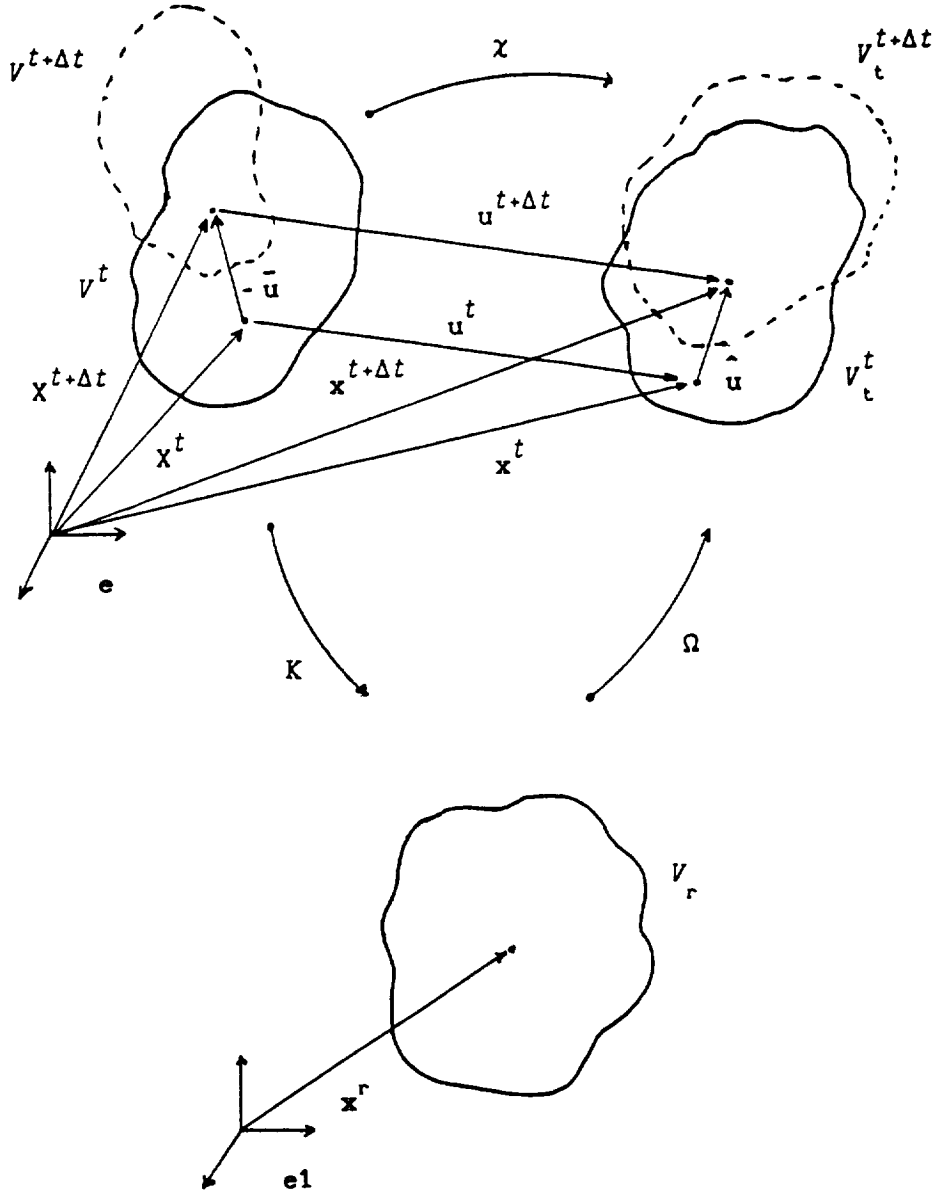

Fig II.4.1

Kinematics of Mixed Eulerian-Lagrangian model, with incremental quantities shown

$$\bar{J}^{t+\Delta t} = \bar{J}^{t} + \Delta \bar{J} \tag{6}$$

$$\tilde{J}^{t+\Delta t} = \tilde{J}^{t} + \Delta \tilde{J} \tag{7}$$

Expanding and neglecting higher order terms, we have

$$\begin{aligned} W_1^{t+\Delta t} = {} & (J^t S^t \cdot \nabla w^{t+\Delta t} \bar{J}^t) \tilde{J}^t + \\ & (\Delta J^t S^t \cdot \nabla w^{t+\Delta t} \bar{J}^t) \tilde{J}^t + \\ & (J^t \Delta S \cdot \nabla w^{t+\Delta t} \bar{J}^t) \tilde{J}^t + \\ & (J^t S^t \cdot \nabla w^{t+\Delta t} \Delta \bar{J}) \tilde{J}^t + \\ & (J^t S^t \cdot \nabla w^{t+\Delta t} \bar{J}^t) \Delta \tilde{J} \end{aligned} \tag{8}$$

Let $\nabla w^{t+\Delta t} = \nabla w^{t} + \circ\nabla w$ (9)

and since we assume that at time t the system is at equilibrium, we have $\nabla w^{t} = 0$.

So then we have :

$$\begin{aligned} W_1^{t+\Delta t} = {} & (J^t S^t \cdot \circ\nabla w \bar{J}^t) \tilde{J}^t + \\ & (\Delta J S^t \cdot \circ\nabla w \bar{J}^t) \tilde{J}^t + \\ & (J^t \Delta S \cdot \circ\nabla w \bar{J}^t) \tilde{J}^t + \\ & (J^t S^t \cdot \circ\nabla w \Delta \bar{J}) \tilde{J}^t + \\ & (J^t S^t \cdot \circ\nabla w \bar{J}^t) \Delta \tilde{J} \end{aligned} \tag{10}$$

The decomposed virtual work equation, after linearizing on $\Delta \underline{S}$ then becomes:

$$\int_{V_r} (J^t \, \Delta^L S \cdot {}^o\nabla w \; \bar{J}^t) \, \tilde{J}^t \, dV_r + \int_{V_r} (\Delta J \; S^t \cdot {}^o\nabla w \; \bar{J}^t) \, \tilde{J}^t \, dV_r = R - \int_{V_r} (J^t S^t \cdot {}^o\nabla w \; \bar{J}^t) \, \tilde{J}^t \, dV_r - \int_{V_r} (J^t S^t \cdot {}^o\nabla w \, \Delta \bar{J}) \, \tilde{J}^t \, dV_r - \int_{V_r} (J^t S^t \cdot {}^o\nabla w \; \bar{J}^t) \, \Delta \tilde{J} \, dV_r \qquad (11)$$

This is the incremental decomposition that is going to be discretized.

II.5 DYNAMIC CASE

If the effect of inertial forces are included, the virtual work equation in the current configuration takes the form

$$\int_{V_t} T \cdot \text{grad } w \, dV_t = \int_{\partial V_t} Tn \cdot w \, dA - \int_{V_t} \rho \, \ddot{u} \cdot w \, dV_t \qquad (1)$$

where $\ddot{u}$ is $(\ddot{\chi})_s$. The L.H.S. and the first R.H.S. term already been treated in section III.3 (static case). The remaining term

that should be treated is the second R.H.S. term. It can be shown(see appendix 4) that if we express $\dot{u}$ in the referential description it will take the form

$$(\dot{u})_r = \overset{\circ}{u} - 2[\text{grad } u]^{\circ} \bar{J} \mathring{X} - \text{grad } u \overset{\circ}{\bar{J}} \mathring{X} - \text{grad } u \bar{J} \overset{\circ}{\mathring{X}} + \text{grad } [\text{grad } u \bar{J} \mathring{X}] \bar{J} \mathring{X} \quad (2)$$

where $^{\circ}$ means time derivative holding x^r constant.

The dynamic parts expressed in reference configuration is

$$\int_{V_r} \rho_0 [\overset{\circ}{u} \cdot w] \tilde{J} \, dV_r - \int_{V_r} \rho_0 [2 \text{ grad } \overset{\circ}{u} \bar{J} \mathring{X} \cdot w] \tilde{J} \, dV_r -$$

$$\int_{V_r} \rho_0 [\text{grad } u \overset{\circ}{\bar{J}} \mathring{X} \cdot w] \tilde{J} \, dV_r - \int_{V_r} \rho_0 [\text{grad } u \tilde{J} \overset{\circ}{\mathring{X}} \cdot w] \bar{J} \, dV_r +$$

$$\int_{\partial V_r} \rho_0 [(\mathring{X} \cdot \bar{J} n) w \cdot \text{grad } u \bar{J} \mathring{X}] \bar{J} \, dA -$$

$$\int_{V_r} \rho_0 [\bar{J} (w \underline{\times} \mathring{X})^T \text{grad } u \bar{J} \mathring{X} \cdot \nabla \tilde{J}] \, dV_r -$$

$$\int_{V_r} \rho_0 [\text{grad } u \bar{J} \mathring{X} \cdot w(\bar{J}^T \cdot \nabla \mathring{X} + \mathring{X} \cdot \text{div } \bar{J}^T)] \tilde{J} \, dV_r -$$

$$\int_{V_r} \rho_0 [\text{grad } u \bar{J} \mathring{X} \cdot \nabla w \bar{J} \mathring{X}] \tilde{J} \, dV_r \quad (3)$$

where $\underline{\times}$ is the tensor product of two vector. The derivation of this formulation can be seen in appendix 4.

II.6 FINITE ELEMENTS IMPLEMENTATION

Equation II.4.11 and II.5.3 will serve as the weak formulation of the problem. As can be seen in Figure II.4.1, this weak formulation contains two sets of unknowns, namely the increment in the motion K (denoted by $\Delta X = -\bar{u}$), and the increment in the motion Ω (denoted by $\Delta x = \hat{u}$). Together they will form the increment of motion χ (given by $\Delta u = \bar{u} + \hat{u}$). If one of the motion is chosen to represent the known translation or rotation, for example, motion K, then the increment $\bar{u}$ is known, and the weak form will contain only one set of unknown variables, namely, the increment of motion Ω (denoted by $\hat{u}$).

Let $\mathcal{S}$ denote the trial solution space and $\mathcal{V}$ the variation space, and let $\mathcal{S}^h$ and $\mathcal{V}^h$ be finite dimensional approximations of $\mathcal{S}$ and $\mathcal{V}$. $\mathcal{S}^h$ and $\mathcal{V}^h$ can be thought of as being subsets of $\mathcal{S}$ and $\mathcal{V}$, respectively,

$$\mathcal{S}^h \subset \mathcal{S}$$

$$\mathcal{V}^h \subset \mathcal{V}.$$

If ϕ_α, $\alpha=1,n$ denotes a set of linearly independent basis function spanning $\mathcal{S}^h$ and $\mathcal{V}^h$, the approximate solution on the domain V_r will be of the form

$$\hat{u} = \sum_{\alpha=1}^{n} \hat{u}_\alpha \phi_\alpha. \qquad (1)$$

The Finite Element method provides a systematic method for constructing appropriate function, ϕ_α. The domain V_r is first partitioned into subdomain, namely the finite elements. Over each

element Ω_e , the solution is approximated as a linear combination of shape function , N_α, which typically are polynomials. The construction of the global basis function ϕ_α can be viewed as a process of patching together element shape functions at the nodes. Hence, the global basis function ϕ_α are non zero only on the element or elements containing the node; that is, the basis function have local support.

Example of an element is shown in Figure II.6.1, along with its shape functions at each node, given by

$$
\begin{aligned}
N_1 &= 0.25\ (1-\xi)\ (1-\eta)\ \xi\ \eta \\
N_2 &= -0.5\ (1-\xi^2)\ (1-\eta)\ \eta \\
N_3 &= -0.25\ (1+\xi)\ (1-\eta)\ \xi\ \eta \\
N_4 &= 0.5\ (1+\xi)\ (1-\eta^2)\ \xi \\
N_5 &= 0.25\ (1+\xi)\ (1+\eta)\ \xi\ \eta \\
N_6 &= 0.5\ (1-\xi^2)\ (1+\eta)\ \eta \\
N_7 &= -0.25\ (1-\xi)\ (1+\eta)\ \xi\ \eta \\
N_8 &= -0.5\ (1-\xi)\ (1-\eta^2)\ \xi \\
N_9 &= (1-\xi^2)\ (1-\eta^2).
\end{aligned}
\qquad (2)
$$

Although the problem is stated in a weak form involving integrals over the entire domain, the fact that function ϕ_α is non zero only on those elements containing the nodal point in the finite element mesh, makes it possible to generate the Galerkin approximation by summing local contributions from each element in

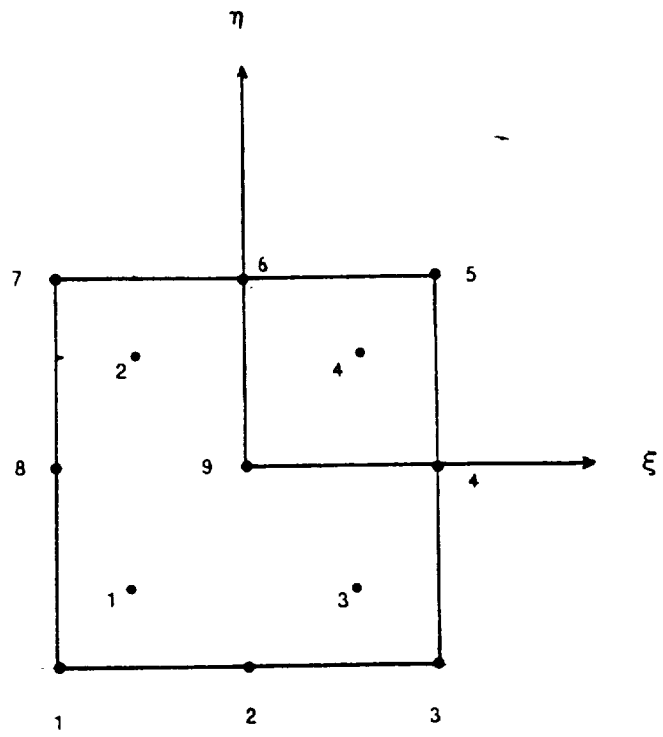

Fig II.6.1
Parent 9 nodes Isoparametric element
in ξ - η space, with four Gaussian
integration point inside.

the mesh.

The variables in each element domain can be represented by

$$X = \sum_{\alpha=1}^{n} N_\alpha X_\alpha \tag{3}$$

$$x = \sum_{\alpha=1}^{n} N_\alpha x_\alpha \tag{4}$$

$$\hat{u} = \sum_{\alpha=1}^{n} N_\alpha \hat{u}_\alpha \tag{5}$$

$$\bar{u} = \sum_{\alpha=1}^{n} N_\alpha \bar{u}_\alpha \tag{6}$$

where X_α, x_α, $\hat{u}_\alpha$, $\bar{u}_\alpha$, are the nodal values of the variables.

The subtitution of this interpolation into the weak form yields

$$M\,{}^{t+\Delta t}\dot{U}^{(k)} + ({}^{t}K_L + {}^{t}K_{NL})\,\Delta\,\hat{U}^{(k)} = {}^{t+\Delta t}R - {}^{t+\Delta t}F^{(k-1)} \tag{7}$$

where

M = Mass matrix

${}^{t}K_L$ = Linear incremental stiffness matrices, from first term of L.H.S. of Equation II.4.11.

${}^{t}K_{NL}$ = Non-Linear incremental stiffness matrices, from the second term of L.H.S. of Equation II.4.11.

${}^{t+\Delta t}R$ = Vector of externally applied nodal point loads at time $t+\Delta t$, from the first term of R.H.S. of Equation II.4.11.

${}^{t+\Delta t}F^{(k-1)}$ = Vectors of nodal point forces equivalent to the element stresses at time $t+\Delta t$, at iteration (k-1), from second, third and fourth terms of R.H.S. of Equation II.4.11.

$^{t+\Delta t}\dot{\hat{U}}^{(k)}$ = Vector of nodal point total spatial description of material accleration, as given by Equation II.5.2, at time $t+\Delta t$ and iteration k.

$\Delta\ \hat{U}^{(k)}$ = Vector of increments of Lagrangian nodal point displacements in iteration k.

This is the incremental semi discrete matrices equation of the weak formulation. In order to put Equation 7 into a form suitable for digital computer implementation, we need to introduce temporal integration for vector $^{t+\Delta t}\dot{\hat{U}}^{(k)}$ which is going to be described in the next section.

II.7. TEMPORAL INTEGRATION

Newmark integration scheme is chosen to integrate the time parameter. The scheme is given as follows

$$^{t+\Delta t}\ddot{u}^{(k)} = a_0(^{t+\Delta t}u^{(k)} - {}^{t}u) - a_2\ {}^{t}\dot{u} - a_3\ {}^{t}\ddot{u} \qquad (1)$$

$$^{t+\Delta t}\dot{u}^{(k)} = a_1(^{t+\Delta t}u^{(k)} - {}^{t}u) + (1-a_7\ a_2)\ {}^{t}\dot{u} + (a_6-a_7\ a_3)\ {}^{t}\ddot{u} \qquad (2)$$

where $t+\Delta t$ means present time step, t means previous time step, k means present iteration. It is assumed that condition in previous time step and previous iteration is known. a_0, a_1...etc are given by

$a_0 = 1/(\alpha^*\ \Delta t^{**}2)$

$a_1 = \delta/(\alpha^*\ \Delta t)$

$$a_2 = 1/(\alpha^* \Delta t)$$

$$a_3 = (1/2^*\alpha)-1$$

$$a_6 = \Delta t(1-\delta)$$

$$a_7 = \delta \Delta t$$

where α and δ are integration parameter. Note that

$$t+\Delta t\,\mathbf{u}^{(k)} = t+\Delta t\,\mathbf{u}^{(k-1)} + \Delta \mathbf{u}^{(k)} \qquad (3)$$

and from II.6

$$\Delta \mathbf{u}^{(k)} = \bar{\mathbf{u}} + \hat{\mathbf{u}}. \qquad (4)$$

Subtituting (3) and (4) to (1) and (2)

$$t+\Delta t\,\ddot{\mathbf{u}}^{(k)} = a_0(t+\Delta t\,\mathbf{u}^{(k-1)} - t\,\mathbf{u}) - a_2\,t\dot{\mathbf{u}} - a_3\,t\ddot{\mathbf{u}} + a_0\,\bar{\mathbf{u}}^{(k)} + a_0\,\hat{\mathbf{u}}^{(k)} \qquad (5)$$

$$t+\Delta t\,\dot{\mathbf{u}}^{(k)} = a_1(t+\Delta t\,\mathbf{u}^{(k-1)} - t\,\mathbf{u}) + (1-a_7\,a_2)\,t\dot{\mathbf{u}} + (a_6-a_7\,a_3)\,t\ddot{\mathbf{u}} + a_1\,\bar{\mathbf{u}}^{(k)} + a_1\,\hat{\mathbf{u}}^{(k)} \qquad (6)$$

Note that the last terms of R.H.S. of (5) and (6) are the unknown. After subtituting (5) and (6) into (II.5.3) the unknown parts will be added into the stiffness matrix (of the static parts), and the known parts will contribute to the loading parts namely, the R.H.S. of (II.4.11).

CHAPTER III

RESULTS

III.1. STATIC CASE

The first problem considered is a 1.0 in x 2.0 in x 1.0 in block subjected to a load P = 1000 lbs on the upper nodes (node 3, 6, 9, 12 and 15) as shown in Figure III.1.1. The boundary conditions for this problem are:

Fixed on node 1, 4, 7, 10 and 13.

Rollers on node 2, 3, 14 and 15.

Due to the imposition of these boundary conditions, the problem can be thought as a continuous slab, with a fixed support. The material properties utilized are Young's Modulus E = 0.3E+08 psi, and Poisson's ratio ν = 0.25. The mesh shown in Figure III.1.1 consists of two 9 nodes Lagrange elements, and lives in the spatial region V_r ,and measured in coordinate system e1, as shown in Figure II.2.1.

A prescribed motion K is introduced in the form of Eulerian displacement of the nodes as follows:

Node	Direction	Displacement
5	x	0.08333 in
6	x	0.16667 in
8	x	0.16667 in

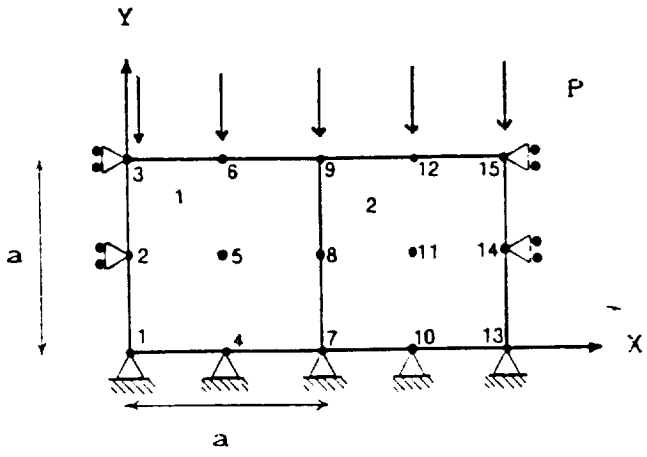

Fig III.1.1

Mesh in spatial region V_r for static case a=1 in. and all P = 1000 lbs

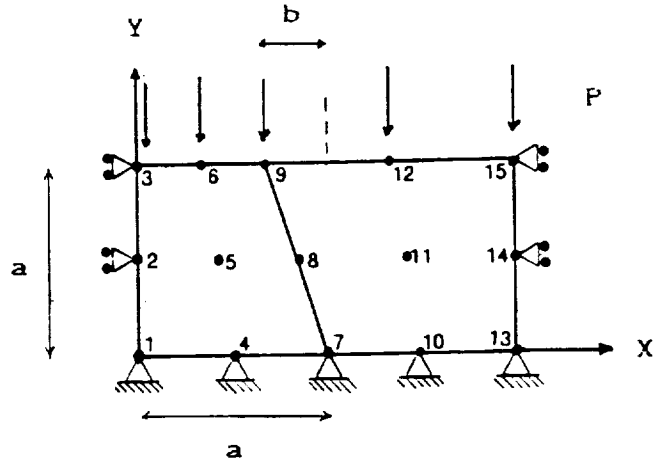

Fig III.1.2

Material discretization after motion K is specified. a=1 in, b=1/3 in, and all P=1000 lbs.

9	x	0.33333 in
11	x	0.08333 in
12	x	0.16667 in

Due to this prescribed motion, the material discretization in the region V in Figure II.2.1 will be in the form as given in Figure III.1.2.

Now we can state the problem as follows:

Given a mesh geometry in the spatial region V_r, with specified loading, and given the prescribed Eulerian motion K, find the Lagrangian motion Ω (or equivalently, find the final configuration V_t).

Since the Eulerian motion is prescribed without any external driving forces, we know that final configuration V_t should only reflects the effects of the (relatively small) prescribed loading. The motion Ω then should contain large deformation which cancel out the prescribed Eulerian displacement. The net displacement will be the displacement due to prescribed loading.

Consider a separate problem with discretization and loading as shown in Figure III.1.2. We solve this problem using a non-linear Finite Elements program. Theoretically, the results of these two problems should be identical. The results are compared in Table III.1.1. The slight difference between them is likely due to round off error, because of the large load generated to compensate the (large) prescribed Eulerian displacement. Thus, the results suggest that our formulation and program does not contain a

serious physical error.

The stresses inside the element 1 and element 2 for both cases above are calculated at each of the Gaussian integration points. The location of the Gaussian points inside the parent element are given in Figure II.6.1. The comparison of the value of the stresses is given in Table III.1.2.

Next, we consider the same problems as described above, but the load P are increased to 100000.0 lbs. The purpose of this is to introduce a set of load large enough to give a large deformation in the final configuration V_t. The results from our formulation for P = 1000.0 lbs and P = 100000.0 lbs are given in Table III.1.4. The results from regular Non-linear Finite Element program for P = 1000.0 lbs and P = 100000.0 lbs are given in Table III.1.3. It can be seen that for P = 100000.0 lbs, the solutions of our formulation compared well with the solutions of regular Non-Linear Finite Element program.

III.2. DYNAMIC, TWO LAYERS OF MATERIALS WITH MOVING POINT LOAD.

The second problem considered is two layers of different materials, with the following dimension and properties.

Material I : 104.0 in x 2.0 in

Young's modulus E = 0.3E+08 psi

Poisson's ratio ν = 0.25

Density ρ = 0.777E-03 lb-sec^2/in^4

Material II : 104.0 in x 26.0 in

Young's modulus E = 1.0E+05 psi

Poisson's ratio ν = 0.20

Density ρ = 0.20E-03 lb-sec^2/in^4

The problem and the boundary conditions are depicted in Figure III.2.2. Material I is shown as the shaded area and lying above the material II. Along the interface between material I and material II, the nodes are constrained to move together. That is, there is no slip between material I and material II. This system is subjected to a load of 1000.0 lbs acting on node 1, as shown in Figure III.2.2.

The load is moving with constant velocity **v** above the material I. The mesh shown in Figure III.2.2 consists of 96 nine nodes Lagrange elements, and lives in the spatial region V_r ,and measured in coordinate system **e1**, as shown in Figure II.2.1. The movement of the load is represented by uniform Eulerian motion K, prescribed in all the nodes in the **x** direction. The deflection in the upper nodes of material I for velocity **v** = 1000.0 in/sec is plotted in Figure III.2.3.

We would like to compare the results with the available solution. In 1958, Mathews [20] solved the problem of a point load moving with constant velocity on a beam on an elastic foundation. He considered two cases, namely systems with damping and without damping. The latter will be examined. His solution gives deflection of the beam at distance **x** measured from the moving load.

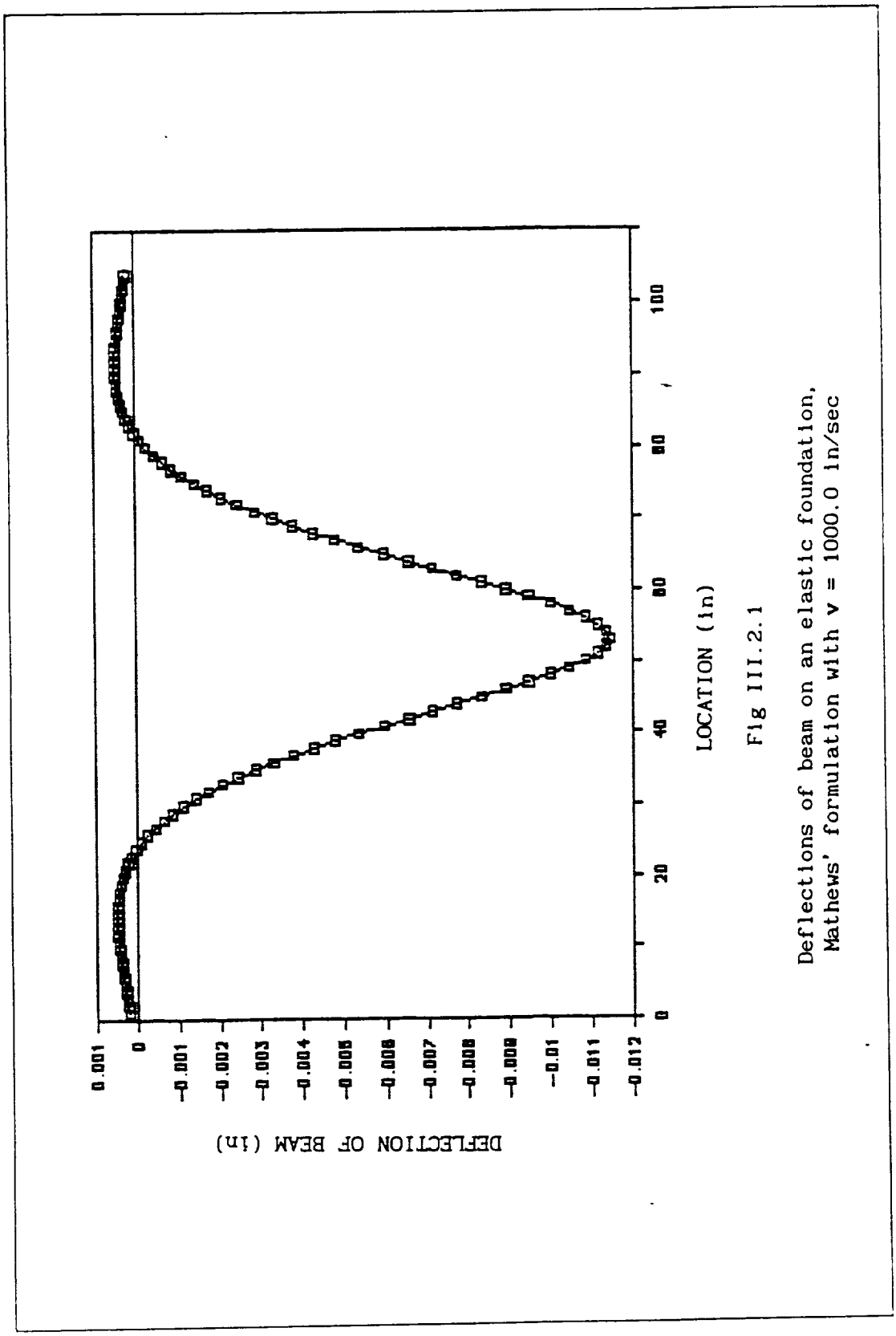

Fig III.2.1

Deflections of beam on an elastic foundation,
Mathews' formulation with v = 1000.0 in/sec

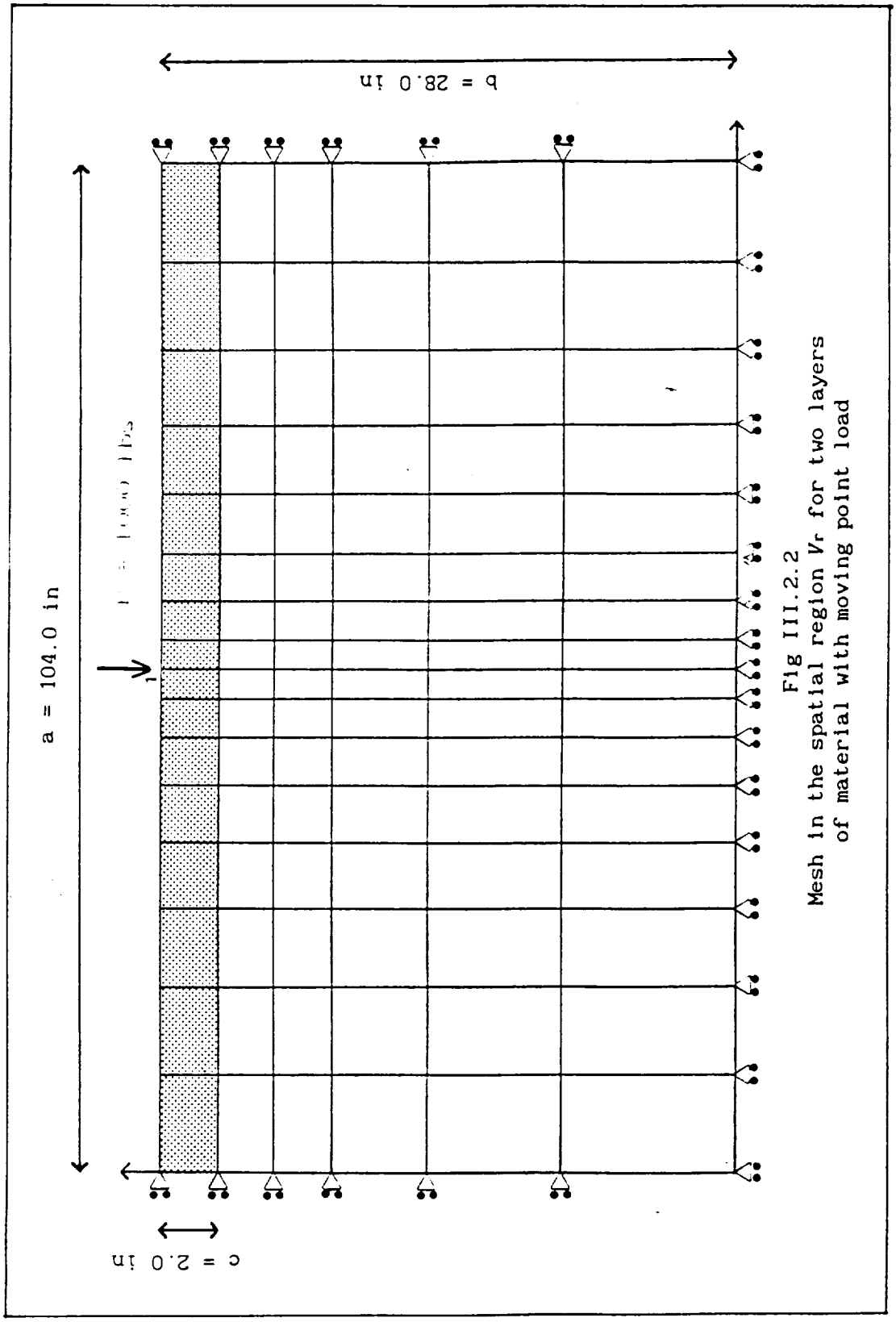

Fig III.2.2
Mesh in the spatial region V_r for two layers of material with moving point load

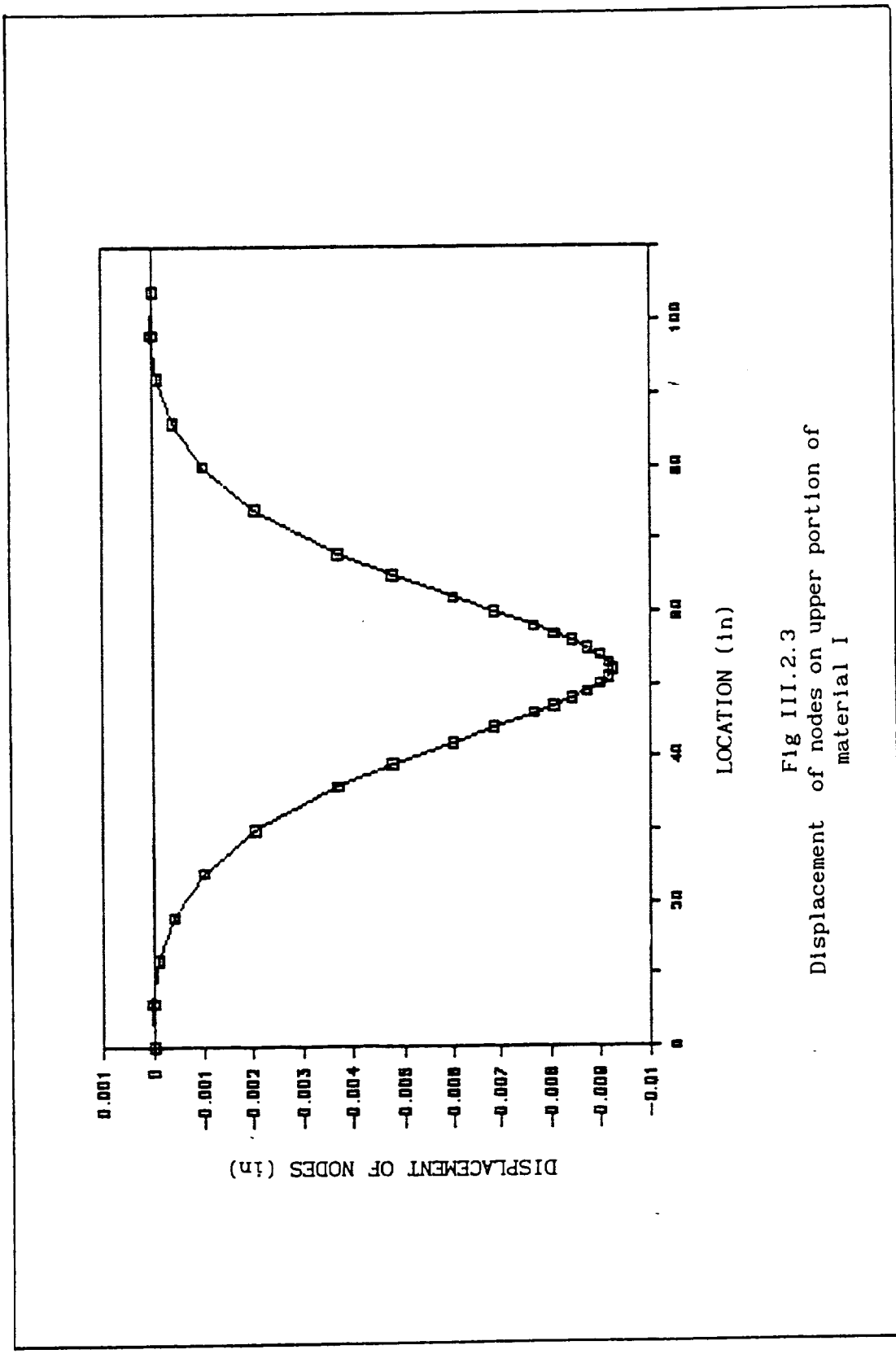

Fig III.2.3
Displacement of nodes on upper portion of material I

The formulation is

$$y = \frac{F_0 \; e^{-b|x-vt|}}{2 E I \; 2ab \; (a^2+b^2)} \; [a \cos a|x-vt| + b \sin a|x-vt|]$$

and a and b are given by

$$a = \left\{ \sqrt{\frac{k}{4 EI}} + \frac{\rho v^2}{4 EI} \right\}^{1/2}$$

$$b = \left\{ \sqrt{\frac{k}{4 EI}} - \frac{\rho v^2}{4 EI} \right\}^{1/2}$$

where

E = Young's modulus for beam material

I = Inertia of the beam

ρ = Mass per unit length of the beam

F_0 = Applied load

k = "Elasticity" of the foundation, defined as the force required to displace unit length of the foundation through unit distance

$|x-vt|$ = Absolute value of the distance between the load and the point where the deflection is calculated.

The result from Mathews' formulation, for velocity of the load of 1000.0 in/sec, evaluated at the same location as we evaluate the deflection of two layered material, is plotted in Figure III.2.1.

The deflections under the load for v = 0.0, 10.0, 1000.0

in/sec and v = 10000.0 in/sec are calculated for both of Mathews' and our formulation. The critical velocity for these materials is found to be 19110 in/sec. The spring constant k in Mathews' is evaluated in two ways. First, k is calculated using the definition that he gives, namely, k is the force required to displace unit length of the foundation through unit distance.

The calculation is done using Finite Element method. A finite element mesh is set to discretize a body consisting of Material II, characterized by two parameters, namely Young's modulus E and Poisson's ratio ν. The dimension of the body is 1.0 in x 26.0 in. The dimension of 26.0 in is the depth of Material II in our model. A force that is needed to displace this system by a unit length is calculated, and this is taken as the value k. We denote this k by k_1. Second, k is evaluated from the formulation he gives, with velocity v = 0.0 in/sec, and the value of deflection y underneath the load is taken from the results of the programs, with v = 0.0 in/sec. We denote this k by k_2. The results are tabulated in Table III.2.1. The deflection under a moving load is greater than that under an identical static load by a factor which increases as the velocity v increases.

The differences of our solution compared with Mathews' are due to the fact that we solve the discretized model of two layered continuum under the action of moving load with constant velocity. It is not a beam problem. Mathews solved a beam on elastic foundation subjected to moving load along the beam. He made use of

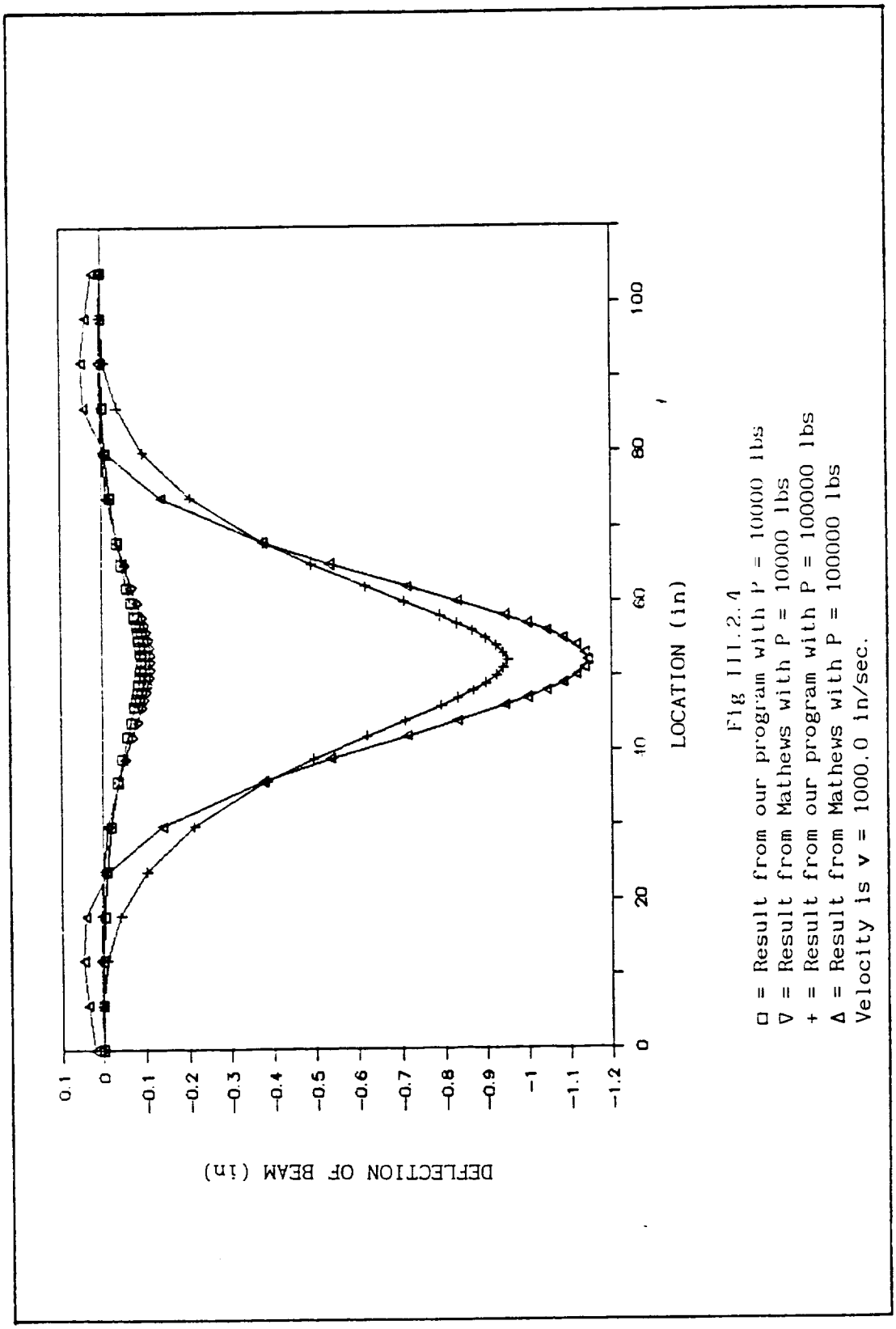

Fig III.2.4

□ = Result from our program with P = 10000 lbs
▽ = Result from Mathews with P = 10000 lbs
+ = Result from our program with P = 100000 lbs
Δ = Result from Mathews with P = 100000 lbs
Velocity is v = 1000.0 in/sec.

Elementary Beam theory in his formulation.

Another two different loads are considered, namely, P = 10000 lbs and P = 100000 lbs. The results from our formulation and from Mathews', for v = 1000 in/sec are plotted in Figure III.2.4. The displacements W of the point under the load for v = 1000 in/sec are as follows:

Mathews' formulation :

For P = 10000 lbs, W = -0.114316 in

For P = 100000 lbs, W = -1.14316 in

Our formulation:

For P = 10000 lbs, W = -0.092471 in

For P = 100000 lbs, W = -0.95413 in.

The results suggest that Load - Displacement relations in Mathews' formulation are linear, and Load - Displacement relations in our formulation are non-linear.

III.3. DYNAMIC, ROTATING HOLLOW DISK

In this problem a hollow disk with inner radius a = 4.0 in and outer radius b = 6.0 in is subjected to non zero initial acceleration $\dot{\omega}$, until constant angular velocity $\omega = 20\pi$ radians/sec, or 600 R.P.M. is attained (we have $\dot{\omega} = 0.0$ radians/sec^2). The rise time for the angular velocity is taken to be 0.00002 second. It will be shown later in this chapter that it is roughly equivalent with 1/8 T, where T is the Period of the

system. Since this problem has two axes of symmetry, we can analyze the quarter plate model together with boundary condition presented in Figure III.3.1. The material properties utilized include a Young's Modulus E = 0.3E+08 psi, and Poisson's ratio ν = 0.25. The mesh shown in Figure III.3.1 consists of six 9 nodes Lagrange elements, and lives in the spatial region V_r ,and measured in coordinate system **e1**, as shown in Figure II.2.1.

A prescribed motion K is introduced to represent the rotation of the disk, in the form of Eulerian displacement of all the nodes in the mesh. This displacement can be easily computed since we know that each node will undego a circular (Eulerian) motion.

Since there are no applied external loads, and due to the symmetry of the problem, the disk will oscillate in the radial directions in the uniform fashion, around its steady state displacement value.This behaviour can be thought of the vibration of one D.O.F. spring-mass system. A closed form solution can be easily computed to check the results of our computation.

Saada [24] give the solution of the steady state displacement of a rotating hollow disk with constant angular velocity. The closed form solution is given in the following formulation:

$$u_r = \rho\ \omega^2\ r\ \frac{(3+\nu)(1-\nu)}{8E}\left(b^2+a^2+\ \frac{1+\nu}{1-\nu}\ \frac{b^2a^2}{r^2}\ -\ \frac{1+\nu}{3+\nu}\ r^2\ \right)$$

where

u_r = steady state radial displacement of rotating disk

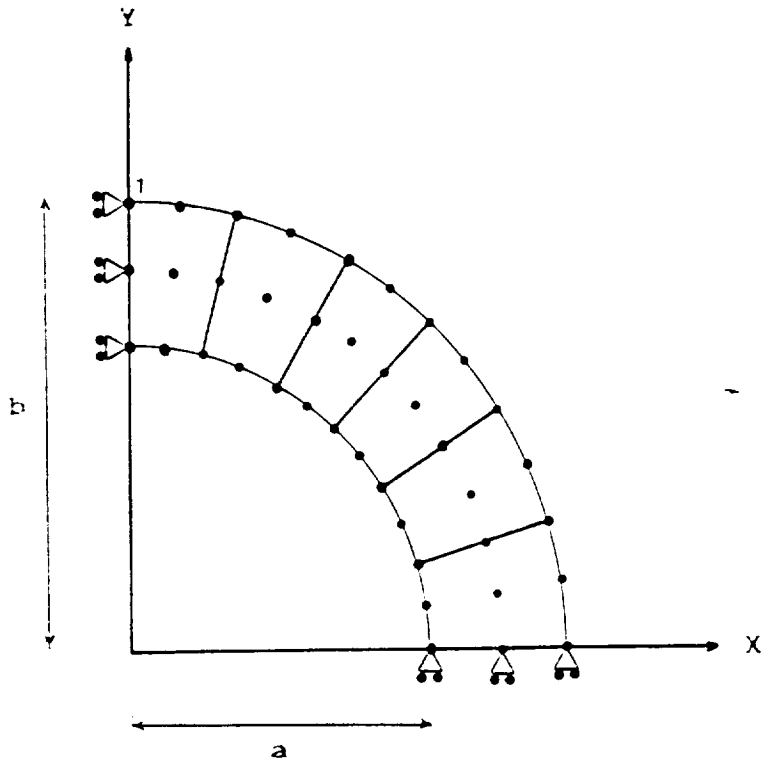

Fig III.3.1

Mesh in the spatial region V_r for first problem
ω = 600 R.P.M, a = 4 in, b = 6 in

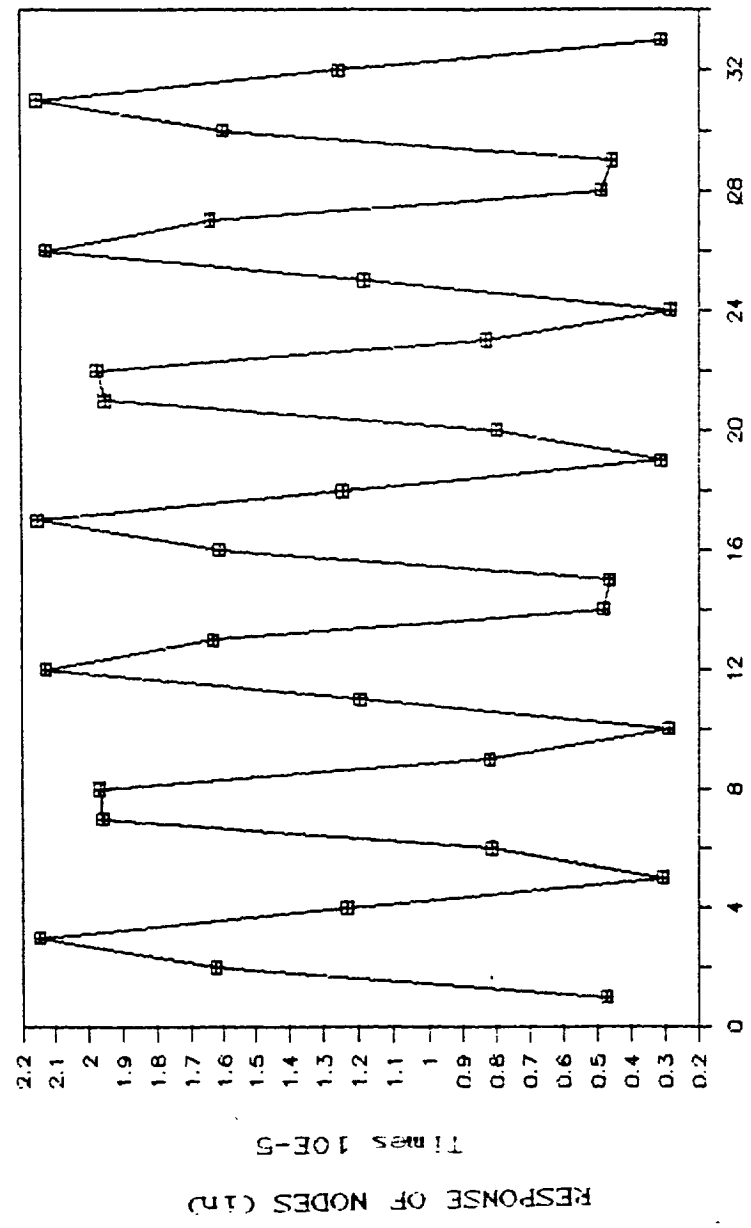

Fig III.3.2

Response of node 1 under initial acceleration until ω = 600 R.P.M. is achieved

r = radial point where displacement is computed = 6 in

a = inner radius of disk = 4 in

b = outer radius of disk = 6 in

E = Young's modulus = 0.3E+08 psi

ν = Poisson's ratio = 0.25

ρ = Density = 0.777E-03 $\frac{\text{lb-sec}^2}{\text{in}^4}$

ω = 20Π rad/sec

and the result is u_r = 1.211E-05 in.

The result of our computation is depicted in Figure III.3.2. This is the response of node 1 shown in Figure III.3.1. We can see from Figure III.3.2 that the response is oscilating around its steady state displacement value (u_r).

The period of the vibration of the spring-mass system can be calculated as follows: We can calculate the force, which is mass times accleration. Since u_r is known, the stiffness of the spring can be obtained. Then the period can be calculated. The result is T = 1.556E-04 sec/cycle. The results of our computation as can be seen in Figure III.3.2 give the period of around 1.6E-04 sec/cycle.

The next problem can be described as follows (the mesh is in Figure III.3.3.). The disk will rotate with constant angular velocity of 600 R.P.M.(exactly like in the first problem), then after a while a load P is applied suddenly in the radial directions (see fig III.3.3). This can be thought of as an impact

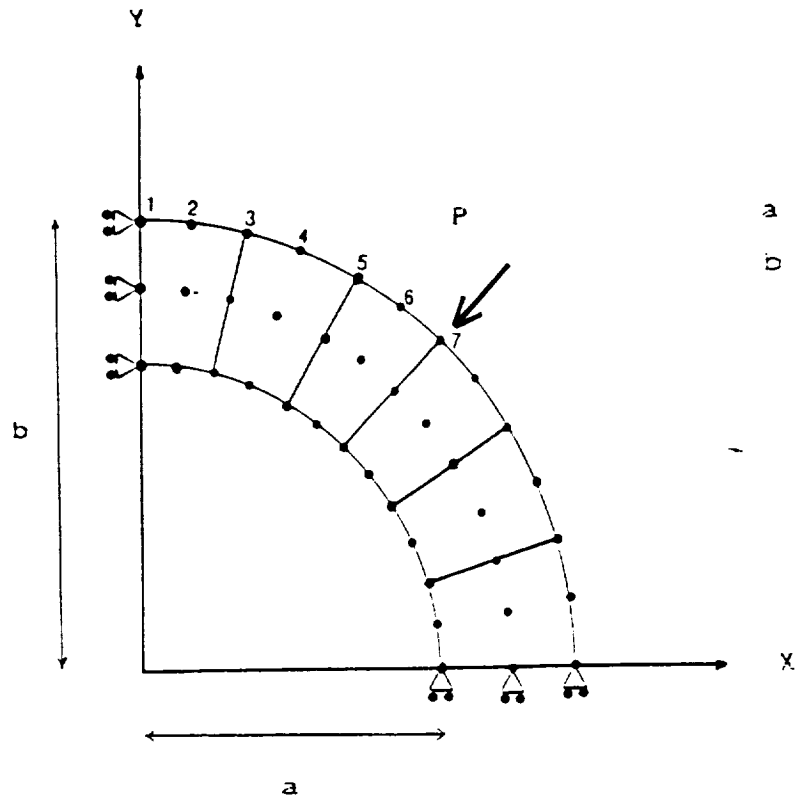

Fig III.3.3

Mesh in the spatial region V_r for second problem
Loading P = 707 lbs

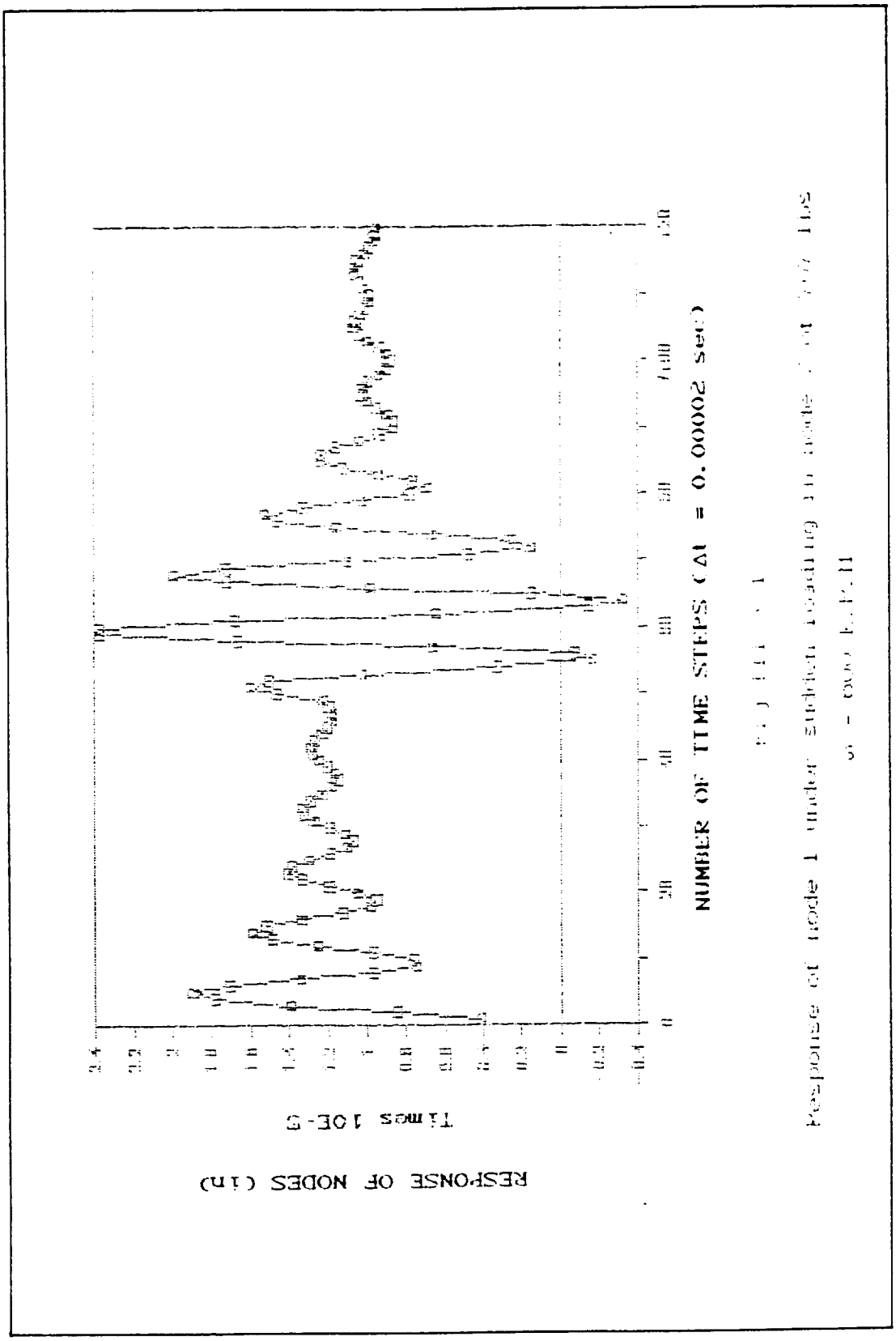
RESPONSE OF NODES (in)
Times 10E-5
NUMBER OF TIME STEPS (Δt = 0.00002 sec)

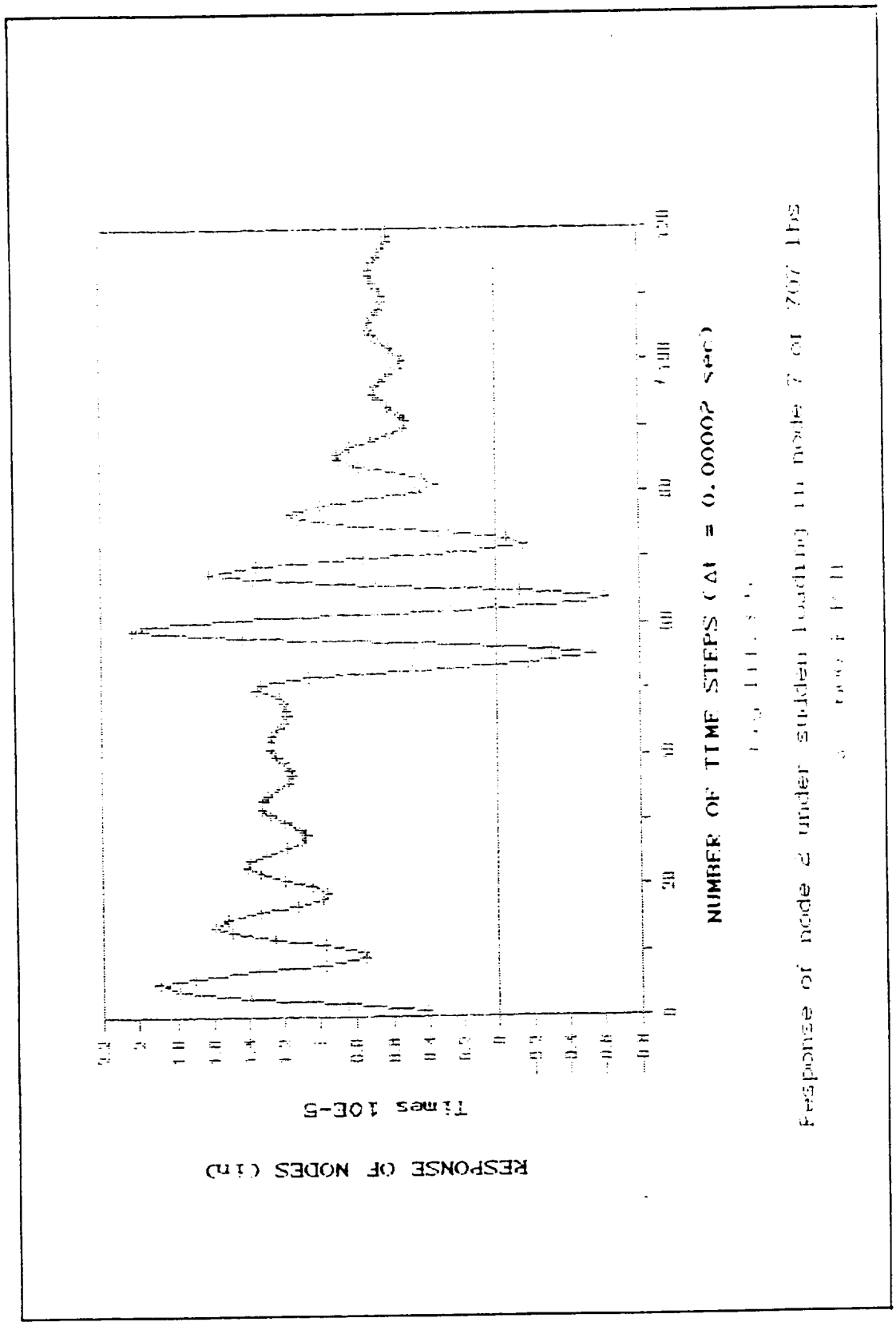

Response of node 2 under sudden loading in node 7 of 200 lbs

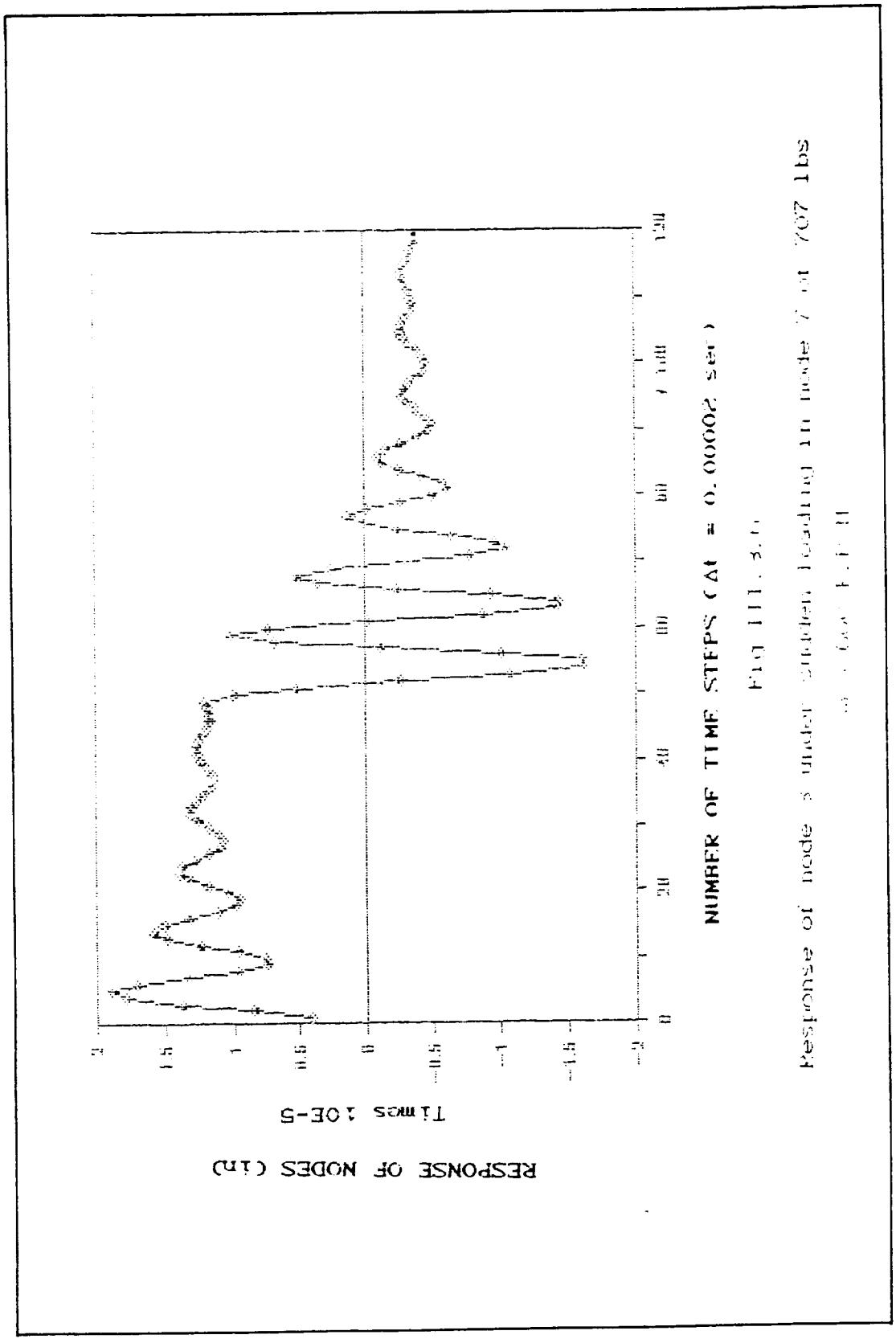

Fig III.3.1

Response of node 3 under sudden loading in mode 7 of 707 lbs

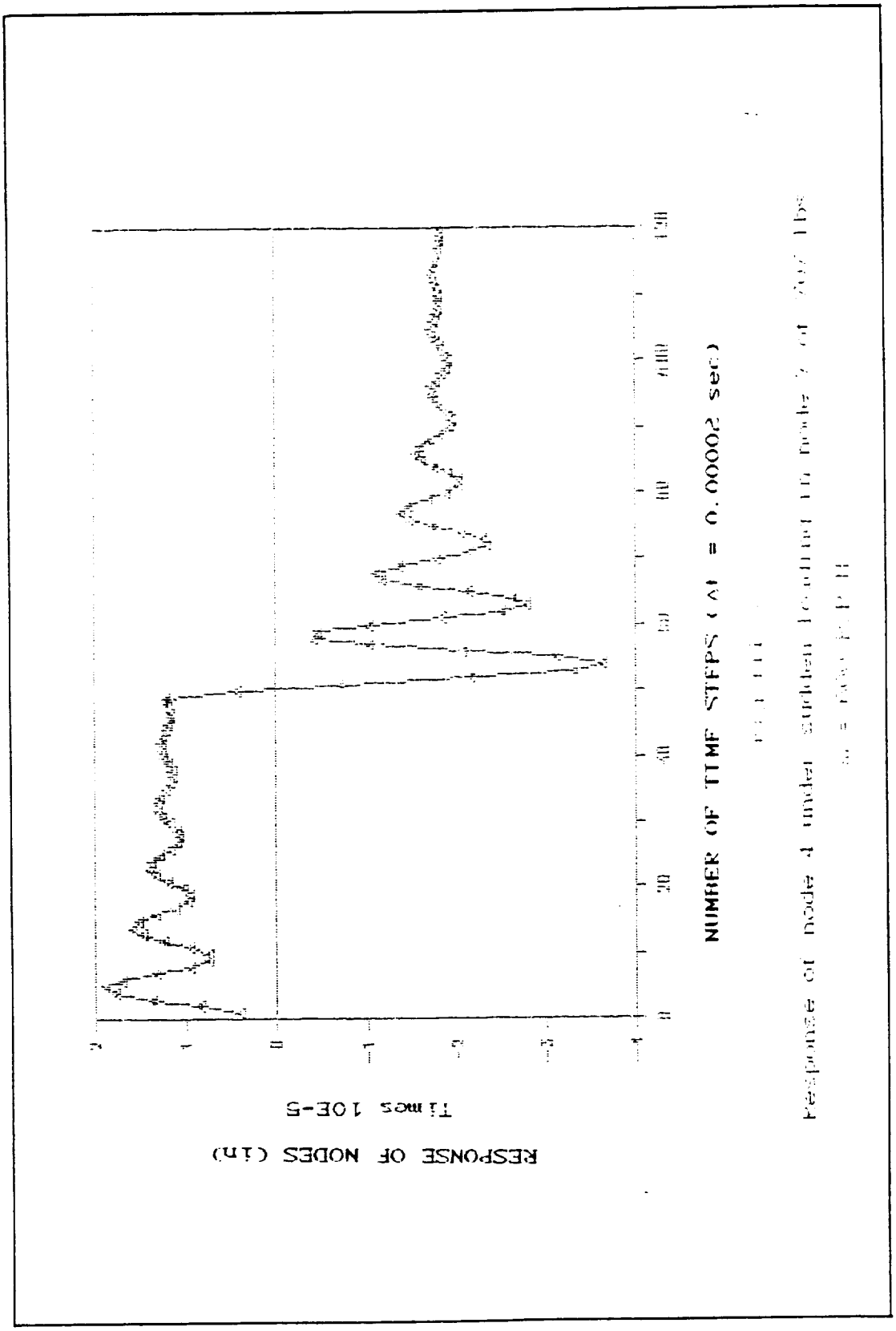

Response of Node 4 under Sudden Loading

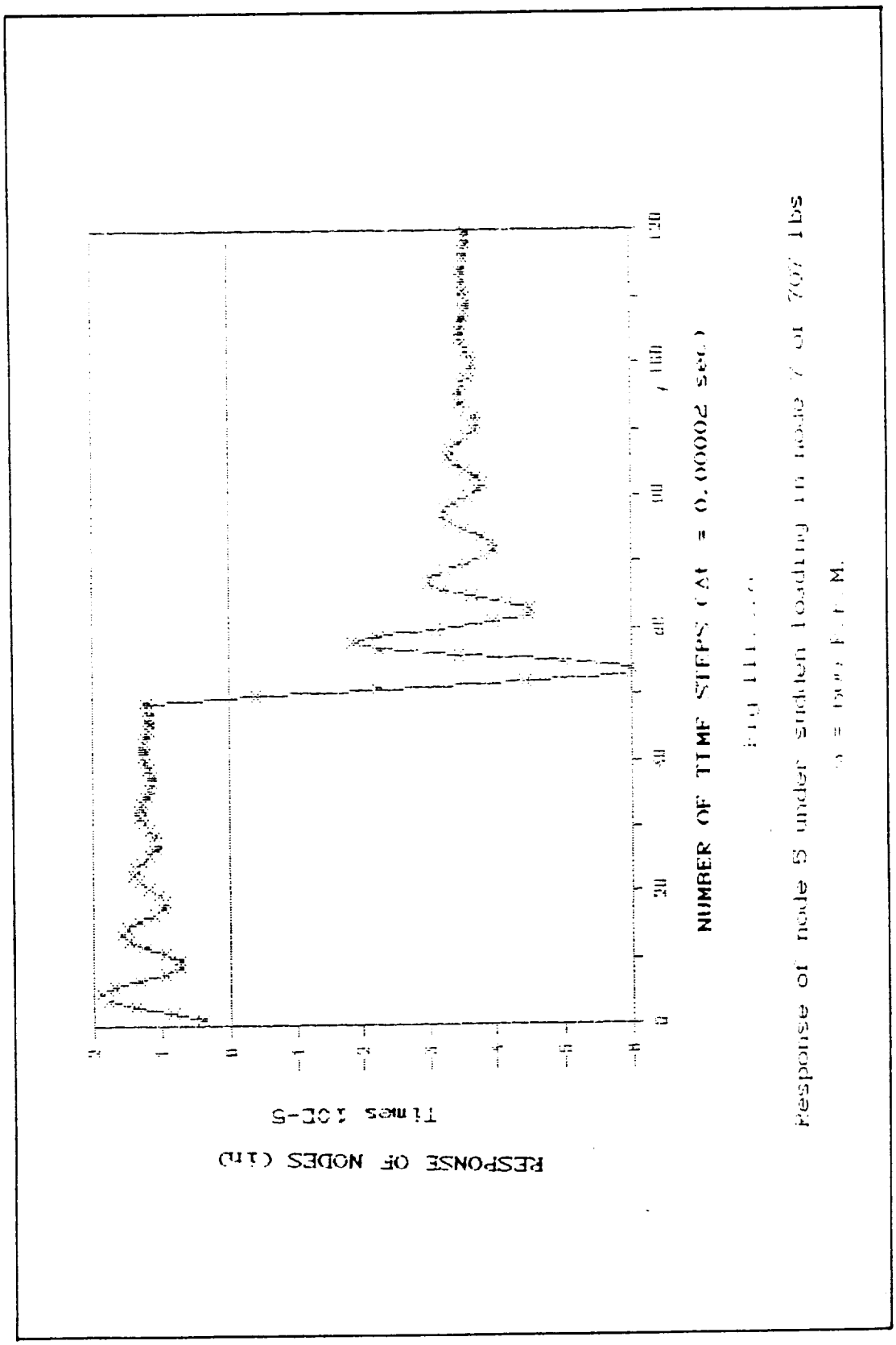

Response of node 5 under sudden loading 10 node 7 of 707 lbs

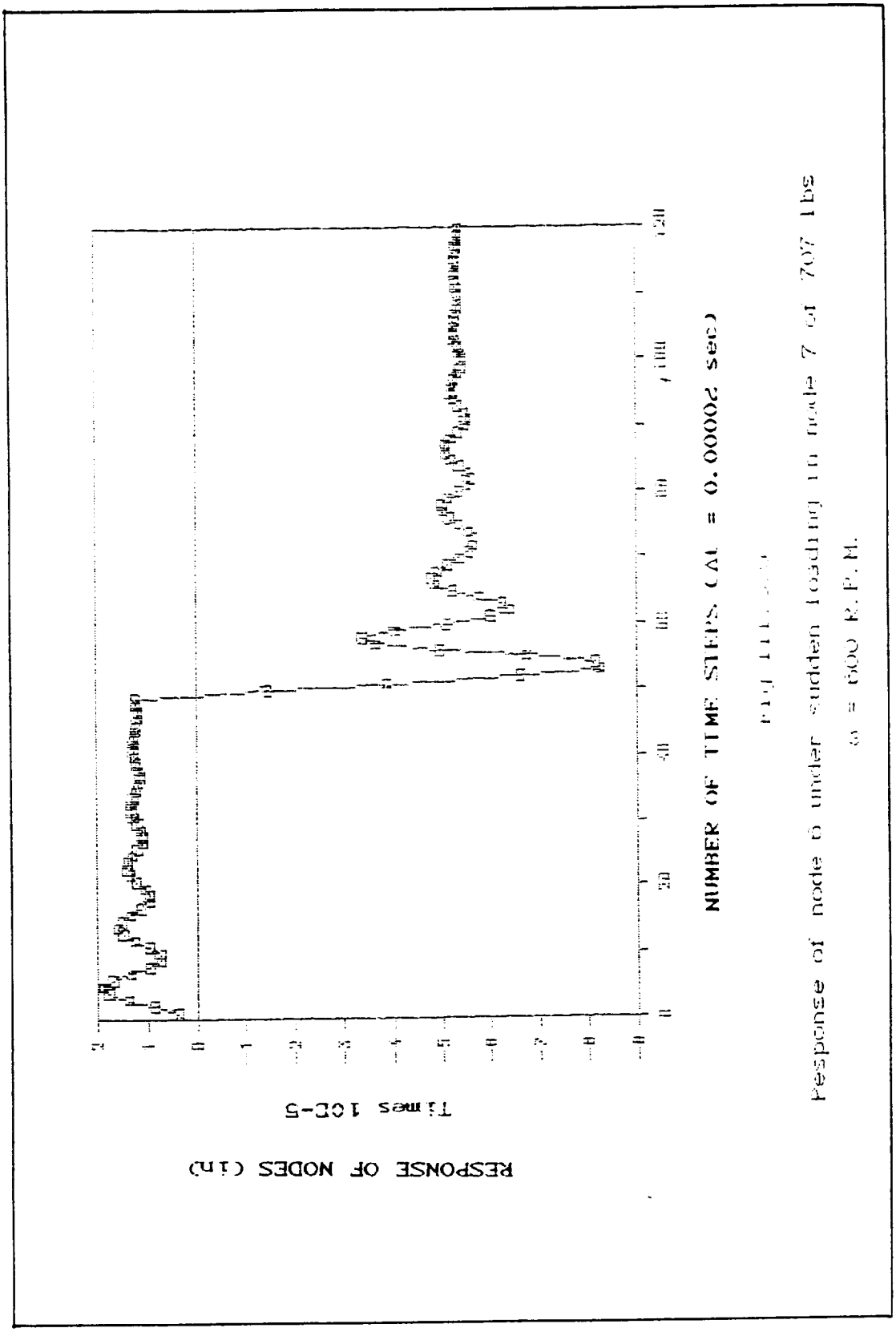

Response of node 6 under sudden loading in node 7 of 707 lbs
ω = 600 R.P.M.

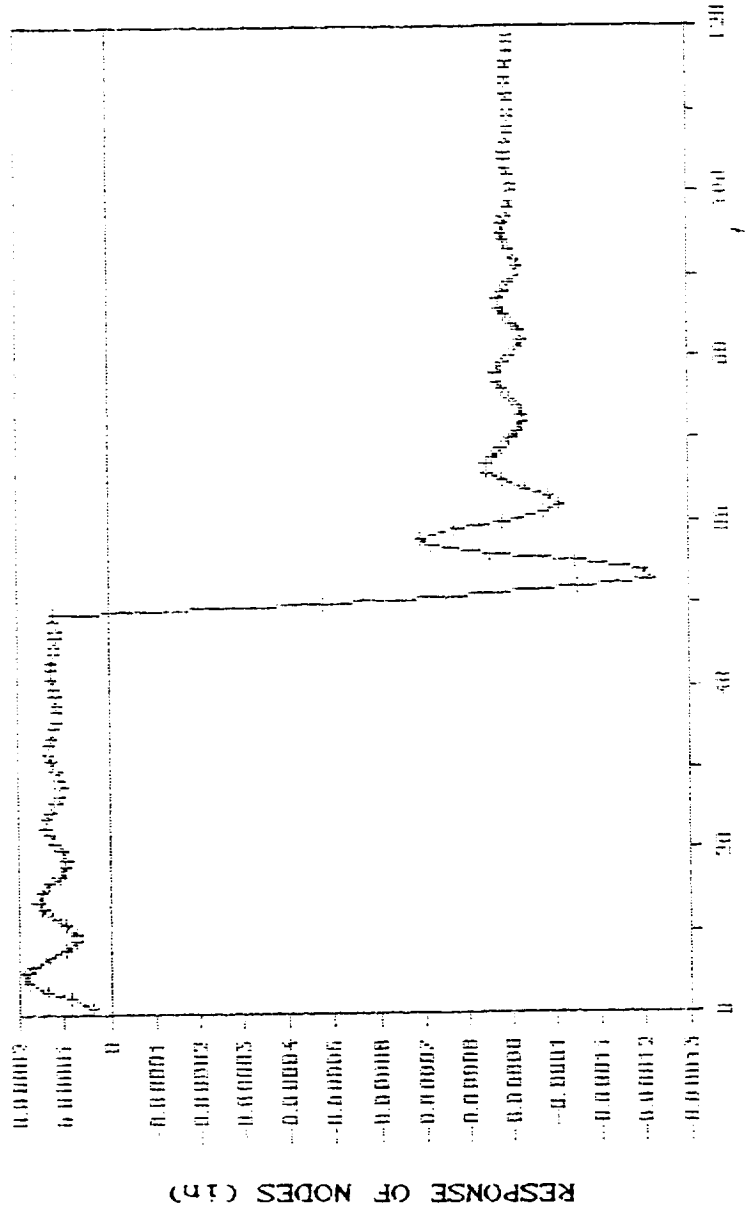

Response of node 7 under sudden loading in node 7 of 707 lbs

C-3

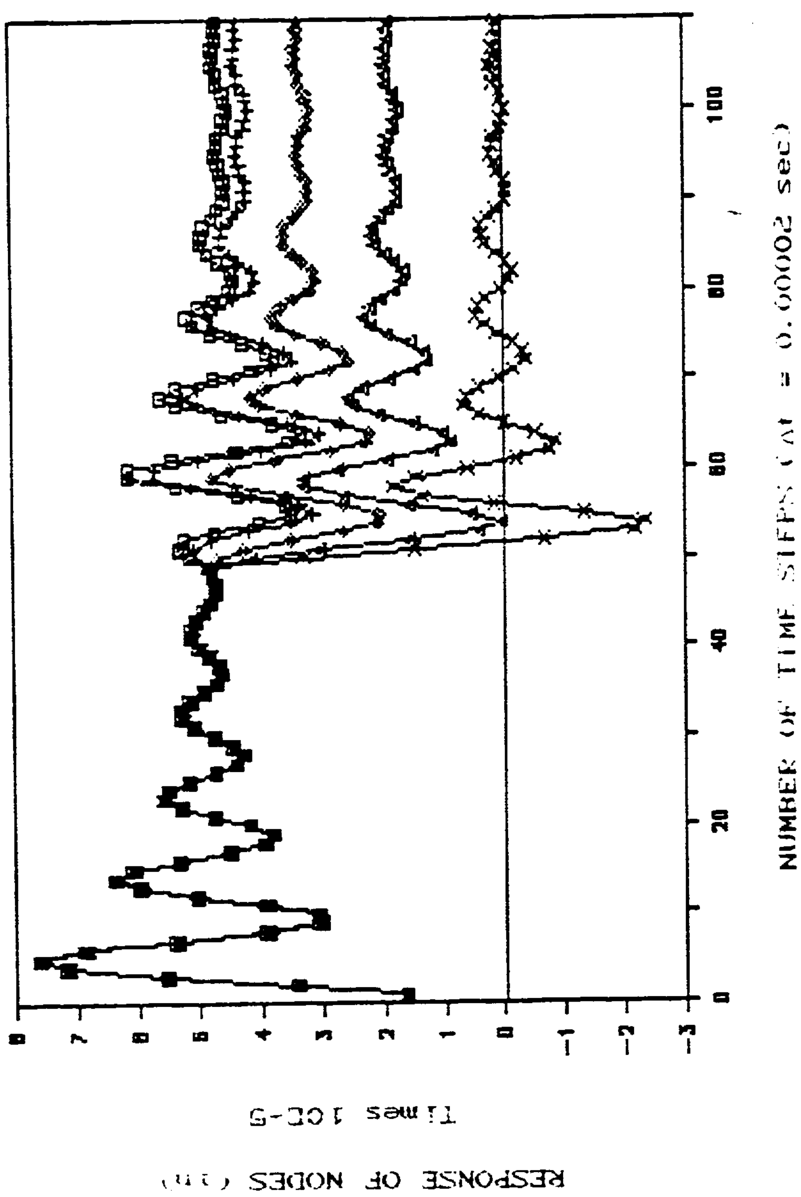

Response of node 1 to node 5 under sudden loading in node 7 of 707 lbs ω = 1200 R.P.M

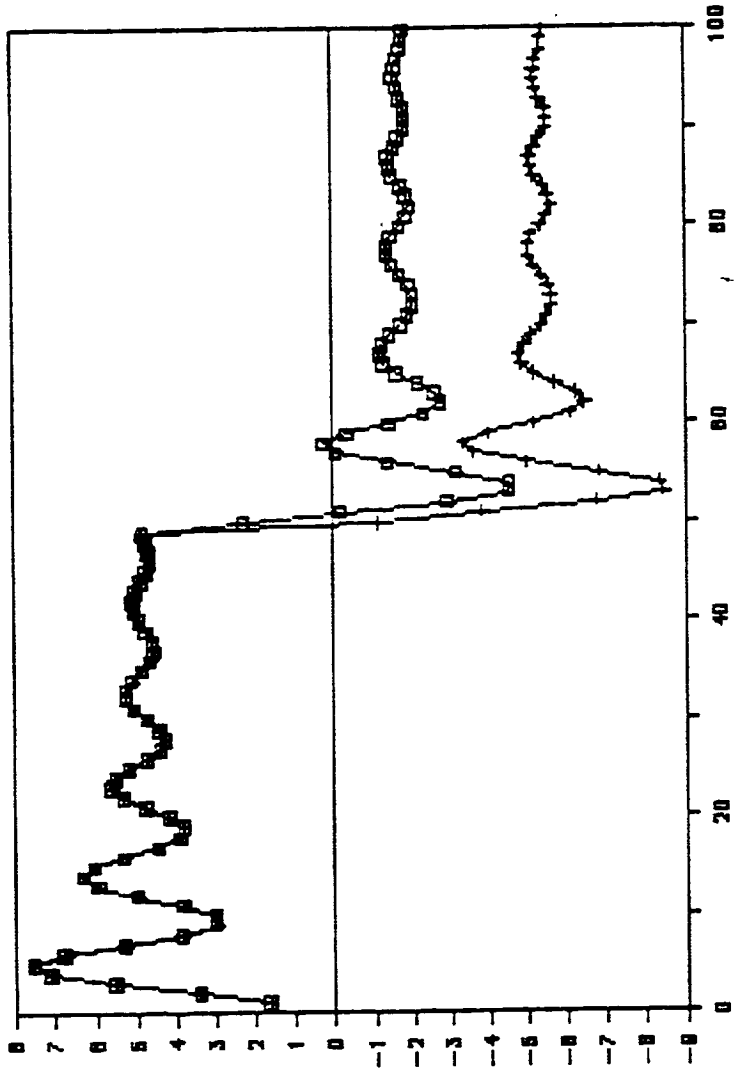

Fig III.3.1.2

Response of node 6 and 7 under sudden loading in mode 7 of
[illegible] E.P.M.

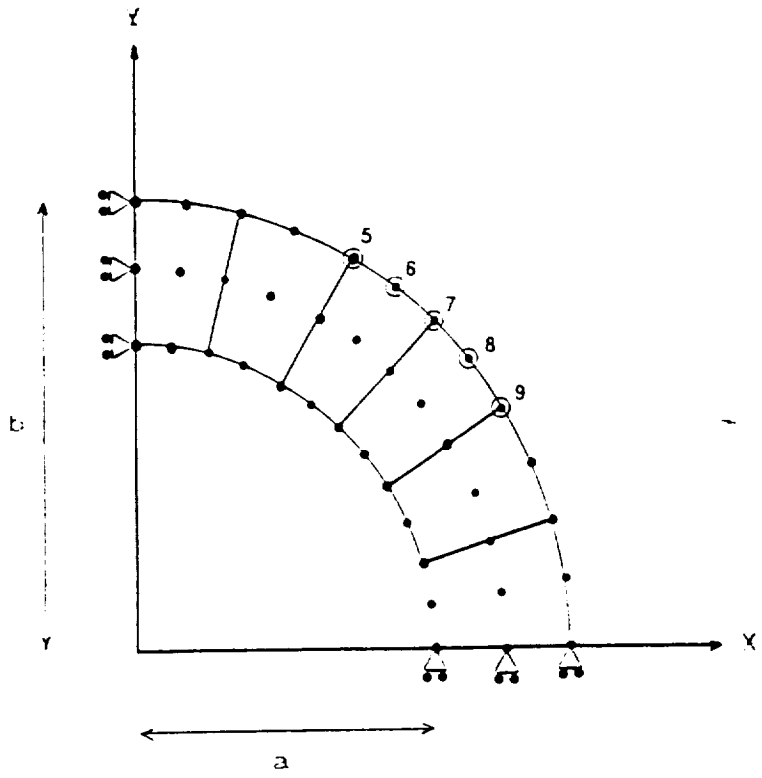

Fig III.3.13

Mesh in the spatial region V_r for third problem.
Constraint will be applied on node 5,6,7,8,9.
Again a=4 in. b=6 in

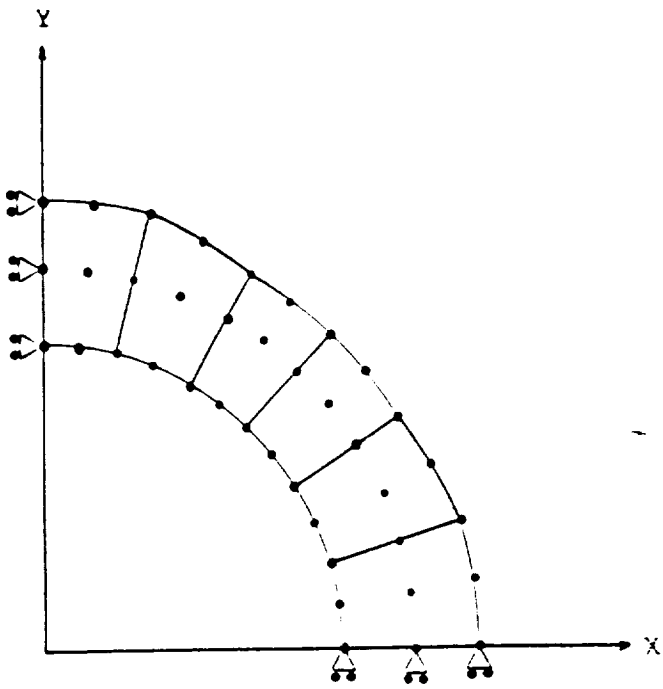

Fig III.3.14

The shape of final configuration after constraint is applied(roughly). a and b are the same with fig III.3.13.

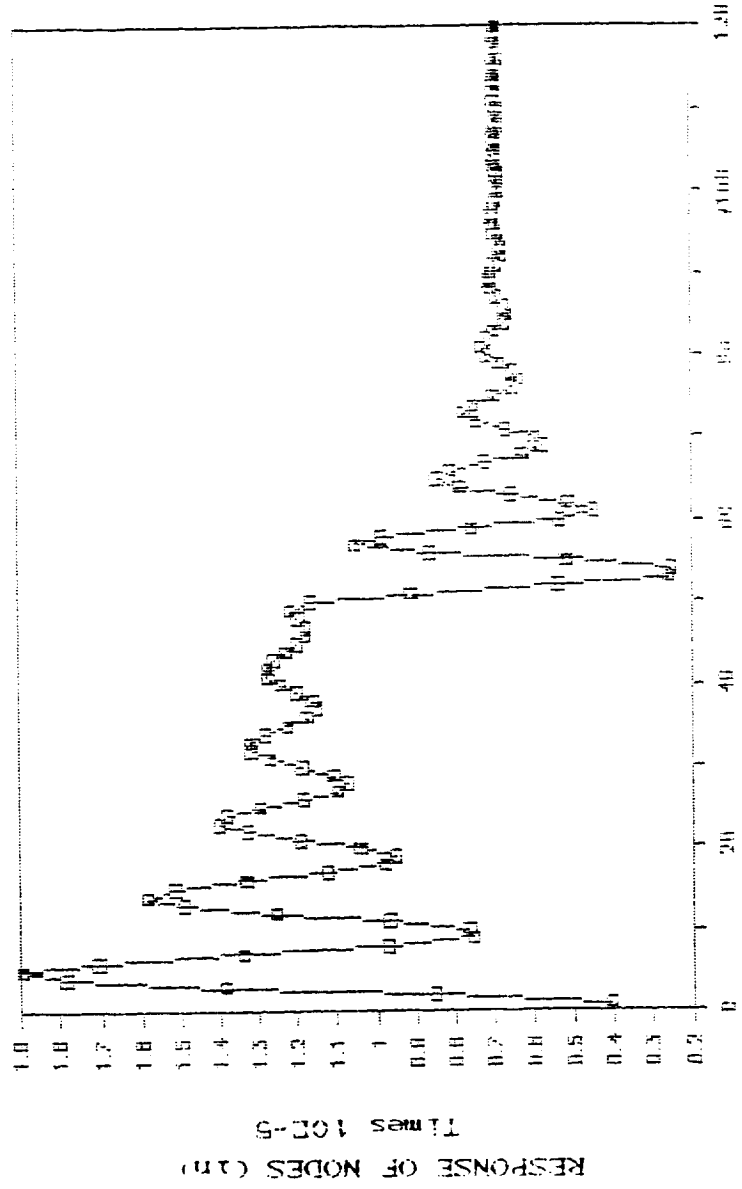

Response of node 1 under sudden constraint in node 5-y.

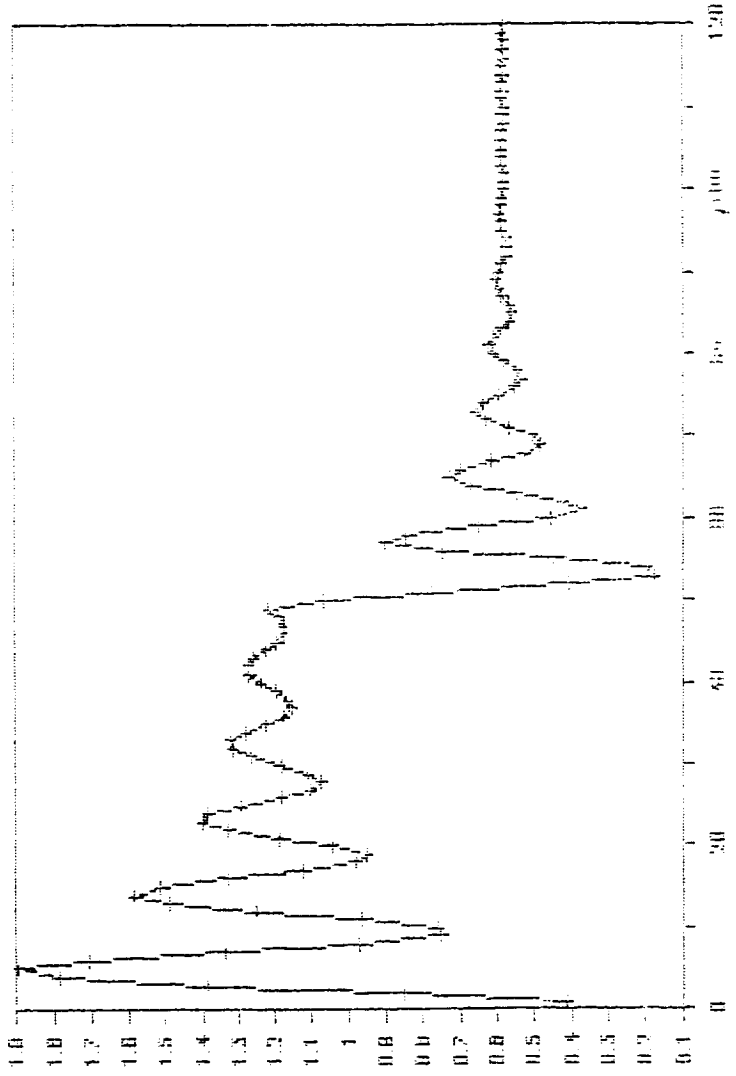

Fig III.3.11

Response of node 2 under sudden constraint in node 5-9.
ω = 600 R.P.M.

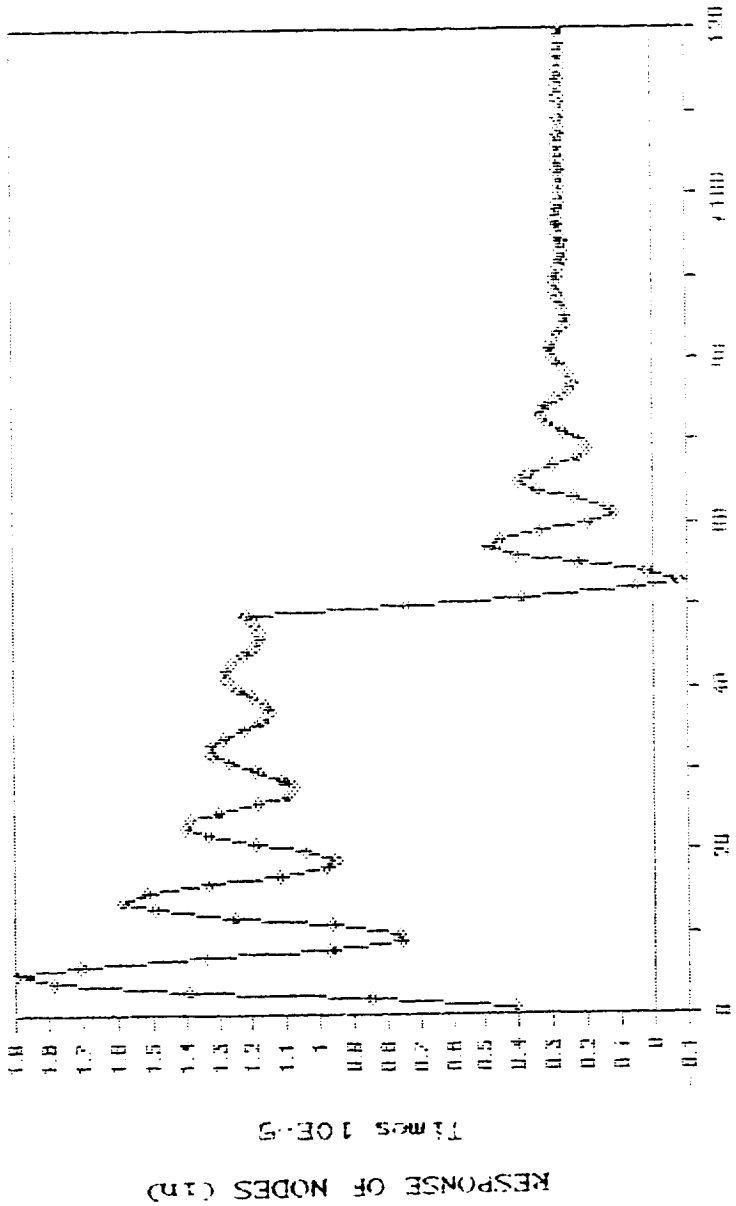

Fig III.3.17

Response of node 3 under sudden constraint in node 5-9.
ω = 600 R.P.M.

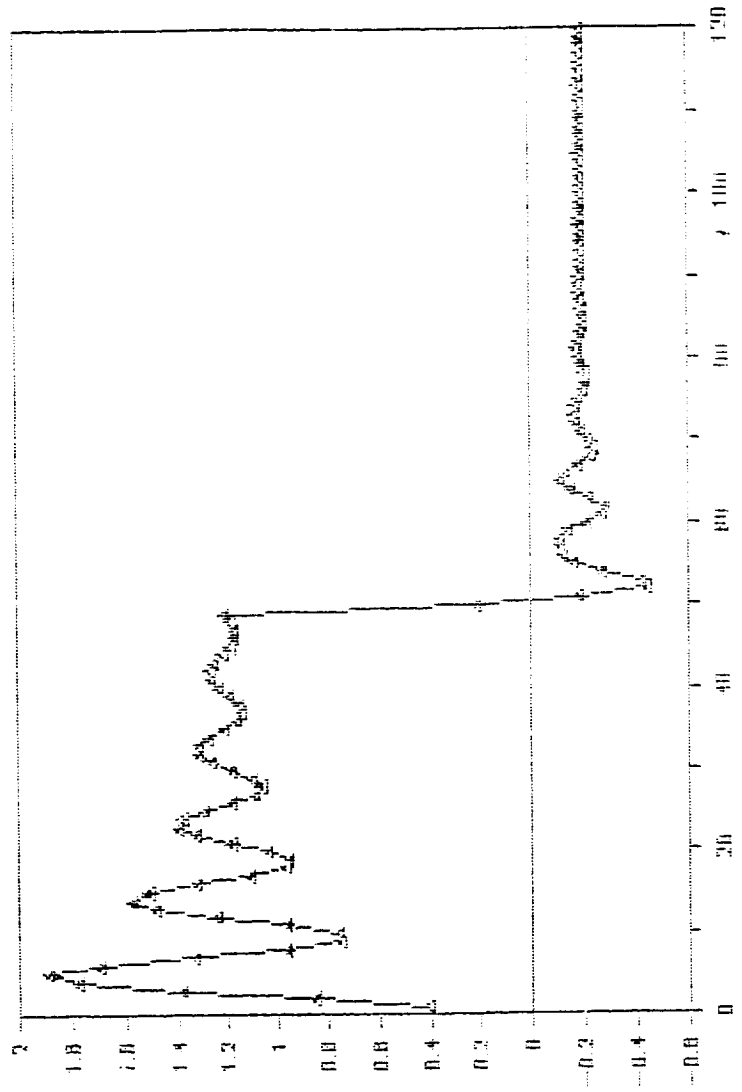

Fig III.3.18

Response of node 4 under sudden constraint in node 5-9.
ω = 600 R.P.M.

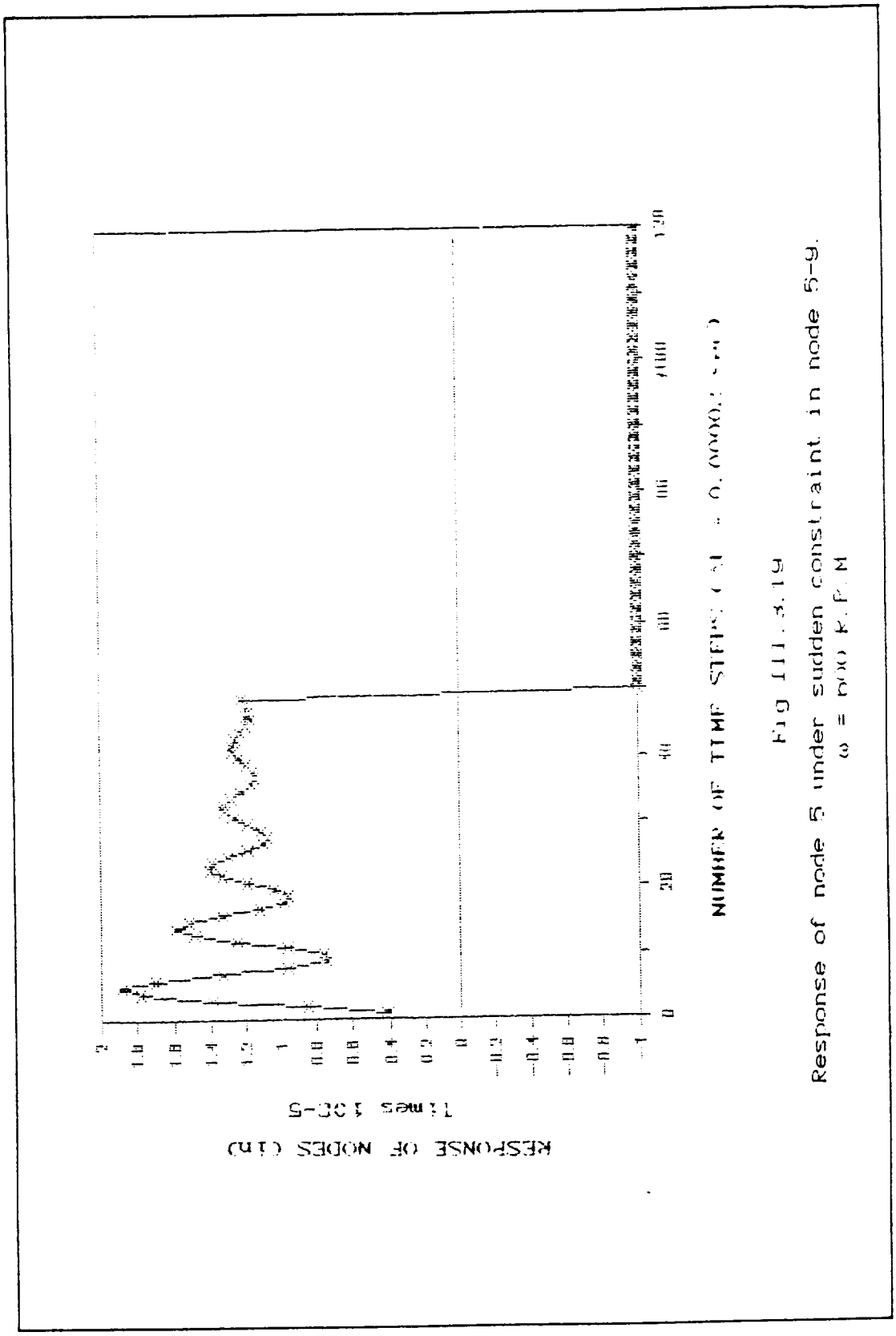

Fig III.3.19

Response of node 5 under sudden constraint in mode 5-9.

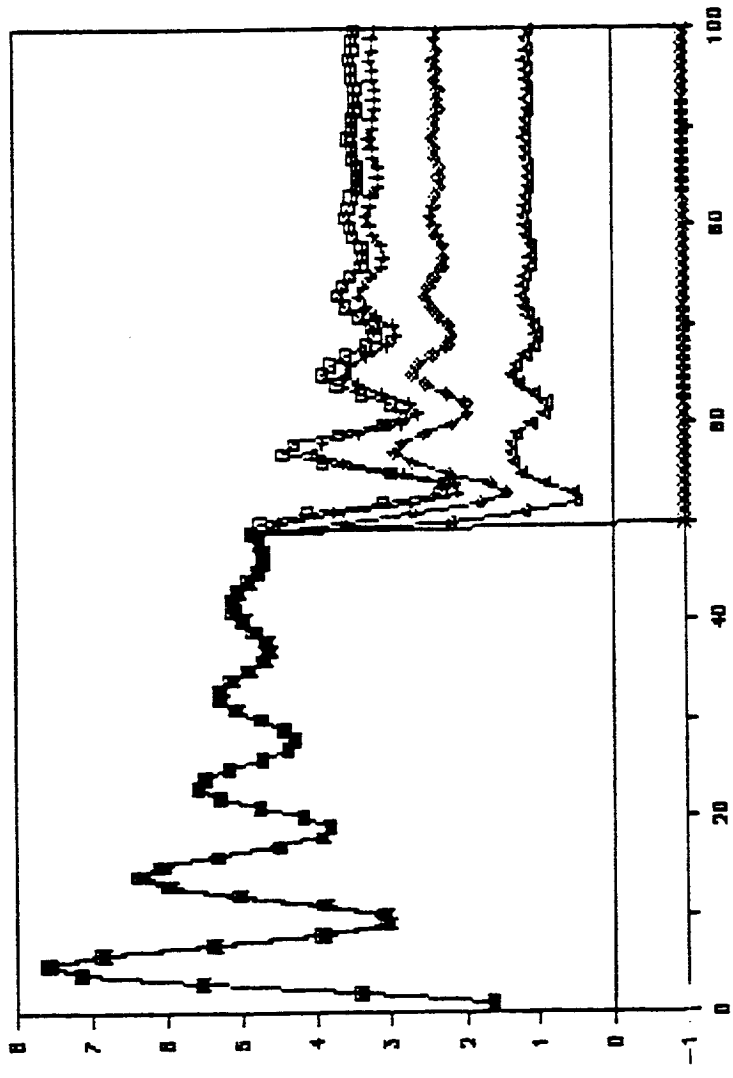

Fig III. 5.20

Response of node 1-node 5 under sudden constraint in node 5-9. ω = 1200 R.P.M

that comes from the sprag to the race. Hughes [10] suggest that we can eleminate the contributions of the response from the higher modes by choosing the integration parameter in the Newmark integration scheme such as $\alpha > 0.25$ and $\delta > 0.5$. We use $\alpha = 0.8$ and $\delta = 0.8$ respectively. The response of node 1 to node 7 are plotted in Figure III.3.4 to Figure III.3.10. The result of ω = 1200 R.P.M. are plotted in Figure III.3.11 and Figure III.3.12.

The mesh for third problem is depicted in Figure III.3.13 (represent the discretization in region V_r). The disk is rotating with specified angular velocity (exactly like in first problem), then a sudden constraints are applied in node 5 to node 9. The constraints are in the form of specified radial displacement. This can be thought of as a brake pad that is applied suddenly on a rotating rotor. The final configuration will be roughly as depicted in Figure III.3.14. The results for ω = 600 R.P.M. are plotted in Figure III.3.15 to Figure III.3.19. The results for ω = 1200 R.P.M. are plotted in Figure III.3.20.

III.4. STRESSES PRODUCED IN A HALF PLANE BY MOVING LOADS

In 1958, Cole and Hut [9] did a study on the stresses produced in a half plane by the uniform motion of a concentrated line load. It was a plane strain problem. In their study, three cases were considered, namely,

(a) The load is moving more slowly than either the longitudinal

or transversal wave speed of the elastic medium (subsonic case).

(b) The load speed is between the two wave speed (transonic case).

(c) The load speed is geater than either wave speed (supersonic case).

For subsonic case, the stresses are found to be

$$-\frac{\pi S_{zz}}{P} = K_1 (2-M_T^2) \frac{\sin\theta_L}{r_L} - 2 K_2 \beta_T \frac{\sin\theta_T}{r_T}$$

$$-\frac{\pi S_{zx}}{P} = 2 K_1 \beta_L \left[\frac{\cos\theta_L}{r_L} - \frac{\cos\theta_T}{r_T} \right]$$

$$-\frac{\pi S_{xx}}{P} = -K_1 (M_T^2 - 2 M_L^2 + 2) \frac{\sin\theta_L}{r_L} + 2 K_2 \beta_T \frac{\sin\theta_T}{r_T}$$

$$C_L = \left\{ \frac{\lambda + 2\mu}{\rho} \right\}^{1/2}$$

$$C_T = \left\{ \frac{\mu}{\rho} \right\}^{1/2}$$

$$M_L = \frac{U}{C_L} \quad ; \quad M_T = \frac{U}{C_T}$$

$$\beta_L = (1 - M_L^2)^{1/2} \quad ; \quad \beta_T = (1 - M_T^2)^{1/2}$$

$$K_1 = \frac{2 - M_T^2}{(2 - M_T^2)^2 - 4\beta_T \beta_L}$$

$$K_2 = \frac{2 \beta_L}{(2 - M_T^2)^2 - 4\beta_T \beta_L}$$

where

S_{zz}, S_{zx}, S_{xx} = Components of the stress tensor

P = Applied line load

ρ = Density of the material

λ and μ = Lame's constants

C_L = Longitudinal wave speed

C_T = Transversal wave speed

U = Speed of the moving load

$$\theta_L = tg^{-1} \frac{\beta_L z}{x}$$

$$\theta_T = tg^{-1} \frac{\beta_T z}{x}$$

z, x = Coordinate of the point where the stress is being evaluated.

To compare the results of our program and the results obtained from Cole's formulation, a plain stress problem with the following dimension and material properties is considered

Material I : 104.0 in x 28.0 in

Young's modulus E = 1.0E+05 psi

Poisson's ratio υ = 0.20

Density ρ = 0.2E-03 lb-sec^2/in^4

The problem and the boundary conditions are depicted in Figure

III.4.1. This system is subjected to a load of 1000.0 lbs acting on node 1, as shown in Figure III.4.1.

The load is moving with constant velocity U above the material I. The mesh shown in Figure III.4.1 consists of 96 nine nodes Lagrange elements, and lives in the spatial region V_r as shown in Figure II.2.1. The movement of the load is represented by uniform Eulerian motion K, prescribed in all the nodes in the **x** direction. We will evaluate the stresses inside the element number 9 as shown in Figure III.4.1. The stresses will be computed using Gaussian integration with 4 points rule. The location of integration points inside the parent element is shown in Figure II.6.1. The stresses inside element 9 will be evaluated on the integration point 1 as shown in Figure III.4.2. The coordinates of integration point 1, measured from a coordinate system with point application of load as the origin are x = 0.4227 in and y (or z in Cole's formulation) = - 1.5774 in.

Three different velocities are used, namely, U = 0.0 in/sec, U = 10000 in/sec, and U = 12000 in/sec. The wave speed for this particular material are found to be C_L = 23570.23 in/sec and C_T = 14433.75 in/sec. The comparisons of the stresses is given in Table III.4.1.

Cole's formulation suggest that as U -> C_T, the solutions becomes singular. However, for this material, the solutions also become unbounded as U —> 13000 in/sec. Our solutions also shows a singularity in the stiffness matrices as U —> 13000 in/sec.

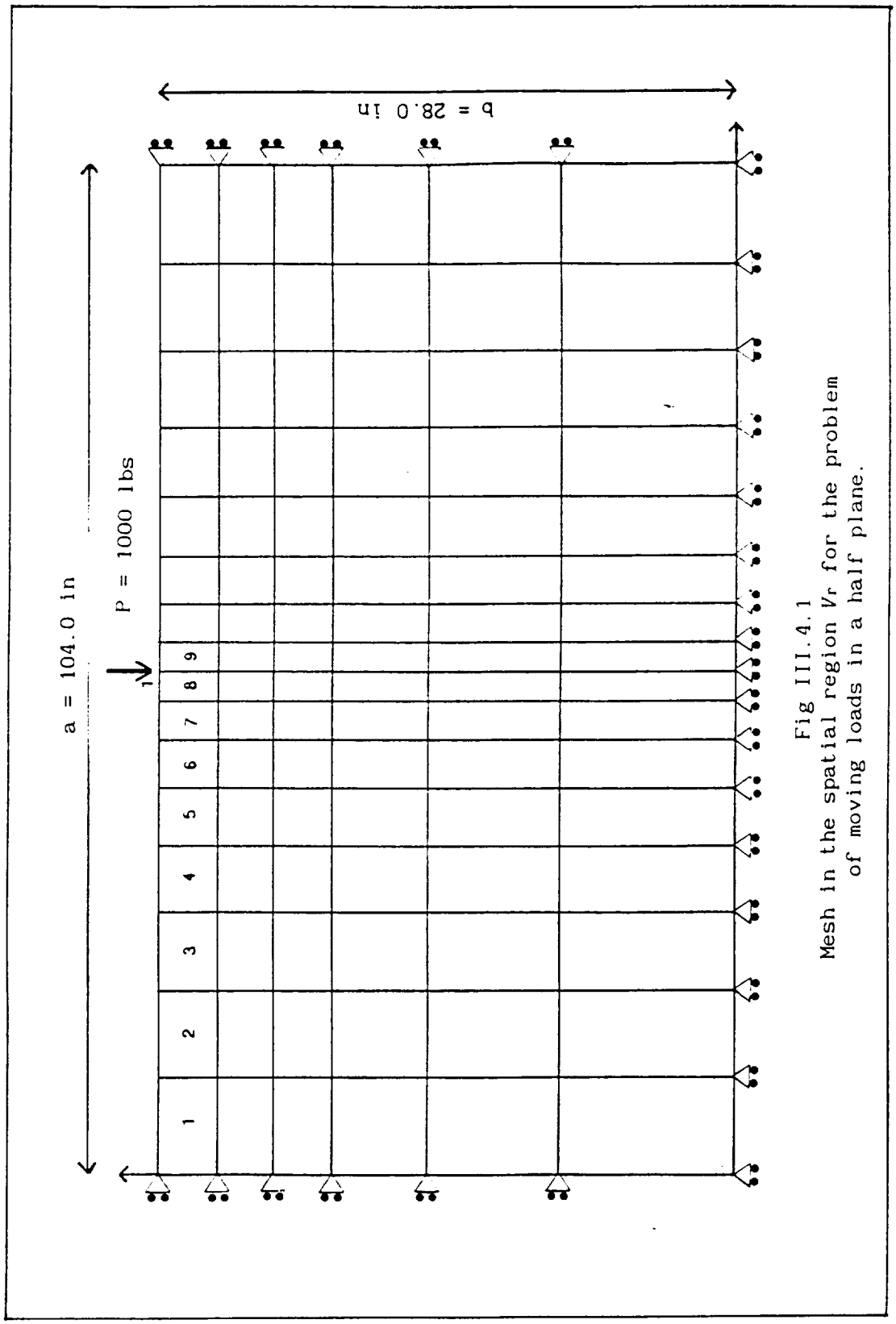

Fig III.4.1
Mesh in the spatial region V_r for the problem of moving loads in a half plane.

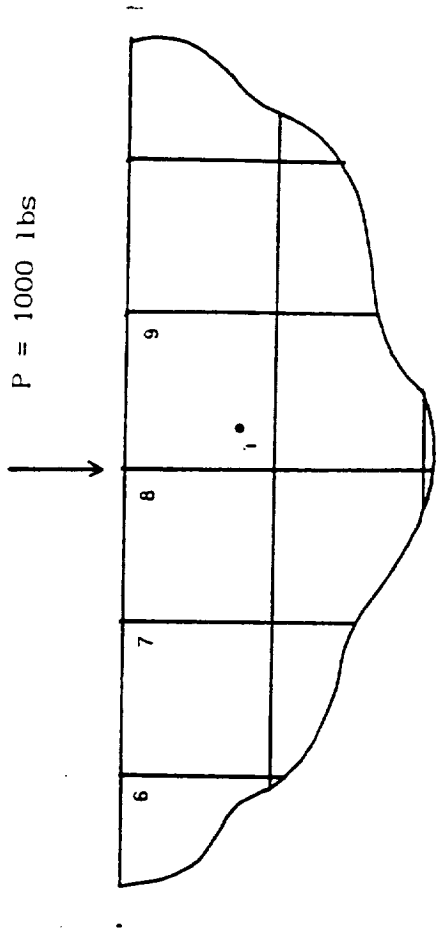

Fig III.4.2
The stresses for half plane problem are evaluated inside element 9, at integration point 1

CHAPTER IV

IV.1. CONCLUSION & FUTURE WORK

The generalized mixed Eulerian-Lagrangian method for solid domain has been formulated, extending previous work by including large strain and dynamic effects. The formulation gives us flexibility to investigate the physics in any choosen spatial region of interest. A FORTRAN program to implement the formulation has been developed. Several different problems have been solved. Comparison with previous solutions show that the implementation of our formulation yields reasonable results.

It is shown that the concept and the method can be applied to a large class of problem. Clutch problem, characterized by sliding contact, is one of them. This tool can be used to build a more realistic model of sliding contact in the clutch. For that, more work is needed.

1) As described in the introduction , the clutch problem is characterized by two (or possibly more) moving bodies. There are two possibilities for the interaction of those bodies. First, since there is oil present in the clutch system, the interactions can be viewed as a coupling between fluid and solid. This is the step that we will pursue immidiately. Second, we can regards the interaction are between two solids. If we assume that stick-slip

conditions occur, an additional contact criteria must be developed

2) A study of experimental results for the clutch suggest that more insight unto the heat transfer problem on the sliding contact in the clutch is needed. Therefore, it is necessary to develop a thermodynamic.

APPENDIX

APPENDIX 1.

This appendix will prove how do we get eq II.1.9 and II.1.10 from eq II.1.7 and II.1.8. Consider eq II.1.7

$$\int_{\partial R} \mathbf{s}(\mathbf{n})\, dA + \int_{R} \mathbf{b}\, dV = \frac{d}{dt} \int_{R} \mathbf{v}\, \rho\, dV + \int_{\partial R} (\rho \mathbf{v}) \mathbf{v} \cdot \mathbf{n}\, dA\,, \qquad (A.1)$$

and focus the attention on the R.H.S. Since R is a fixed region, we can bring time differentiation inside

$$\int_{R} (\, \mathbf{v}\, \rho\,)'\, dV + \int_{\partial R} (\rho \mathbf{v}) \mathbf{v} \cdot \mathbf{n}\, dA. \qquad (A.2)$$

The following relations are useful

$$\operatorname{div}(\mathbf{v} \times \mathbf{w}) = \mathbf{v} \operatorname{div} \mathbf{w} + (\nabla \mathbf{v})\mathbf{w} \qquad (A.3)$$

$$\dot{\mathbf{v}} = \mathbf{v}' + (\operatorname{grad} \mathbf{v})\, \mathbf{v} \qquad (A.4)$$

$$\rho' + \operatorname{div}(\rho\, \mathbf{v}) = 0. \qquad (A.5)$$

Using (A.3) to (A.5)

$$\rho\, \dot{\mathbf{v}} = \rho \mathbf{v}' + \rho(\operatorname{grad} \mathbf{v})\mathbf{v} = (\rho \mathbf{v})' - \rho' \mathbf{v} + (\operatorname{grad} \mathbf{v})(\rho \mathbf{v})$$

$$= (\rho \mathbf{v})' + \mathbf{v} \operatorname{div}(\rho \mathbf{v}) + (\operatorname{grad} \mathbf{v})(\rho \mathbf{v}) =$$

$$= (\rho \mathbf{v})' + \operatorname{div}(\mathbf{v} \times \rho \mathbf{v}) \qquad (A.6)$$

Using the divergence theorem we have the following

$$\int_{\partial R} (\rho \mathbf{v})\mathbf{v}\cdot\mathbf{n}\, dA = \int_{\partial R} (\mathbf{v} \underline{\times} \rho\mathbf{v})\mathbf{n}\, dA = \int_{R} \mathrm{div}(\mathbf{v} \underline{\times} \rho\mathbf{v})\, dV. \qquad (A.7)$$

Combining (A.2), (A.6) and (A.7) we get

$$\int_{\partial R} \mathbf{s}(\mathbf{n})\, dA + \int_{R} \mathbf{b}\, dV = \int_{R} \dot{\mathbf{v}}\, \rho\, dV \qquad (A.8)$$

which is eq II.1.9.

We now start with eq II.1.8

$$\int_{R} \mathbf{r} \times \mathbf{s}(\mathbf{n})\, dA + \int_{R} \mathbf{r} \times \mathbf{b}\, dV = \frac{d}{dt} \int_{R} \mathbf{r} \times \mathbf{v}\, \rho\, dV + \int_{\partial R} \mathbf{r} \times (\rho\mathbf{v})\mathbf{v}\cdot\mathbf{n}\, dA \qquad (A.9)$$

Consider the integrand of the first R.H.S. term after taking time differentiation inside:

$$(\mathbf{r} \times \mathbf{v}\, \rho)' = \mathbf{r}' \times \mathbf{v}\, \rho + \mathbf{r} \times (\mathbf{v}\rho)' \qquad (A.10)$$

since $\mathbf{r}' = \mathbf{v}$, and $\mathbf{v} \times \mathbf{v} = 0$,

$$(\mathbf{r} \times \mathbf{v}\, \rho)' = \mathbf{r} \times (\mathbf{v}\rho)' = \mathbf{r} \times (\mathbf{v}'\rho) + \mathbf{r} \times (\mathbf{v}\rho'). \qquad (A.11)$$

Using divergence theorem the second R.H.S. of (A.9) can be written

$$\int_{\partial R} \mathbf{r} \times (\rho\mathbf{v})\mathbf{v}\cdot\mathbf{n}\, dA = \int_{\partial R} (\mathbf{r} \times \mathbf{v})(\rho\mathbf{v}\cdot\mathbf{n})\, dA = \int_{\partial R} [(\mathbf{r} \times \mathbf{v}) \underline{\times} \rho\mathbf{v}]\mathbf{n}\, dA$$

$$= \int_{R} \mathrm{div}[(\mathbf{r} \times \mathbf{v}) \underline{\times} \rho\mathbf{v}]\, dV \qquad (A.12)$$

The integrand of (A.12) can be written as

$$\mathrm{div}[(\mathbf{r} \times \mathbf{v}) \times \rho\mathbf{v}] = (\mathbf{r} \times \mathbf{v})\ \mathrm{div}\ \rho\mathbf{v} + \mathrm{grad}(\mathbf{r} \times \mathbf{v})\ \rho\mathbf{v}. \qquad (A.13)$$

Using the following relationship

$$\mathrm{grad}(\mathbf{r} \times \mathbf{v})\ \mathbf{v} = \mathbf{r} \times (\mathrm{grad}\ \mathbf{v})\ \mathbf{v} \qquad (A.14)$$

together with (A.4), (A.5) and (A.11), the R.H.S. of (A.9) becomes

$$\int_R \mathbf{r} \times \dot{\mathbf{v}}\rho\ dV \quad , \qquad (A.15)$$

Therefore

$$\int_{\partial R} \mathbf{r} \times \mathbf{s}(\mathbf{n})\ dA \ + \ \int_R \mathbf{r} \times \mathbf{b}\ dV \ = \ \int_R \mathbf{r} \times \dot{\mathbf{v}}\rho\ dV \qquad (A.16)$$

which is eq II.1.10

□

APPENDIX 2.

This appendix will prove that eq II.1.9 and II.1.10 are equivalent with eq II.1.11. First, by using eq II.1.12

$$\mathbf{b}_* = \mathbf{b} - \rho\dot{\mathbf{v}} \ , \qquad (A.17)$$

eq II.1.9 and II.1.10 can be written as

$$\int_{\partial R} \mathbf{s}(\mathbf{n})\ dA \ + \ \int_R \mathbf{b}_* dV \ = 0 \qquad (A.18)$$

$$\int_{\partial R} \mathbf{r} \times \mathbf{s}(\mathbf{n})\ dA \ + \ \int_R \mathbf{r} \times \mathbf{b}_* dV \ = 0 \qquad (A.19)$$

Defining

$$\int_{\partial R} \mathbf{s}(\mathbf{n})\, dA + \int_{R} \mathbf{b}_* dV = \mathbf{f}_* , \tag{A.20}$$

$$\int_{\partial R} \mathbf{r} \times \mathbf{s}(\mathbf{n})\, dA + \int_{R} \mathbf{r} \times \mathbf{b}_* dV = \mathbf{m}_* , \tag{A.21}$$

the momentum balance laws takes the simple form

$$\mathbf{f}_* = 0, \qquad \mathbf{m}_* = 0 , \tag{A.22}$$

Eq II.1.13 with $\mathbf{p} = \mathbf{x}$, $\mathbf{q} = \mathbf{o}$, and $\nabla \mathbf{w} = \mathbf{W}$ will take the form

$$\mathbf{w}(\mathbf{x}) = \mathbf{w}_0 + \mathbf{W}\,(\mathbf{x} - \mathbf{o}) \tag{A.23}$$

with $\mathbf{w}_0$ a vector and $\mathbf{W}$ a skew tensor. Since $(\mathbf{x} - \mathbf{o}) = \mathbf{r}(\mathbf{x})$, where $\mathbf{r}(\mathbf{x})$ is position vector, $\mathbf{w}$ can be written as

$$\mathbf{w} = \mathbf{w}_0 + \omega \times \mathbf{r}, \tag{A.24}$$

with ω the axial vector corresponding to $\mathbf{W}$. Define $\varphi(\mathbf{w}_0, \omega)$ as

$$\varphi(\mathbf{w}_0, \omega) = \int_{\partial R} \mathbf{s}(\mathbf{n}) \cdot \mathbf{w}\, dA + \int_{R} \mathbf{b}_* \cdot \mathbf{w}\, dV \tag{A.25}$$

with $\mathbf{w}$ given by (A.24). Then $\varphi(\mathbf{w}_0, \omega)$ involves integrals of the fields

$$\mathbf{s} \cdot \mathbf{w} = \mathbf{s} \cdot \mathbf{w}_0 + \mathbf{s} \cdot (\omega \times \mathbf{r}), \quad \mathbf{b}_* \cdot \mathbf{w} = \mathbf{b}_* \cdot \mathbf{w}_0 + \mathbf{b}_* \cdot (\omega \times \mathbf{r})$$

where $\mathbf{s}$ is abreviation of $\mathbf{s}(\mathbf{n})$, and since

$$\mathbf{k} \cdot (\omega \times \mathbf{r}) = \omega \cdot (\mathbf{r} \times \mathbf{k}),$$

it follows that

$$\mathbf{s} \cdot \mathbf{w} = \mathbf{w}_0 \cdot \mathbf{s} + \omega \cdot (\mathbf{r} \times \mathbf{s})$$

$$\mathbf{b}_* \cdot \mathbf{w} = \mathbf{w}_0 \cdot \mathbf{b}_* + \omega \cdot (\mathbf{r} \times \mathbf{b}_*)$$

Thus, by (A.20) and (A.21),

$$\varphi(\mathbf{w}_0,\omega) = \mathbf{w}_0\cdot\mathbf{f}_* + \omega\cdot\mathbf{m}_*,$$

and $\varphi(\mathbf{w}_0,\omega) = 0$ for all vectors $\mathbf{w}_0$ and ω if and only if (A.22) hold.

□

APPENDIX 3.

This appendix will prove that eq II.1.11 is equivalent with eq II.1.14, which is

$$\int_{\partial R} \mathbf{s}(\mathbf{n})\cdot\mathbf{w}\, dA + \int_R \mathbf{b}_*\cdot\mathbf{w}\, dV = \int_R \mathbf{T}\cdot\operatorname{grad}\mathbf{w}\, dV \qquad (A.26)$$

in which w is admissible virtual displacement.

Lets start the proof. Let T be Cauchy stress during a motion and let w be any smooth vector field on R. Using the relationship

$$\operatorname{div}(\mathbf{S}^T\mathbf{v}) = \mathbf{S}\cdot\operatorname{grad}\mathbf{v} + \mathbf{v}\cdot\operatorname{div}\mathbf{S} \qquad (A.27)$$

where S and v are smooth tensor and vector field respectively, and using divergence theorem, we have

$$\int_{\partial R} \mathbf{T}\mathbf{n}\cdot\mathbf{w}\, dA = \int_{\partial R} (\mathbf{T}^T\mathbf{w})\cdot\mathbf{n}\, dA = \int_R \operatorname{div}(\mathbf{T}^T\mathbf{w})\, dV$$

$$= \int_R (\mathbf{w}\cdot\operatorname{div}\mathbf{T} + \mathbf{T}\cdot\operatorname{grad}\mathbf{w})\, dV \qquad (A.28)$$

Using eq II.1.6a and (A.17) we get

$$\int_{\partial R} \mathbf{s}(\mathbf{n})\cdot\mathbf{w}\, dA + \int_{R} (\mathbf{b}_*\cdot\mathbf{w})\, dV = \int_{R} (\mathbf{T}\cdot\text{grad}\ \mathbf{w})\, dV \qquad (A.29)$$

Since $\mathbf{w}$ is any smooth vector field on R, we can take $\mathbf{w}$ as admissible virtual displacement and in particular, if we take $\mathbf{w}$ as an infinitesimal rigid displacement, then (A.29) will become eq II.1.11. □

APPENDIX 4.

In this appendix we derive eq II.5.2 and II.5.3. Eq II.5.2 is actually the expression of material time derivative of spatial field $\mathbf{u}$. By (A.4) we can express first material time derivative of $\mathbf{u}$ as

$$(\mathbf{u})^{\cdot}_{\mathrm{m}} = (\mathring{\mathbf{u}})_{\mathrm{m}} + (\text{grad}\ \mathbf{u})_{\mathrm{m}}\ \frac{\partial K}{\partial t} \qquad (A.30)$$

where $\mathring{}$ means spatial time derivative, $\cdot$ is material time derivative, grad $\mathbf{u}$ is spatial gradient of $\mathbf{u}$, motion K is defined in fig II.2.1. This following relationship will be useful.

Define $\Phi = K^{-1}$ so we can express

$$X = \Phi(\mathbf{x}^{\mathrm{r}}, t), \qquad \mathbf{x}^{\mathrm{r}} = K(X, t) \qquad (A.31)$$

Using the fact that

$$\left.\frac{\partial X}{\partial t}\right|_{X\ \text{fixed}} = 0 \qquad (A.32)$$

we can expand

$$\left.\frac{\partial X}{\partial t}\right|_{X\ \text{fixed}} = \frac{\partial\ \Phi(K(X,t),t)}{\partial t} =$$

$$\frac{\partial\, \Phi(K(X,t),t)}{\partial\, K(X,t)} \quad \frac{\partial K}{\partial t} + \frac{\partial \Phi(K,t)}{\partial t}\Bigg|_{K \text{ fixed}} =$$

$$\frac{\partial\, \Phi(\mathbf{x}^r,t)}{\partial\, \mathbf{x}^r}\Bigg|_{\mathbf{x}^r=K(X,t)} \quad \frac{\partial K}{\partial t} + \frac{\partial \Phi(\mathbf{x}^r,t)}{\partial t}\Bigg|_{\mathbf{x}^r=K(X,t)} =$$

$$\text{grad } \Phi(\mathbf{x}^r,t)\Big|_{\mathbf{x}^r=K(X,t)} \quad \frac{\partial K}{\partial t} + \frac{\partial \Phi(\mathbf{x}^r,t)}{\partial t}\Bigg|_{\mathbf{x}^r=K(X,t)} =$$

Evaluating at $X = \Phi(\mathbf{x}^r, t)$ we have

$$\text{grad } \Phi(\mathbf{x}^r,t) \quad \frac{\partial K(X,t)}{\partial t}\Bigg|_{X=\Phi(\mathbf{x}^r,t)} + \frac{\partial \Phi(\mathbf{x}^r,t)}{\partial t}. \qquad (A.33)$$

Using eq $II.3.4_1$ and (A.31), (A.33) can be written as

$$\tilde{J} \quad \frac{\partial K(X,t)}{\partial t}\Bigg|_{X=\Phi(\mathbf{x}^r,t)} + \mathring{X}(\mathbf{x}^r,t) = 0 \qquad (A.34)$$

Putting $\mathring{X}$ into R.H.S. and premultiplying by $\tilde{J}^{-1} = \bar{J}$, we have

$$\frac{\partial K(X,t)}{\partial t}\Bigg|_{X=\Phi(\mathbf{x}^r,t)} = -\bar{J}\ \mathring{X}(\mathbf{x}^r,t) \qquad (A.35)$$

Subtituting (A.35) into (A.30) and evaluating in the refferential variable $\mathbf{x}^r$ we get

$$(\dot{u}) = (\mathring{u}) - (\text{grad } u)\ \bar{J}\ \mathring{X} \qquad (A.36)$$

where $\dot{u}$ is spatial description of $(u)^{\cdot}_{m}$. Viewing $\dot{u}$ as another spatial variable, and using (A.36) we get

$$\dot{\dot{u}} = [(\mathring{u}) - (\text{grad } u)\ \bar{J}\ \mathring{X}\ ]^{\circ} - \text{grad } [(\mathring{u}) - (\text{grad } u)\ \bar{J}\ \mathring{X}\ ]\bar{J}\ \mathring{X}$$

(A.37)

and after expanding we get

$$\dot{u} = \overset{\circ}{\dot{u}} - 2[\text{grad } u]^{\circ} \bar{J} \overset{\circ}{X} - \text{grad } u \overset{\circ}{\bar{J}} \overset{\circ}{X} - \text{grad } u \bar{J} \overset{\circ}{\dot{X}}$$

$$+ \text{grad } [\text{grad } u \ \bar{J} \overset{\circ}{X}] \bar{J} \overset{\circ}{X} \qquad \text{(A.38)}$$

which is eq II.5.2.

If we look at eq II.5.1

$$\int_{V_t} T \cdot \text{grad } w \, dV_t = \int_{\partial V_t} Tn \cdot w \, dA - \int_{V_t} \rho \, \dot{u} \cdot w \, dV_t \qquad \text{(A.39)}$$

and consider at second R.H.S. term, express it in the spatial configuration, we get

$$\int_{V_r} \rho_0 [\dot{u} \cdot w] \tilde{J} \, dV_r \, . \qquad \text{(A.40)}$$

If we subtitute (A.38) to (A.40) we get

$$\int_{V_r} \rho_0 [\overset{\circ}{\dot{u}} \cdot w] \tilde{J} \, dV_r - \int_{V_r} \rho_0 [2 \text{ grad } \overset{\circ}{\dot{u}} \ \bar{J} \overset{\circ}{X} \cdot w] \tilde{J} \, dV_r -$$

$$\int_{V_r} \rho_0 [\text{grad } u \ \overset{\circ}{\bar{J}} \overset{\circ}{X} \cdot w] \tilde{J} \, dV_r - \int_{V_r} \rho_0 [\text{grad } u \ \bar{J} \overset{\circ}{\dot{X}} \cdot w] \tilde{J} \, dV_r +$$

$$\int_{V_r} [\text{grad}(\text{ grad } u \ \bar{J} \overset{\circ}{X}) \bar{J} \overset{\circ}{X} \cdot w] \tilde{J} \, dV_r \, . \qquad \text{(A.41)}$$

Now if we integrate by part the last term to relax the derivative with respect to x^r we get

$$\int_{V_r} \rho_0 [\overset{\circ}{\dot{u}} \cdot w] \tilde{J} \, dV_r - \int_{V_r} \rho_0 [2 \text{ grad } \overset{\circ}{\dot{u}} \ \bar{J} \overset{\circ}{X} \cdot w] \tilde{J} \, dV_r -$$

$$\int_{V_r} \rho_0[\text{grad } u \;\; \mathring{\bar{J}}\, \mathring{X}\cdot w]\tilde{J}\, dV_r \;-\; \int_{V_r} \rho_0[\text{grad } u \;\; \bar{J}\, \mathring{\circ}\mathring{X}\cdot w]\bar{J}\, dV_r \;+$$

$$\int_{\partial V_r} \rho_0[(\mathring{X}\cdot\bar{J}n)w \cdot \text{grad } u \;\; \bar{J}\, \mathring{X}\,]\tilde{J}\, dA \;-$$

$$\int_{V_r} \rho_0[\bar{J}\,(w \times \mathring{X}\,)^T \text{grad } u \;\; \bar{J}\, \mathring{X} \cdot \nabla\tilde{J}\,]\, dV_r \;-$$

$$\int_{V_r} \rho_0[\text{grad } u \;\; \bar{J}\, \mathring{X} \cdot w(\bar{J}^T\cdot\nabla\mathring{X} + \mathring{X}\cdot \text{div } \bar{J}^T)]\tilde{J}\, dV_r \;-$$

$$\int_{V_r} \rho_0[\text{grad } u \;\; \bar{J}\, \mathring{X} \cdot \nabla w\, \bar{J}\, \mathring{X}\,]\, \tilde{J}\, dV_r\,, \qquad \text{(A.42)}$$

which is eq II.5.3.

APPENDIX 5.

In this appendix we will derive the governing equation, without the assumption that the reference frame is inertial. In fact, we assume that the reference frame moves relative to the inertial frame, and they are related by a change in observer. We now make this idea precise.

Let χ and χ^* be motions of $\mathcal{B}$. Then χ and χ^* are related by a change in observer if

$$\chi^*(p,t) = q(t) + Q(t)\,[\,\chi(p,t) - o] \qquad \text{(A.43)}$$

for every material point $\mathbf{p}$ and time t, where $\mathbf{q}(t)$ is a point of space and $\mathbf{Q}(t)$ is a rotation [7]. That is, writing

$$\mathbf{f}(\mathbf{x}, t) = \mathbf{q}(t) + \mathbf{Q}(t)(\mathbf{x} - \mathbf{o}), \tag{A.44}$$

then at each time t the deformation $\chi^*(.,t)$ is simply the deformation $\chi(.,t)$ followed by the rigid deformation $\mathbf{f}(.,t)$:

$$\chi^*(.,t) = \mathbf{f}(.,t) \circ \chi(.,t). \tag{A.45}$$

Intuitively it is clear that if $\mathbf{x} \in \mathcal{B}_t$ and $\mathbf{x}^* \in \mathcal{B}_t^*$ are related through

$$\mathbf{x}^* = \mathbf{f}(\mathbf{x}, t), \tag{A.46}$$

then $\mathbf{x}$ and $\mathbf{x}^*$ must correspond to the same material point. To verify that this is indeed the case, note that, by (A.45),

$$\chi(.,t) = \mathbf{f}(.,t)^{-1} \circ \chi^*(.,t),$$

which is easily inverted to give

$$\mathbf{p}(.,t) = \mathbf{p}^*(.,t) \circ \mathbf{f}(.,t)$$

where $\mathbf{p}$ and $\mathbf{p}^*$ are the reference maps corresponding to the motion χ and χ^*, respectively. Thus

$$\mathbf{p}(\mathbf{x}, t) = \mathbf{p}^*(\mathbf{f}(\mathbf{x}, t), t),$$

or equivalently, by (A.46),

$$\mathbf{p}(\mathbf{x}, t) = \mathbf{p}^*(\mathbf{x}^*, t), \tag{A.47}$$

so that $\mathbf{x}$ and $\mathbf{x}^*$ correspond to the same material point.

As a consequence of (A.43),

$$\dot{\chi}^*(\mathbf{p}, t) = \dot{\mathbf{q}}(t) + \mathbf{Q}(t)\,\dot{\chi}(\mathbf{p}, t) + \dot{\mathbf{Q}}(t)\,[\,\chi(\mathbf{p}, t) - \mathbf{o}\,].$$

If we take $\mathbf{p} = \mathbf{p}^*(\mathbf{x}^*, t)$ in the left side and $\mathbf{p} = \mathbf{p}(\mathbf{x}, t)$ in the right side of this relation - a subtitution justified by (A.47) provided $\mathbf{x}$ and $\mathbf{x}^*$ are related by (A.46) - we conclude that

$$\mathbf{v}^*(\mathbf{x}^*, t) = \dot{\mathbf{q}}(t) + \mathbf{Q}(t)\mathbf{v}(\mathbf{x}, t) + \dot{\mathbf{Q}}(t)(\mathbf{x}-\mathbf{o}), \tag{A.48}$$

where

$$\mathbf{v}^* = (\dot{\chi}^*)_{\mathcal{A}}, \qquad \mathbf{v} = (\dot{\chi})_{\mathcal{A}}$$

are the spatial description of the velocity in the two motions. Let $\mathcal{f}$ be a framing with respect to the inertial frame and $\mathcal{f}^*$ be a framing with respect to the moving observer. Equation (A.48) can be written as

$$\mathbf{v}^*(\mathbf{x}^*, t) - \mathbf{Q}(t)\mathbf{v}(\mathbf{x}, t) = \dot{\mathbf{q}}(t) + \mathbf{A}\,(\mathbf{x}^* - \mathbf{o}) \tag{A.49}$$

where

$$\mathbf{A} = \dot{\mathbf{Q}}\,\mathbf{Q}^{\mathrm{T}}.$$

The skew tensor $\mathbf{A}$ is the spin of $\mathcal{f}$ with respect to $\mathcal{f}^*$ [17]. If we differentiate (A.49) with respect to to t, we obtain

$$\dot{\mathbf{v}}^* - \mathbf{Q}\,\dot{\mathbf{v}} = \ddot{\mathbf{q}} + 2\mathbf{A}(\,\mathbf{v}^* - \dot{\mathbf{q}}\,) + (\dot{\mathbf{A}} - \mathbf{A}^2)\,(\mathbf{x}^* - \mathbf{q})$$

and if we rearrange, we obtain

$$\dot{\mathbf{v}}^* - \ddot{\mathbf{q}} - 2\mathbf{A}(\,\mathbf{v}^* - \dot{\mathbf{q}}\,) - (\dot{\mathbf{A}} - \mathbf{A}^2)\,(\mathbf{x}^* - \mathbf{q}) = \mathbf{Q}\,\dot{\mathbf{v}}\,. \tag{A.50}$$

Let $\mathbf{Q}\,\dot{\mathbf{v}} \equiv \mathbf{a}_{\mathcal{f}}$. Then $\mathbf{a}_{\mathcal{f}}$ is the frame - indifferent vector field over $\mathcal{B}$ which in $\mathcal{f}$ is the accleration field of $\mathcal{B}$.

Cauchy's laws assert that $\mathbf{T}^{\mathrm{T}} - \mathbf{T}$ and $\rho\dot{\mathbf{v}} - \operatorname{div}\mathbf{T} - \mathbf{b}$ vanish in an inertial frame. Since $\mathbf{T}$ is frame indifferent, so is $\mathbf{T}^{\mathrm{T}} - \mathbf{T}$. Thus Cauchy's second law is a frame - indifferent statement. That is, it holds for one framing if and only if it holds for all framings.

Cauchy's first law as stated is not frame - indifferent, but of course it can be modified so as to become so [17]. Cauchy's first law in general framing $\mathcal{f}^*$ assumes the form

$$\text{div } \mathbf{T}^{*} + \mathbf{b}^{*} = \rho\, \mathbf{a}_{\mathcal{F}} \; ; \tag{A.51}$$

where $\mathbf{a}_{\mathcal{F}}$ is given by (A.50), and

$$\mathbf{T}^{*} = \mathbf{Q}\, \mathbf{T}\, \mathbf{Q}^{T}$$

$$\mathbf{b}^{*} = \mathbf{Q}\, \mathbf{b} \; .$$

Using (A.29), (A.51), and the assumption that the body force is due to inertial effect, we obtain

$$\int_{\partial R^{*}} \mathbf{T}^{*}\, \mathbf{n}^{*} \cdot \mathbf{w}^{*}\, dA^{*} - \int_{R^{*}} (\rho\, \mathbf{a}_{\mathcal{F}} \cdot \mathbf{w}^{*})\, dV^{*} = \int_{R^{*}} (\mathbf{T}^{*} \cdot \text{grad } \mathbf{w}^{*})\, dV^{*} \tag{A.52}$$

Equation (A.52) is the governing equation as seen by the moving observer.

By using (A.38), the accleration field in R^{*} as seen by the moving observer is

$$\dot{\mathbf{u}}^{*} = \overset{\circ}{\mathbf{u}}^{*} - 2[\text{grad } \mathbf{u}^{*}]\, \bar{\mathbf{J}}\, \mathring{\mathbf{X}} - \text{grad } \mathbf{u}^{*} \dot{\bar{\mathbf{J}}}\, \mathring{\mathbf{X}} - \text{grad } \mathbf{u}^{*}\, \bar{\mathbf{J}}\, \overset{\circ}{\mathring{\mathbf{X}}} + \text{grad } [\text{grad } \mathbf{u}^{*}\, \bar{\mathbf{J}}\, \mathring{\mathbf{X}}]\, \bar{\mathbf{J}}\, \mathring{\mathbf{X}} \; . \tag{A.53}$$

By using (A.50) and (A.53), we obtain

$$\mathbf{a}_{\mathcal{F}} = \overset{\circ}{\mathbf{u}}^{*} - 2[\text{grad } \mathbf{u}^{*}]\, \bar{\mathbf{J}}\, \mathring{\mathbf{X}} - \text{grad } \mathbf{u}^{*} \dot{\bar{\mathbf{J}}}\, \mathring{\mathbf{X}} - \text{grad } \mathbf{u}^{*}\, \bar{\mathbf{J}}\, \overset{\circ}{\mathring{\mathbf{X}}} + \text{grad } [\text{grad } \mathbf{u}^{*}\, \bar{\mathbf{J}}\, \mathring{\mathbf{X}}]\, \bar{\mathbf{J}}\, \mathring{\mathbf{X}} - \ddot{\mathbf{q}} - 2\mathbf{A}(\, \mathring{\mathbf{u}}^{*} - \text{grad } \mathbf{u}^{*}\, \bar{\mathbf{J}}\, \mathring{\mathbf{X}} - \dot{\mathbf{q}}\,) - (\dot{\mathbf{A}} - \mathbf{A}^{2})\, (\mathbf{x}^{*} - \mathbf{q}). \tag{A.54}$$

The governing equation can be obtained by subtituting (A.54) to (A.52).

□

FLOW CHART FOR GENERALIZED

MIXED EULERIAN-LAGRANGIAN PROGRAM

1) INITIALIZE

XBGD1	(Time rate of change of Material Coordinate)
XBGDD1	(Time rate of change of XBGD1)
UVD1	(Velocity of motion χ)
UVDD1	(Accleration of motion χ)
XXBIG	(Current value of Material Coordinate)
XXBIG1	(Initial value of Material Coordinate)
XXBIG2	(Material Coordinate from previous step)

2) ZERO OUT

STR1	(Second Piola-Kirchhoff stress)
UVTOT1	(Total displacement from previous iteration)
UVTOT2	(Total displacement from previous step)
UVHAT	(Total of Lagrangian displacement)
UVBAR	(Total of Eulerian displacement)
UVBAR1	(Increment of Eulerian displacement)
UVBAR2	(Total Eulerian displa from previous step)

3) START INCREMENT

4) DEFINE KNOWN EULERIAN DISPLACEMENT
   Define UVBAR and UVBAR1

5) START ITERATION (Iteration is denoted by "k")

6) ZERO OUT

BIGK	(Stiffness matrix)
ALOAD	(Loading from stress and dynamics)

7) TEMPORAL INTEGRATION FOR EULERIAN MOTION

Calculate:

XBGD2 (Current value of XBGD1)

XBGDD2 (Current value of XBGDD1)

using old value:

XBGD1, XBGDD1, and UVBAR1

8) ELEMENT LOOP, BUILD STIFFNESS AND LOADING, AND SOLVE

$$M\ {}^{t}\ddot{U}^{(k)} + ({}^{t}K_{L} + {}^{t}K_{NL})\ \Delta\ \hat{U}^{(k)} = {}^{t}R - {}^{t}F^{(k)}$$

9) CALCULATE CURRENT LAGRANGIAN DISPLACEMENT

$$UVHAT^{(k)} = UVHAT^{(k-1)} + UVHAT1^{(k)}$$

10) CALCULATE CURRENT TOTAL DISPLACEMENT

$$UVTOT^{(k)} = UVHAT^{(k)} + UVBAR^{(k)}$$

11) CALCULATE CURRENT MATERIAL COORDINATES

XXBIG = XXBIG1 - UVBAR

12) SWAP THE VALUE OF UVTOT INTO UVTOT1

$$UVTOT1 = UVTOT^{(k)}$$

13) TEMPORAL INTEGRATION FOR TOTAL MOTION

Calculate:

UVD (Current value of UVD1)

UVDD (Current value of UVDD1)

using old value:

UVD1, UVDD1, UVTOT and UVTOT2

14) CHECK THE CONVERGENCE

$$\frac{|UVHAT1|}{|UVHAT|} \leq TOL$$

15) IF NO, THEN GO TO 5)

16) IF YES THEN

Swap the value

XBGD1=XBGD2
XBGDD1=XBGDD2
UVD1=UVD
UVDD1=UVDD
UVTOT2=UVTOT
UVBAR2=UVBAR
XXBIG2=XXBIG

Go to 3) until increment completed

REFERENCES

1. ANSYS Engineering Analysis System User's Manual, Swanson Analysis Systems, Inc., Houston, (1978)

2. Ayoub, N.J., Test Result and Technology Development Report: HLH/ATC (Heavy Lift Helicopter/Advanced Technology Component) Transmission Overrunning Clutch, Boeing Vertol Company, Philadelphia, (1974)

3. Bathe, K.J., Finite Element Procedures in Engineering Analysis, Prentice-Hall, Inc., Englewood Cliffs, New Jersey 07632, (1982)

4. Belytschko, T., Hsieh, B.J.,"Nonlinear Transient Finite Element Analysis with Convected Coordinates," International Journal for Numerical Methods in Engineering, vol.7, pp.255-271 (1973)

5. Belytschko, T., Chiapetta, R.L. and Bartell, H., International Journal for Numerical Methods in Engineering, vol.10, pp.579 (1976)

6. Bogner, F.K., Mallet, R.H., Minich, M.D., and Schmit, L.A. Jr., "Development and Evaluation of Energy Search Methods of Nonlinear Structural Analysis," AFFDL-TR-65-113, Wright-Patterson Air Force Base, Ohio, (1965)

7. Burden, R.L. and Faires, J.D., Numerical Analysis, Prindle, Weber & Schmidt, Boston, (1985)

8. Clough, R.W. and Penzien, J., Dynamics of Structures, McGraw-Hill, Inc., (1975)

9. Cole, J. and Hut, J., "Stresses Produced in a Half Plane by Moving Loads," Journal of Applied Mechanics, vol.25,pp.433-436 (1958)

10. Donea, J., Fasoli-Stella, P. and Giuliani, S., "Lagrangian and Eulerian Finite Element Techniques for Transient Fluid-Structure Interaction Problems," 4th International Conference on Structural Mechanics in Reactor Technology, San Francisco, (1977)

11. Fowles, G.R., Analytical Mechanics, Holt, Rinehart and Winston, New York, (1977)

12. Frank, R.M. and Lazarus, R.B.,"Mixed Eulerian - Lagrangian Method," Methods in Computational Physics, vol.3, pp.47-66 (1964)

13. Gurtin, M.E., An Introduction to Continuum Mechanics, Academic Press, Inc., New York, (1981)

14. Haber, R.B., "A Mixed Eulerian-Lagrangian Displacement Model For Large-Deformation Analysis In Solid Mechanics," Computer Methods In Applied Mechanics and Engineering, vol.43, pp.277-292 (1984)

15. Hirt, C.W., Amsden, A.A. and Cook, J.L.,"An arbitrary Lagrangian Eulerian Computing Method for all Flow Speeds," Journal of Computational Physics, pp.227-254 (1974)

16. Hughes, T.J.R., Liu, W.K. and Zimmermann, T.K., "Lagrangian-Eulerian Finite Element Formulation for Incompressible Viscous-Flows," Interdisciplinary Finite Element Analysis, Proc. U.S.-Japan Seminar; School of Civil and Environmental Engineering, Cornell University, pp.179-216 (1980)

17 Hughes, T.J.R., The Finite Element Method Linear Static and Dynamic Finite Element Analysis, Prentice-Hall, Inc., Englewood Cliffs, New Jersey 07632, (1987)

18. Kikuchi, N. and Oden, J.T., Contact Problems in Elasticity: A study of Variational Inequalities and Finite Element Methods, SIAM, Philadelphia, (1988)

19. Koh, H.M. and Haber, R.B., "Elastodynamic Formulation of the Eulerian-Lagrangian Kinematic Discription," Journal of Applied Mechanics, vol.53,pp.839-845 (1986)

20. Mathews, P.M., "Vibrations of A Beam on Elastic Foundation," Z. angew. Math. Mech, vol.38,pp.105-115 (1958)

21. Mullen, R.L.,"Numerical Methods for the Analysis of Fluid - Solid Interaction Problems," Ph.D. Thesis, Northwestern University, Chicago, (1981)

22. Noh, W.F., "CEL: A Time Dependent Two-Space Dimensional Coupled Eulerian-Lagrangian Code," Methods in Computational Physics, vol.3, pp.117 (1964)

23. Oden, J.T. and Carey, G.F., Finite Element: A second Course volume II, Prentice-Hall, Inc., Englewood Cliffs, New Jersey 07632, (1983)

24. Saada, A.S., Elasticity Theory and Applications, Robert E. Krieger Publishing Company, Malabar, Florida, (1983)

25. Truesdell, C., The Elements of Continuum Mechanics, Springer-Verlag New York Inc., New York, (1966)

26. Truesdell, C., A First Course In Rational Continuum Mechanics, Academic Press, Inc., New York, (1977)

	Y deflection in inches	
Node	Non-linear F.E.M. program	New program
1	-0.0000	-0.0000
2	-0.62323E-04	-0.62327E-04
3	-0.16672E-03	-0.16672E-03
4	-0.0000	-0.0000
5	-0.51305E-04	-0.51307E-04
6	-0.98338E-04	-0.98340E-04
7	-0.0000	-0.0000
8	-0.32815E-04	-0.32816E-04
9	-0.90460E-04	-0.90648E-04
10	-0.0000	-0.0000
11	-0.27737E-04	-0.27738E-04
12	-0.43420E-04	-0.43421E-04
13	-0.0000	-0.0000
14	-0.43517E-04	-0.43520E-04
15	-0.11380E-03	-0.11381E-03

Table III.1.1

Comparison of value from problem III.1 for deflection in Y directions

Stresses calculated from regular F.E.M. program (psi)

Element no 1

Integration point			
1	σ_x = -450.9	σ_y = -3574.	σ_{xy}= 88.57
2	σ_x = -1178.	σ_y = -4436.	σ_{xy}= 1014.
3	σ_x = -739.8	σ_y = -2453.	σ_{xy}= 530.5
4	σ_x = -636.0	σ_y = -2563.	σ_{xy}= -66.97

Element no 2

1	σ_x = -837.7	σ_y = -1932.	σ_{xy}= -38.20
2	σ_x = -366.5	σ_y = -1404.	σ_{xy}= -405.9
3	σ_x = -463.8	σ_y = -2176.	σ_{xy}= -86.99
4	σ_x = -554.6	σ_y = -2429.	σ_{xy}= -833.6

Stresses calculated from ELD program (psi)

Element no 1

1	σ_x = -450.9	σ_y = -3575.	σ_{xy}= 88.60
2	σ_x = -1178.	σ_y = -4437.	σ_{xy}= 1015.
3	σ_x = -739.9	σ_y = -2453.	σ_{xy}= 530.7
4	σ_x = -636.0	σ_y = -2563.	σ_{xy}= -67.09

Element no 2

1	σ_x = -837.7	σ_y = -1932.	σ_{xy}= -38.22
2	σ_x = -366.4	σ_y = -1405.	σ_{xy}= -406.0
3	σ_x = -463.8	σ_y = -2176.	σ_{xy}= -87.01
4	σ_x = -554.7	σ_y = -2429.	σ_{xy}= -833.9

Table III.1.2
The comparison of the stresses of Problem III.1 inside element 1 and 2, in each of the Gaussian integration points

Displacement from Non linear FEM with P=1000.0 lbs

NODE	X-DISPLACEMENT	Y-DISPLACEMENT
1	.00000	.00000
2	.00000	-.62330E-04
3	.00000	-.16672E-03
4	.00000	.00000
5	.71694E-05	-.51305E-04
6	-.12223E-04	-.98347E-04
7	.00000	.00000
8	.55443E-05	-.32804E-04
9	-.98024E-05	-.90410E-04
10	.00000	.00000
11	-.14001E-05	-.27739E-04
12	-.15527E-06	-.43420E-04
13	.00000	.00000
14	.00000	-.43520E-04
15	.00000	-.11380E-03

Displacement from Non linear FEM with P=100000 lbs

NODE	X-DISPLACEMENT	Y-DISPLACEMENT
1	.00000	.00000
2	.00000	-.63276E-02
3	.00000	-.17029E-01
4	.00000	.00000
5	.74899E-03	-.51913E-02
6	-.12749E-02	-.99538E-02
7	.00000	.00000
8	.57336E-03	-.32980E-02
9	-.10268E-02	-.91264E-02
10	.00000	.00000
11	-.14338E-03	-.27832E-02
12	-.18885E-04	-.43547E-02
13	.00000	.00000
14	.00000	-.43886E-02
15	.00000	-.11524E-01

Table III.1.3.
Comparison of the displacements in problem III.1 for P = 1000.0 lbs and P = 100000.0 lbs using regular Non-Linear F.E.M.

Displacement from ELD with P=1000.0 lbs

NODE	X-DISPLACEMENT	Y-DISPLACEMENT
1	0.00000E+00	0.00000E+00
2	0.00000E+00	-0.62327E-04
3	0.00000E+00	-0.16672E-03
4	0.00000E+00	0.00000E+00
5	0.71674E-05	-0.51307E-04
6	-0.12216E-04	-0.98340E-04
7	0.00000E+00	0.00000E+00
8	0.55446E-05	-0.32816E-04
9	-0.98428E-05	-0.90468E-04
10	0.00000E+00	0.00000E+00
11	-0.14010E-05	-0.27738E-04
12	-0.17100E-06	-0.43421E-04
13	0.00000E+00	0.00000E+00
14	0.00000E+00	-0.43520E-04
15	0.00000E+00	-0.11381E-03

Displacement form ELD with P=100000.0 lbs

NODE	X-DISPLACEMENT	Y-DISPLACEMENT
1	0.00000E+00	0.00000E+00
2	0.00000E+00	-0.63810E-02
3	0.00000E+00	-0.17206E-01
4	0.00000E+00	0.00000E+00
5	0.74652E-03	-0.52203E-02
6	-0.13065E-02	-0.10014E-01
7	0.00000E+00	0.00000E+00
8	0.56921E-03	-0.33063E-02
9	-0.10394E-02	-0.91754E-02
10	0.00000E+00	0.00000E+00
11	-0.14392E-03	-0.27898E-02
12	-0.16930E-04	-0.43631E-02
13	0.00000E+00	0.00000E+00
14	0.00000E+00	-0.44114E-02
15	0.00000E+00	-0.11601E-01

Table III.1.4.
Comparison of the displacements in problem III.1 for P = 1000.0 lbs and P = 100000.0 lbs using our formulation

Velocity in/sec	Result from Mathews (k_1)	Result from programs	Result from Mathews (k_2)
0	1.1415 E-02	0.9200 E-02	0.9199 E-02
10	1.1416 E-02	0.9244 E-02	0.9200 E-02
1000	1.1432 E-02	0.9261 E-02	0.9211 E-02
10000	1.3396 E-02	1.1200 E-02	1.0533 E-02

Table III.2.1
Deflection under the load P = 1000.0 lbs
for various velocities

	σ_{yy} (psi)	σ_{xx} (psi)	σ_{xy} (psi)	Velocity (in/sec)
Cole	-351.340	-25.225	-94.141	0.0
ELD	-355.700	-3.014	-76.900	
Cole	-559.895	-59.78	-280.573	10000
ELD	-587.500	-21.36	-256.89	
Cole	-986.840	-220.00	-850.009	12000
ELD	-1144.00	-173.17	-812.000	

Table III.4.1
Comparison of stresses for half plane problem.
Stresses are computed at integration point 1
(inside element 9) with various velocities.